Issue 2 2014 | Volume 10

The Journal on Advanced Studies in Theoretical and Experimental Physics, including Related Themes from Mathematics

PROGRESS IN PHYSICS

"All scientists shall have the right to present their scientific research results, in whole or in part, at relevant scientific conferences, and to publish the same in printed scientific journals, electronic archives, and any other media." — Declaration of Academic Freedom, Article 8

ISSN 1555-5534

The Journal on Advanced Studies in Theoretical and Experimental Physics, including Related Themes from Mathematics

PROGRESS IN PHYSICS

A quarterly issue scientific journal, registered with the Library of Congress (DC, USA). This journal is peer reviewed and included in the abstracting and indexing coverage of: Mathematical Reviews and MathSciNet (AMS, USA), DOAJ of Lund University (Sweden), Zentralblatt MATH (Germany), Scientific Commons of the University of St. Gallen (Switzerland), Open-J-Gate (India), Referativnyi Zhurnal VINITI (Russia), etc.

Electronic version of this journal:
http://www.ptep-online.com

ISSN: 1555-5534 (print)
ISSN: 1555-5615 (online)

Standard Address Number: 297-5092
Printed in the United States of America

April 2014 **Vol. 10, Issue 2**

CONTENTS

Information for Authors and Subscribers

Progress in Physics has been created for publications on advanced studies in theoretical and experimental physics, including related themes from mathematics and astronomy. All submitted papers should be professional, in good English, containing a brief review of a problem and obtained results.

All submissions should be designed in LaTeX format using *Progress in Physics* template. This template can be downloaded from *Progress in Physics* home page http://www.ptep-online.com. Abstract and the necessary information about author(s) should be included into the papers. To submit a paper, mail the file(s) to the Editor-in-Chief.

All submitted papers should be as brief as possible. We accept brief papers, no larger than 8 typeset journal pages. Short articles are preferable. Large papers can be considered in exceptional cases to the section *Special Reports* intended for such publications in the journal. Letters related to the publications in the journal or to the events among the science community can be applied to the section *Letters to Progress in Physics*.

All that has been accepted for the online issue of *Progress in Physics* is printed in the paper version of the journal. To order printed issues, contact the Editors.

This journal is non-commercial, academic edition. It is printed from private donations. (Look for the current author fee in the online version of the journal.)

LETTERS TO PROGRESS IN PHYSICS

General Relativity Theory Explains the Shnoll Effect and Makes Possible Forecasting Earthquakes and Weather Cataclysms

Dmitri Rabounski and Larissa Borissova

E-mails: rabounski@ptep-online.com; borissova@ptep-online.com

The Shnoll effect manifests itself in the fine structure of the noise registered in very stable processes, where the magnitude of signal and the average noise remain unchanged. It is found in the periodic fluctuation of the fine structure of the noise according to the cosmic cycles connected with stars, the Sun, and the Moon. The Shnoll effect is explained herein, employing the framework of General Relativity, as the twin/entangled synchronization states of the observer's reference frame. The states are repeated while the observer travels, in common with the Earth, through the cosmic grid of the geodesic synchronization paths that connect his local reference frame with the reference frames of other cosmic bodies. These synchronization periods match the periods that are manifested due to the Shnoll effect, regardless of which process produces the noise. These synchronization periods are expected to exist in the noise of natural processes of any type (physics, biology, social, etc.) as well as in such artificial processes as computer-software random-number generation. This conclusion accords with what was registered according the Shnoll effect. The theory not only explains the Shnoll effect but also allows for forecasting fluctuations in the stock exchange market, fluctuations of weather, earthquakes, and other cataclysms.

1 The whole truth about the Shnoll effect

Fundamental misunderstandings of the Shnoll effect can be found in published articles as reported by journalists and scientists. Therefore, now is a good time to tell the whole truth about the Shnoll effect, to dot all the i's and to cross all the t's. We express our deep appreciation to Prof. Simon Shnoll, with whom we have enjoyed many years of friendly acquaintance and scientific collaboration.

The principal error in understanding the Shnoll effect is that some people think it is a periodical fluctuation of the magnitude of the signal that is measured. This is incorrect, since the magnitude of the signal and the average noise remain the same during the long-term measurements done by Shnoll and his workgroup. Further, such processes are specifically chosen for the study that are very stable in time. Simply put, nothing allegedly changes in the experiments which continue during days, months, and even years. The subject of the measurement is the *fine structure of the noise* registered in stable processes.

Every process contains noise. The noise originates due to the influence of random factors and satisfies the Gaussian distribution (i.e., the Gauss continuous distribution function of the probability of the measured value between any two moments of time). Gaussian distribution is attributed to any random process, such as noise, and is based on the averaging and smoothing of the noise fluctuation measured during a long enough interval of time. Nevertheless, if considering very small intervals of time, the real noise has a bizarre structure of the probability distribution function, which differs for each interval of time. Each of these real functions being considered "per se" cannot be averaged to a Gaussian curve. This is what Shnoll called the fine structure of noise and is the object of research studies originally conducted by Simon Shnoll, commencing in 1951–1954 to this day.

So, the magnitude of noise is measured in a very stable process during a long enough duration of time (days, months, and even years). Then the full row of the measured data is taken under study. The full duration of time is split into small intervals. A histogram of the probability distribution function is then created for each of the small intervals. Each interval of time has its own bizarre distribution function (form of the histogram) that differs from Gaussian function. Nevertheless, Shnoll found that "paired histograms," which have a very similar (almost identical) form, exist along the row of the measured data. That is, the histogram created for each interval of time has its own "twin" which has a similar form. The similar form was found in the histograms which were registered with the following periods of repetition connected with stars, the Sun, and the Moon:

- 24 hours = 1440 min (solar day);
- 365 days = 525 600 min (calendar year);
- 23 hours, 56 min = 1436 min (stellar day);
- 365 days, 6 hours, 9 min = 525 969 min (stellar year);
- 24 hours, 50 min = 1490 min (lunar day);
- 27 days, 7 hours, 43 min = 39 343 min (lunar month);
- 31 days, 19 hours, 29 min = 45 809 min (period of the lunar evection).

Also, aside as the similar forms of histograms, appearance the mirrored forms of histograms was registered by Shnoll with periods of:

- 720 min (half of the calendar/solar day);
- 182 days, 12 hours = 262 800 min (half of the calendar/solar year).

Shnoll called this phenomenon the "palindrome effect". It is one of Shnoll's newest findings: despite his having started the research studies in 1951, the possibility of the appearance of the mirrored forms of histograms only came to his attention in 2004. The "palindrome effect" was first registered in December 2007. Aside from these two periods of the "palindromes", a number of other palindrome cycles were found. However, certain circumstances have not allowed a continuation of these studies in full force yet.

As was shown by Shnoll after many experiments done synchronously at different locations from South Pole to North Pole, an appearance of the similar form (or the mirrored form) of the histograms does not depend on the geographical latitude, but depends only on the geographical longitude, i.e., the same *local time* at the point of observation. In other words, the Shnoll effect is manifested equally at any location on the Earth's surface, according to the local time, meaning the same locations of the celestial objects in the sky with respect to the visible horizon.

It is significant that the process producing the noise that we measure can be absolutely anything. Initially, in 1951, Shnoll started his research studies from measurements of the speed of chemical reactions in the aqueous solutions of proteins. Then many other biochemical processes attracted his attention. After decades of successful findings, he focused on such purely physical processes as α-decay and β-decay of the atomic nuclei. It was shown that not only all the random natural processes of different origins, but even artificial processes as random-number generation by computer software manifest the Shnoll effect. In other words, this is a fundamental effect.

That in a nutshell is the whole truth about the Shnoll effect. A detailed history of these research studies can be found in Shnoll's book [1], which also contains hundreds of references to the primary publications on this theme commencing in the 1950s to this day. A brief description of the Shnoll effect can also be found in his short presentation of 2006 [2].

A theoretical explanation of the Shnoll effect on the basis of General Relativity follows. But first, we need to explain two important misunderstandings which are popular among the general public.

2 The two most popular mistakes in the understandings of General Relativity

There are two main mistakes in the understanding of General Relativity. These mistakes originate due to the popular explanations of the theory provided by the reporters and other writers unfamiliar with the details of Riemannian geometry. The first is the prejudice that an absolute reference frame allegedly is impossible according to Einstein's theory. The second is the prejudice that Einstein's theory allegedly "prohibits" speeds of information transfer faster than the speed of light, including the instantaneous transfer of information.

These two prejudices originate due to the superficial explanation of Einstein's theory, which can be encountered in the majority of books on the subject. The superficial explanation limits the reader by the historical path in which Special Relativity and General Relativity were created, and by the simplest analysis of the basics of the theory of space-time-matter. As a result, the aforementioned two prejudices became widely popular among laymen as well as among the scientists who did not study the special aspects of Einstein's theory connected with these two problems.

Nevertheless there are a number of fundamental research studies that cover the aforementioned two problems in detail. While these research results may be unknown to reporters or the majority of the scientific community, relativists who work in the field of reference frames and observable quantities have long been aware of them.

So, in 1944 Abraham Zelmanov published his massive theoretical study [3], where he first determined physical observable quantities as the projections of four-dimensional quantities onto the line of time and the three-dimensional spatial section of the observer's reference frame. His mathematical apparatus for calculating physically observable quantities in the space-time of General Relativity then became known as the theory of chronometric invariants [4, 5]. Roger Penrose, Kip Thorne, and Stephen Hawking as young researchers visited Zelmanov in Sternberg Astronomical Institute (Moscow), and listened to his presentations about physical reference frames and observable quantities at his seminar. In particular, Zelmanov showed [3] that an absolute reference frame is allowed in a finite closed universe, if such a reference frame is linked to the global rotation or the global deformation of the universe.

Later, Zelmanov's followers also voiced, in their scientific presentations, the possibility of an absolute reference frame in a finite closed universe.

It should be noted that an absolute reference frame is impossible in the space-time of Special Relativity. This is because Special Relativity considers the simplified version of the four-dimensional pseudo-Riemannian space (space-time), which is always infinite, and also is free of curvature, rotation, and deformation. Therefore, an absolute reference frame is allowed only in the space-time of General Relativity, and only in those cosmological models where the universe exists as a finite closed volume of space, which rotates or deforms as a whole.

The second of the aforementioned prejudices claim that Einstein's theory allegedly "prohibits" the particles which travel faster than light. This claim is not true. The theoretical possibility of faster-than-light particles — tachyons — was

first considered in 1958 by Frank Tangherlini, in the space-time of Special Relativity. He presented this theoretical research in his PhD thesis [6] prepared under the supervision of Sidney Drell and Leonard Schiff, in the Department of Physics at Stanford University. A similar theory of tachyons in the framework of Special Relativity was suggested, independently of Tanglerlini, in 1979 by Torgny Sjödin [7] (he was a Swedish scientist working in Theoretical Physics Department at Vrije Universiteit in Brussels). The most important surveys on tachyons such as [8,9] referred to Tangherlini. Tachyons were first illuminated in the journal publications on the theory of relativity in a principal paper of 1960 [10], authored by Jakov Terletski. Then a more detailed paper [11] was published in 1962 by Bilaniuk, Deshpande, and Sudarshan. The term "tachyons" first appeared later, in 1967 by Gerald Feinberg [12]. See the newest historical survey and analysis of this problem in [13]. Detailed consideration of tachyons in the space-time of General Relativity was included in our books [14, 15].

The main problem with tachyons is that they cannot be registered by means of direct experimentation by a regular observer [16]. Really, regular observers synchronize their reference frames by light signals. In this case, as was already pointed out by Einstein, the speed of light is the ultimate maximum speed that can be registered by an observer: in this case superluminal displacements cannot be registered. More precisely, in reference frames synchronized by light signals, any superluminal displacement will still be registered as a light signal. See [16] or §1.15 of our book [14] for details. This problem arises not from the ideology of Einstein's theory (as many people erroneously think), but only from the general theory of physical experiments.

So, as was explained by international experts on reference frames, an absolute reference frame is allowed in the space-time of General Relativity, in a finite closed universe, if such a reference frame is linked to the global rotation or the global deformation of the universe. But an absolute reference frame is impossible in the space (space-time) of Special Relativity, because the space is infinite, and is free of rotation and deformation.

Faster-than-light particles (tachyons) are allowed in the space (space-time) of both Special Relativity and General Relativity. But superluminal speeds of such particles cannot be registered by a regular observer because his reference frame is synchronized to others by light signals. Such an observer will register any superluminal motion as motion with the speed of light.

Aside from the tachyon problem, there is also the problem of the instant transfer of information. We mean the instant transfer of information without applying quantum mechanics methods (we call it non-quantum teleportation). This problem was first investigated by us, in 1991–1995. These theoretical results were first published in 2001, in the first edition of our book [14]. A short explanation of the theory can also be found in our presentation [17].

The know-how of our theoretical research was that we considered the four-dimensional pseudo-Riemannian space (the space-time of General Relativity) without any limitations pre-imposed on the space geometry according to physical sense or philosophical concepts. In other words, we studied the space-time of General Relativity "per se". We found that, in addition to the regular state of space-time, a fully degenerate state is possible. From the point of view of a regular observer, whose home is our regular space-time, the fully degenerate space-time appears as a point: all four-dimensional (space-time) intervals, all three-dimensional intervals, and all intervals of time are zero therein. We therefore called the fully degenerate space-time *zero-space*. But this fact does not mean that zero-space is nonsense. Once the observer enters zero-space, he sees that the space and time intervals are nonzero therein.

We showed that zero-space is inhabited by light-like particles which are similar to regular photons. We called these particles *zero-particles*. Zero-particles travel in zero-space with the speed of light. But their motion is perceived by a regular observer as instantaneous displacement. This is one of the effects of relativity theory, which is due to the space-time geometry. We only see that particles travel instantaneously while they travel at the speed of light in their home space (zero-space), which appears to us, the external observers, as the space wherein all intervals of time and all three-dimensional intervals are zero.

We also showed that the regular relation between energy and momentum is not true for zero-particles. Zero-particles bear the properties of virtual photons, which are known from Quantum Electrodynamics (i.e., they transfer interactions between regular particles). This means that zero-particles play the rôle of virtual photons, which are material carriers of interaction between regular particles of our world.

Zero-space as a whole is connected to our regular space-time in every point: at every point of our regular space-time, we have full access to any location inside zero-space. Once a regular photon has entered into such a zero-space "gate" at one location of our regular space, it can be instantly connected to another regular photon which has entered into a similar "gate" at another location. This is a way for non-quantum teleportation of photons.

We also showed that zero-particles manifest themselves as standing light waves (stopped light) while zero-space as a whole is filled with the global system of the standing light waves (the world-hologram). This matches with what Lene Hau registered in the frozen light experiment [18, 19]: there, a light beam being stopped is "stored" in atomic vapor, remaining invisible to the observer until that moment of time when it is set free again in its regularly "travelling state". The complete theory of stopped light according to General Relativity was first given in 2011, in our presentations [20, 21], then again in 2012, in the third edition of our book [14]. The

obtained theoretical results mean that the frozen light experiment pioneered at Harvard by Lene Hau is an experimental "foreword" to the discovery of zero-particles and, hence, a way for non-quantum teleportation.

Until recently, teleportation has had an explanation given only by Quantum Mechanics [22]. It was previously achieved only in the strict quantum way: e.g., quantum teleportation of photons, in 1998 [23], and of atoms, in 2004 [24, 25]. Now the situation changes: with our theory we can find physical conditions for non-quantum teleportation of photons, which is not due to the probabilistic laws of Quantum Mechanics but according to the laws of General Relativity following the space-time geometry.

Thus, the instant transfer of information is allowed in the space-time of General Relativity (though the real speeds of the particles do not exceed the velocity of light). But this is impossible in the space-time of Special Relativity, because it is free of rotation and a gravitational field (whereas by contrast, the main physical condition of zero-space is a strong gravitational potential or a near-light-speed rotation).

Of course, the general reader cannot find all these important details in general-purpose books explaining Einstein's theory. Special skills in Riemannian geometry are needed to understand what has been written in the special publications that we surveyed herein. It is not surprising, therefore, that the majority of people are still puzzled by the aforementioned prejudices and misunderstandings about Einstein's theory.

3 General Relativity Theory explains the Shnoll effect: the scanning of the world-hologram along the Earth's path in the cosmos

As we shall set forth, the instantaneous synchronization of remote reference frames in our Universe via non-quantum teleportation has a direct connection with the Shnoll effect.

First, let us understand what is the Shnoll effect in terms of the theory of relativity.

The form of a histogram obtained as a result from a series of measurements of noise (note that the average magnitude of the noise remains the same) shows the fine structure of the countdown of the measured value, according to the structure of the physical coordinates and of the physical time of the observer. It does not matter which type of processes produces the registered noise; only the physical reference frame of the observer is substantial. In other words, the form of the histogram's resulting measurement of noise shows the fine structure of the physical coordinates and of the physical time of the observer. If two histograms' resulting measurements of noise taken at two different time intervals have the same form, then two of these different states of the same system that generates the noise are synchronized to each other. If these two synchronized states appear periodically in the moments of time associated with the same coordinates of a cosmic body on the celestial sphere, the two synchronized states are also synchronized with the cosmic body.

Therefore, we arrive at the following conclusion. In terms of relativity theory, the Shnoll effect means that the reference frame of a terrestrial observer is somehow synchronized with remote cosmic bodies. This synchronization is done at each moment of time with respect to coordinates connected with stars (cycles of the stellar day and the sidereal year), and with respect to the coordinates connected with the Sun (cycles of the solar day and the calendar year). Also, the synchronization condition (the form of the histogram) is repeated in the reversed mode in time at each of two opposite points in the Earth's orbit around the Sun, and at each of two opposite points of the observer's location with respect to stars (due to the daily rotation of the Earth): this is the "palindrome effect", including the half-year and half-day palindromes.

Now the second question arises. How is this synchronization accomplished? Regularly, and according to the initial suggestion of Einstein (which was introduced in the framework of Special Relativity), reference frames are synchronized by light signals. But in the case of experiments where the Schnoll effect was registered, the noise source and the measurement equipment were located in a laboratory building under a massive roof. So the laboratory is surely isolated from light signals and other (low-magnitude) electromagnetic radiations which come from stars... The answer comes from General Relativity.

First, as is known from General Relativity, two remote reference frames can be synchronized through the shortest path (known as geodesic line) connecting them in the space (space-time). A geodesic path can be paved between any two points at every fixed moment of time. If these points oscillate with respect to each other, the synchronized states are repeated with the period of the oscillation. In terms of a regular terrestrial observer, who is located on the surface of the Earth, this means that his reference frame can be synchronized with the reference frame of a celestial object, which is located in the depths of the cosmos, at any moment of time. Each single state (moment of time) of the synchronization has twin states of synchronization. The twin states are repeated due to the daily rotation and to the yearly rotation of the observer (at his location on the Earth's surface) with respect to stars*, with respect to the Sun, and also due to his cyclic motion with respect to the Moon. Thus the respective cycles of repetition of the synchronized twin states of the observer's reference frame (the cycles of appearance of the similar forms of histograms) must exist. The cycles of repetition of the twin states are, with precision, to the nearest minute:

*This refers to the International Celestial Reference System, which is the standard celestial coordinate system centered at the barycentre of the Solar System, with axes that are fixed with respect to objects in far-reaches of the cosmos. These coordinates are approximately the same as the equatorial coordinates on the celestial sphere. The International Celestial Reference System is defined by the measured positions of more than two hundred extragalactic objects (mainly quasars). It is the standard stellar reference system accepted by the International Astronomical Union.

- Solar day (24 hours = 1440 min), the period of daily rotation of the terrestrial observer together with the Earth with respect to the Sun;
- Calendar year (365 days = 525 600 min), the period of orbital revolution of the terrestrial observer together with the Earth around the Sun;
- Sidereal (stellar) day: 23 hours, 56 min = 1436 min. It is the period of daily rotation of the terrestrial observer, together with the Earth with respect to stars;
- Sidereal (stellar) year: 365 days, 6 hours, 9 min = 525 969 min. It is the period of orbital revolution of the terrestrial observer, together with the Earth around the Sun with respect to stars;
- Lunar day (24 hours, 50 min = 1490 min), the period between two observed moonrises. It is longer than a 24-hour solar day, because the Moon revolves around the Earth in the same direction that the Earth rotates around her own axis;
- Sidereal month: 27 days, 7 hours, 43 min = 39 343 min. It is the period of the Moon's revolution around the Earth with respect to stars;
- Period of the lunar evection (31 days, 19 hours, 29 min = 45 809 min), which is the period of the oscillatory deviation of the Moon's orbit from its average position with respect to the Earth.

Also, the cycles of reverse synchronization (appearance of the mirrored forms of histograms, that means the "palindrome effect") shall exist according to the half-periods:

- Half of the solar day (12 hours = 720 min);
- Half of the calendar year (182 days, 12 hours = 262 800 min);
- Half of the stellar day (11 hours, 58 min = 718 min);
- Half of the sidereal year (182 days, 15 hours, 5 min = 262 985 min);
- Half of the lunar day (12 hours, 25 min = 745 min);
- Half of the sidereal month (13 days, 15 hours, 52 min = 19 672 min);
- Half-period of the lunar evection (15 days, 21 hours, 45 min = 22 905 min).

Also there exist a number of other periods of appearance of the synchronized states of the observer's reference frame (appearance of the similar form of histograms), which manifest cyclic synchronization with some other celestial objects. We do not discuss them herein because of brevity of this presentation.

Second. Synchronization is possible not only of light signals or other electromagnetic signals moving at the speed of light. Instant synchronization of remote reference frames is possible in the space-time of General Relativity [14, 17]. This can be done through zero-space — the fully degenerate space-time. It will appear to a regular observer as a point; that is the necessary condition of non-quantum teleportation at any distance in our world. Therefore the "non-quantum teleportation channel" is constantly allowed between any two points of our space. Zero-particles — the particles that are hosted by zero-space — are material carriers in non-quantum teleportation. Zero-particles are standing light waves (i.e. stopped light), thus zero-space is filled with a global system of standing light waves — the world-hologram of non-quantum teleportation channels. According to space topology, there is univalent mapping of zero-space (the world-hologram) onto our regular space (our universe). This means that the local physical reference frame of a terrestrial observer, travelling together with the Earth in the cosmos, "scans" the world-hologram of teleportation channels.

Each point of the Earth's surface, including the observer's location, makes a daily revolution around the Earth's centre. The Earth revolves around the Sun at a speed of 30 km/sec. The Sun revolves, at a speed of 250 km/sec, around the centre of our Galaxy called the Milky Way. As a result, the observer located on the surface of the Earth travels in the Galaxy along the highly elongated double helix (which is like the DNA helix), through the cosmic grid of the "stargates" into the non-quantum teleportation channels which instantly synchronize his local reference frame with stars, the Sun, and other cosmic objects. Because of the cycles of the turbinal motion of the observer, each single stargate has its own twin respectively to the periods of the motion. The states of the observer's reference frame at these twin locations, due to entering into the same teleportation channel, are not only synchronized but also entangled with each other.*

The moments of a terrestrial observer's entering into the gate of the same teleportation channel are the same as the moments of repetition of the twin synchronized states of his local reference frame. Therefore, it is obvious that the appearance of the similar forms of histograms (and the appearance of the mirrored forms of histograms) manifests not only the synchronized (and, respectively, — reverse synchronized) twin states of the observer's reference frame, but also that these states are entangled with each other.

Such a synchronization occurs regardless of whether the observer sees the sky or is isolated in a laboratory building. It is done by zero-particles through zero-space, independently of the obstacles that can be met by electromagnetic signals in our regular space.

Recall, the Shnoll effect is periodic repetition of a similar form (or mirrored forms) of the histograms' resulting measurement of noise. Most of the periods that are expected according to the theory and listed above coincide with the periods registered by Shnoll and his workgroup [1]. These are the solar day (1440 min), the stellar day (1436 min), the calendar year (525 600 min), the stellar year (525 969 min),

*In a sense similar to the quantum entangled states, according to Quantum Mechanics.

the lunar day (1490 min), the lunar month (registered as the "near-27-day period"), and the period of the lunar evection (45 809 min). The mirrored forms of histograms were registered with periods of half of a solar day (720 min), and half of the calendar year (262 800 min), while analysis of the measurements is still under development. Nevertheless, there are enough coincidences of the theory with Shnoll's experimental data.

We therefore conclude that the Shnoll effect manifests the scanning of the world-hologram of the non-quantum teleportation channels along the Earth's path in the cosmos. So, the Shnoll effect has been explained according to General Relativity Theory.

It is important to understand the following: to find entangled moments of time (the "gates" into the same teleportation channel in the cosmos), it does not matter which stable process (which type of processes) produces the random noise that we register. Not only natural processes, but also the processes such as random-number generation by a computer's software will show the Shnoll effect, as well as such social phenomena as fluctuations in the stock exchange market. This means that the theoretical explanation that is given here on the basis of General Relativity provides a theoretical ground for a wide range of fundamental effects in physics, biology, geophysics, social behaviour and other fields of science. This fact leads us to a number of important sequels and applications, which can be achieved from further research studies of the Shnoll effect.

4 Forecasting earthquakes and other cataclysms on the basis of the scanning of the Earth's path in the cosmos

So, we have arrived at a conclusion that the Shnoll effect is a fundamental effect, which is explained according to General Relativity. Therefore, we expect the Shnoll effect to be found not just in noise that the terrestrial observer registers in such processes as biochemical reactions or nuclear decay. The noise of other terrestrial processes which have natural and artificial origin should also show the Shnoll effect. Because practical applications are important, the following important types of noise should be taken into account:

- Random mass migrations of people;
- Fluctuations in the stock exchange market;
- Fluctuations of the sickness rate among the masses of people, animals, and plants;
- Fluctuations of social unrest (local conflicts, etc.)
- Fluctuations of the Earth's crust — earthquakes;
- Fluctuations of weather (weather events and weather cataclysms);
- and many others.

Here within we've touched so far only on the last two items on this list. These are earthquakes and weather.

Our planet Earth is so large that earthquakes can be considered as the noise fluctuations of the Earth's crust, while weather events and weather cataclysms are the noise fluctuations in the atmosphere. Therefore, this is a proper background where the Shnoll effect should be manifested.

Indeed, there is a huge scientific study that shows the statistical behaviour of background earthquakes and weather events [26–32]. The study was done in the 1930–1940's. It was conducted by Nikolai Morozov, Hon. Member of the USSR Academy of Sciences.*

Morozov and his assistants analysed the observational data about the background earthquakes and weather events that were collected at all the world-known weather observatories and seismic stations of the world (located from the equator to the extreme north and south). The observational data were recorded throughout all periods of the systematic scientific observations, during the second half of the 19th century and the first half of the 20th century, which has then been accessed from yearbooks of the observatories and stations.

In addition to the statistical behaviour of the background earthquakes and weather events, Morozov found that air temperature, barometric pressure, humidity and other geophysical parameters depend on the height of the centre of our Galaxy (and other compact star clusters in our Galaxy) above the horizon. In other words, the weather factors depend on the stellar (sidereal) time at the point of observations. As a result, Morozov arrived at the following fundamental conclusion. All previous forecasts of earthquakes and weather cataclysms did not give satisfying results because the forecasters took into account only the influence of the Sun and Moon on the Earth's crust and the atmosphere (which influences were dated according to solar time), while the influence of objects in the farther-reaches of the cosmos, such as the centre of our Galaxy and other (as visible and invisible) compact stellar clusters, which are dated according to the stellar (sidereal) time, were not taken into account.

We can therefore say that Morozov's geophysical studies show that we can surely consider micro-earthquakes as random noise, which always exist in the Earth's crust. The same is true about weather where random noise is nothing but small fluctuations of air temperature, barometric pressure, humidity, etc.

A confirmation of the conclusion follows from Shnoll's experiments. Already by the 1980s, synchronous fluctuations of forms of the histograms (the Shnoll effect) were registered on the basis of seismic observations [33]. This means, according to our theoretical explanation herein, that the twin entangled synchronization states of the local physical reference frame of the terrestrial observer (the Shnoll effect, according to General Relativity) coincide with the seismic noise registered in the Earth's crust.

*This study was not continued after the death of its author, Prof. Morozov, in 1946.

Therefore, proceeding from our theoretical explanation of the Shnoll effect, we can forecast how, where, and when powerful earthquakes will appear in the Earth's crust; how, where, and when weather cataclysms will occur in the atmosphere. Essentially, here's how to go about doing it.

Two things are needed to understand this method. First, we need to understand that every real observer has his own local physical reference frame. The physical reference frame consists of real coordinate grids spanning over the real physical bodies around him (his real reference bodies), and also of the real clocks that are fixed on the real coordinate grids.* In the case of a terrestrial observer (us, for instance), the real coordinate grids and clocks are connected with the physical environment around us. Therefore, noise fluctuations of the environment mean noise fluctuations of the real physical measurement units of the observer.

Second, as follows from the theory of physical observable quantities in General Relativity, if the fine structure of noises in two physical reference frames match with each other, these two reference frames are synchronized with each other. Therefore, as we've shown above, the Shnoll effect manifests the twin/entangled states of the local physical reference frame of the observer. These twin/entangled states are instantly synchronized with each other, along with other cosmic bodies located along the entire synchronization path in the cosmos. If their physical reference frames are synchronized at a very close frequency, a resonance of noise fluctuations occurs. In this case, concerning seismic noise, a powerful earthquake occurs in the background of the noise from micro-earthquakes (that exist continuously and everywhere in the Earth's crust). Concerning the weather, this means that a weather cataclysm occurs in the background of noise fluctuations of the weather.

In other words, if one or more of the powerful cosmic bodies appear on the same path of synchronization with a terrestrial observer, noise fluctuations of these cosmic bodies become synchronized with the background noise of the observer's physical reference frame. A resonance occurs in the physical reference frame of the observer that is the local environment in the point of his observation. The background noise of the environment experiences a huge fluctuation: i.e., a powerful earthquake, a weather cataclysm, etc.

Thank to Morozov's geophysical studies we conclude that the Sun and the Moon are not the main "synchronizers" that cause a significant resonance in the physical reference frame of a terrestrial observer. We must therefore take into account the convergence of several "celestial synchronizers" of the Solar System and our Galaxy in one synchronization path.

Therefore, all that is required for forecasting earthquakes and weather cataclysms, according to our theoretical explanation of the Shnoll effect, is as follows.

1. First step — daily registrations of the basic noise fluctuations in different environments at different locations on the Earth. Analysis of the measurements, according to the histogram techniques that were used by Shnoll, in order to fix the details of the periods as determined by the Shnoll effect. In other words, this is the "scanning" of the local space of the planet in order to create the complex map of the background noise fluctuations of different environments of the Earth, according to solar time and stellar time;
2. Second step — creating a detailed list of the more or less powerful cosmic sources, which can be the main "synchronizers" affecting the physical reference frame of a terrestrial observer. The stellar (sidereal) coordinates of the cosmic sources, and their ephemerides will be needed in the third stage of the forecasting;
3. Third step — determining the moments of time when these celestial synchronizers converge on the same synchronization path, that is, their crossing the celestial meridian (hour circle) at approximately the same moment of time as the point of observation, then comparing these with the moments of time of the noise fluctuations registered due to the Shnoll effect (in the first step). As a result we will find those celestial synchronizers whose synchronization with the terrestrial environment produces the most powerful effect;
4. Fourth step — calculate further convergences of the most powerful synchronizers at every location on the Earth's surface. As a result, by taking into account the delay time of interaction rate in the respective terrestrial environment (the ground, the atmosphere, etc.), we will be able to forecast where and when the resonant states will occur in the Earth's crust (earthquakes) and in the atmosphere (weather cataclysms).

Forecasting the other events of the above list such as random mass migrations of people, fluctuations in the stock exchange market, fluctuations of the sickness rate, fluctuations of social unrest, and others, is possible analogously. The events predicted according to this method may have different periods of delay from the synchronization moment. The delay time depends on inertia in the medium that is being affected: the Earth's crust, atmosphere, interaction in the social medium, etc. Therefore, despite this, the moments of the resonant synchronization are the same for all processes that are registered at the point of observation; the resonant fluctuations will appear at different moments of time in different environments (including the technogenic environments and the social medium). Nevertheless the method of forecasting remains consistent for all the events around us.

So, forecasting powerful earthquakes and weather cataclysms is possible on the basis of our theoretical explanation of the Shnoll effect. Other practical applications of the the-

*See details about physical reference frames, and about physical observable quantities in Zelmanov's publications [3–5], or in our books [14, 15].

ory and experiment are also possible, but they are outside the scope of this short communication.

Acknowledgements

The authors are grateful to Prof. Simon Shnoll and his wife, Prof. Maria Kondrashova, for years of fruitful scientific collaboration and friendly acquaintance. We are also thankful to Prof. Joseph Hafele and Patrick Ivers for a discussion of these issues and useful tips.

Submitted on January 25, 2014 / Accepted on January 27, 2014

References

1. Shnoll S. E. Cosmophysical Factors in Stochastic Processes. American Research Press, Rehoboth (NM, USA), 2012.
2. Shnoll S. E. Changes in the fine structure of stochastic distributions as a consequence of space-time fluctuations. *Progress in Physics*, 2006, v. 2, issue 2, 39–45.
3. Zelmanov A. Chronometric Invariants. Dissertation, 1944. American Research Press, Rehoboth (NM, USA), 2006.
4. Zelmanov A. L. Chronometric invariants and accompanying frames of reference in the General Theory of Relativity. *Soviet Physics Doklady*, 1956, vol. 1, 227–230 (translated from *Doklady Academii Nauk USSR*, 1956, vol. 107, no. 6, 815–818).
5. Zelmanov A. L. On the relativistic theory of an anisotropic inhomogeneous universe. A 1957 Cosmogony Meeting thesis. *The Abraham Zelmanov Journal*, 2008, vol. 1, 33–63.
6. Tangherlini F. R. The velocity of light in uniformly moving frame. A dissertation. Stanford University, 1958. *The Abraham Zelmanov Journal*, 2009, vol. 2, 44–110.
7. Sjödin T. Synchronization in special relativity and related theories. *Nuovo Cimento B*, 1979, v. 51, 229–246.
8. Recami E. Classical tachyons and possible applications. *Rivista del Nuovo Cimento*, 1986, vol. 9, 1–178.
9. Liberati S., Sonego S., and Visser M. Faster-than-*c* signals, special relativity, and causality. *Annals of Physics*, 2002, vol. 298, 151–185.
10. Terletski Ya. P. The causality principle and the second law of thermodynamics. *Soviet Physics Doklady*, 1961, vol. 5, 782–785 (translated from *Doklady Academii Nauk USSR*, 1960, vol. 133, no. 2, 329–332).
11. Bilaniuk O.-M. P., Deshpande V. K., and Sudarshan E. C. G. "Meta" relativity. *American Journal of Physics*, 1962, vol. 30, no. 10, 718–723.
12. Feinberg G. Possibility of faster-than light particles. *Physical Review*, 1967, vol. 159, no. 5, 1089–1105.
13. Malykin G. B. and Malykin E. G. Tangherlini's dissertation and its significance for physics of the 21th century. *The Abraham Zelmanov Journal*, 2009, vol. 2, 121–143.
14. Rabounski D. and Borissova L. Particles Here and beyond the Mirror. Third expanded edition. American Research Press, Rehoboth (NM, USA), 2012. Re-printed in French as: Rabounski D. et Borissova L. Particules de l'Univers et au delà du Miroir. Traduit de l'anglais par Patrick Marquet, American Research Press, Rehoboth (NM, USA), 2012.
15. Borissova L. and Rabounski D. Fields, Vacuum, and the Mirror Universe. Svenska fysikarkivet, Stockholm, 2009. Re-printed in French as: Borissova L. et Rabounski D. Champs, Vide, et Univers miroir. Traduit de l'anglais par Patrick Marquet, American Research Press, Rehoboth (NM, USA), 2010.
16. Rabounski D. A blind pilot: who is a super-luminal observer? *Progress in Physics*, 2008, v. 4, issue 2, 171.
17. Borissova L. and Rabounski D. On the possibility of instant displacements in the space-time of General Relativity. *Progress in Physics*, 2005, v. 1, issue 1, 17–19.
18. Hau L. V. Frozen light. *Scientific American*, 17 July 2001, v. 285, no. 1, 52–59.
19. Hau L. V. Frozen light. *Scientific American Special Edition* "*The Edge of Physics*", 31 May 2003, 44–51.
20. Rabounski D. and Borissova L. A theory of frozen light according to General Relativity. A presentation delivered at the *2011 APS March Meeting*, held in March 21–25, 2011, in Dallas, Texas.
21. Rabounski D. and Borissova L. A theory of frozen light according to General Relativity. *The Abraham Zelmanov Journal*, 2011, v. 4, 3–27.
22. Bennett C. H., Brassard G., Crepeau C., Jozsa R., Peres A., and Wootters W. K. Teleporting an unknown quantum state via dual classical and Einstein-Podolsky-Rosen channels. *Physical Review Letters*, 1993, v. 70, 1895–1899.
23. Boschi D., Branca S., De Martini F., Hardy L., and Popescu S. Experimental realization of teleporting an unknown pure quantum state via dual classical and Einstein-Podolsky-Rosen Channels. *Physical Review Letters*, 1998, v. 80, 1121–1125.
24. Riebe M., Häffner H., Roos C. F., Hänsel W., Benhelm J., Lancaster G. P. T., Korber T. W., Becher C., Schmidt-Kaler F., James D. F. V., and Blatt R. Deterministic quantum teleportation with atoms. *Nature*, 2004, v. 429, 734–736.
25. Barrett M. D., Chiaverini J., Schaetz T., Britton J., Itano W. M., Jost J. D., Knill E., Langer C., Leibfried D., Ozeri R., and Wineland D. J. Deterministic quantum teleportation of atomic qubits. *Nature*, 2004, v. 429, 737–739.
26. Morozov N. A. On the possibility of a scientific prognosis of weather. *Bulletin de l'Académie des Sciences de l'URSS*, Série géographique et géophisique, 1944, tome VIII, no. 2–3, 63–71.
27. Morozov N. A. Influence of the central body of the galaxy and its other dark super-suns on the geophysical and meteorological phenomena that appear around us. *Archive of Russian Academy of Sciences*, fund 543 (personal fund of N. A. Morozov, Hon. Member of the USSR Academy of Sciences), folder 01, file 72 (188 pages).
28. Morozov N. A. On the cosmic factors affecting the frequency of earthquakes. *Ibidem*, file 96 (461 pages).
29. Morozov N. A. On the celestial influences on the frequency of earthquakes. *Ibidem*, file 98 (297 pages).
30. Morozov N. A. On the influence of the cosmic effects on the frequency of earthquakes. *Ibidem*, file 99 (110 pages).
31. Morozov N. A. Earthquakes: the cosmic studies. *Ibidem*, file 100 (282 pages).
32. Morozov N. A. Basics of Theoretical Meteorology and Geophysics. Manuscript of the book. *Ibidem*, files 128–139.
33. Shnoll S. E. Private communications with the authors.

On the Origin of Elementary Particle Masses

Johan Hansson

Department of Physics, LuleåUniversity of Technology, SE-971 87 Luleå, Sweden.

The oldest enigma in fundamental particle physics is: Where do the observed masses of elementary particles come from? Inspired by observation of the empirical particle mass spectrum we propose that the masses of elementary particles arise solely due to the self-interaction of the fields associated with a particle. We thus assume that the mass is proportional to the strength of the interaction of the field with itself. A simple application of this idea to the fermions is seen to yield a mass for the neutrino in line with constraints from direct experimental upper limits and correct order of magnitude predictions of mass separations between neutrinos, charged leptons and quarks. The neutrino interacts only through the weak force, hence becomes light. The electron interacts also via electromagnetism and accordingly becomes heavier. The quarks also have strong interactions and become heavy. The photon is the only fundamental particle to remain massless, as it is chargeless. Gluons gain mass comparable to quarks, or slightly larger due to a somewhat larger color charge. Including particles outside the standard model proper, gravitons are not exactly massless, but very light due to their very weak self-interaction. Some immediate and physically interesting consequences arise: i) Gluons have an effective range $\sim$1 fm, physically explaining why QCD has finite reach; ii) Gravity has an effective range $\sim$100 Mpc coinciding with the largest known structures, the cosmic voids; iii) Gravitational waves undergo dispersion even in vacuum, and have all five polarizations (not just the two of $m = 0$), which might explain why they have not yet been detected.

The standard model of particle physics [1–4] is presently our most fundamental *tested* [5] description of nature. Within the standard model there are some 18 parameters (several more if neutrinos are non-massless) which cannot be predicted but must be supplied by experimental data in a global best-fit fashion. There are coupling constants, mixing parameters, and, above all, values for the different fundamental particle masses. The theory is silent on where and how these parameters arise, and even more speculative theories, such as string theory, have so far not been able to predict (postdict) their values. Even if the Higgs particle is confirmed, and the Higgs mechanism [6] is validated in one form or another, it still does not explain "the origin of mass" as often erroneously stated. Unknown/incalculable parameters for particle masses are in the Higgs model replaced by equally unknown/incalculable coupling constants to the Higgs field; the higher the coupling, the larger the mass, while no coupling to the Higgs field gives massless particles like the photon and gluons. So nothing is gained in the *fundamental* understanding of masses. Fifteen of the free parameters in the standard model are due to the Higgs. Thirteen of them are in the fermion sector, and the Higgs interactions with the fermions are not gauge invariant so their strengths are arbitrary. So to make progress we must understand masses.

There is no hope of predicting elementary masses from renormalized quantum field theory as the very process of renormalization itself forever hides any physical mass-generating mechanism; the renormalized masses are taken as the experimentally measured values, *i.e.* any possible physical connection for predicting particle masses is lost. But surely, nature herself is not singular, the infinities appearing in quantum field theory instead arising from the less-than-perfect formulation of the theory. If a truly non-perturbative description of nature would be found it might be possible to calculate particle masses from first principles, but we still seem far from such a description.

In this article we will instead take a more phenomenological approach, but still be able to deduce a number of physical results and some interesting consequences.

From standard (perturbative) quantum field theory, the lowest order contribution to the self-mass is [7] (see Fig. 1)

$$\Delta m = \alpha \int \bar{u}\,\gamma_\mu K(1,2)\gamma^\mu\, u\, e^{ipx_{12}}\,\delta(s_{12}^2)\,\mathrm{d}^4x, \qquad (1)$$

where the loop integral is logarithmically UV divergent $\propto log(\frac{1}{r})$ as the cut-off radius $r \to 0$.* So (in perturbation theory) the contribution is divergent but as all gauge fields diverge in the same way, the *quotients* are finite. (Another way would be to assume that there exists a "shortest length" in nature that would serve as a natural cut-off and give finite integrals.) As an aside, as all expressions are relativistically invariant the usual relativistic factor $\gamma = 1/\sqrt{1 - v^2/c^2}$ is automatic if $v \neq 0$, *i.e.* if we are not in the rest frame of the particle.

*Also for a classical electron of radius r, $\Delta m = C\alpha \propto \alpha$, but there the coefficient is linearly divergent $C \propto 1/r$. Additionally, the classical result is exact, *i.e.* non-perturbative.

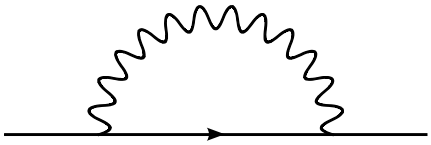

Fig. 1: Feynman diagram for self-mass contribution from a gauge field (squiggly line). Each vertex contributes one charge factor $\sqrt{\alpha} \propto q$.

We will thus imagine the following pragmatic scenario: a quantum field without any charges corresponds to a massless particle; when charges, q, are attached the mass is $m \propto q^2 \propto \alpha$, where α is the relevant coupling constant. This significantly reduces the number of *ad hoc* parameters. Also, the lagrangian can still be completely massless (as in the Higgs scenario), preserving attractive features such as gauge invariance that would be broken by explicit mass terms, the generation of mass being a secondary *physical* phenomenon.

So we get

$$m(electron) \propto \alpha_{QED} \tag{2}$$

$$m(quark) \propto \alpha_{QCD} \tag{3}$$

$$m(neutrino) \propto \alpha_{QFD} \tag{4}$$

where the dominating coupling constant is α_{QED} for quantum electrodynamics, α_{QCD} for quantum chromodynamics (strong interactions) and α_{QFD} for quantum flavordynamics (weak interactions).

If we now assume that all gauge fields give a contribution of roughly the same order of magnitude, so that the proportionality factors cancel up to a constant of order unity (coming from the different gauge groups), we get results for the quotients of elementary masses without having to know the exact (non-perturbative) contribution. Using the observed mass for the electron, and $\alpha_{QED} \sim 137^{-1}$, $\alpha_{QCD} \sim 1$, we get

$$m(quark) \simeq 50\,\mathrm{MeV}, \tag{5}$$

(although physical quark masses are notoriously hard to define [8]) and pretending as if we knew nothing of the electroweak theory (in order not to get entangled with the Higgs mechanism again), using the old Fermi theory for weak interactions (or quantum flavordynamics, QFD) as appropriate for the low energies where observations of physical masses are actually made, using the *physical* coupling derived from typical scattering cross sections or decay rates ($\tau^{-1} \propto \alpha^2$) , we get, using $\tau^{-1}_{QFD} \sim 10^6\mathrm{s}^{-1}$ (*e.g.* $\mu \to e\nu_\mu\bar{\nu}_e$) and $\tau^{-1}_{QED} \sim 10^{16}\mathrm{s}^{-1}$ (*e.g.* $\pi^0 \to \gamma\gamma$),

$$m(neutrino) \simeq 0.5 \times 10^{-5}\mathrm{MeV} \simeq 5\,\mathrm{eV}. \tag{6}$$

This is a *prediction* resulting from our simple assumption, compatible with upper limits from direct experiments, whereas in the Higgs model *no* predictions of masses are possible (being connected to free parameters).

We see that we immediately get the right hierarchy of masses, with the right magnitudes, which is encouraging considering the approximations made.

A clear indication of the relative effect of QED compared to QCD is seen in the case of pions: π^+ and π^- both have mass 139.6 MeV, while the neutral pion π^0 has a mass of 135 MeV. The small difference $\Delta m = 4.6$ MeV, attributable to QED, predicts a charge radius ∼1 fm, consistent with scattering experiments using pions.

One issue still remaining is why not $m(Z) \sim m(neutrino)$ or $m(W) \sim m(electron)$. We take it as a sign that the intermediate vector bosons W and Z really are not fundamental, but instead are composite [9, 10].

If we, disregarding renormalization issues, also include the graviton as the force carrier of gravity (which is expected to hold for weak gravitational fields) we see that QCD, QFD and gravity all should disappear exponentially at sufficiently large distances due to the non-zero physical masses of their force carrier particles, only electromagnetism (QED) having truly infinite reach as the physical mass of the photon is equal to zero, as the photon carries no charge. The range can be estimated by the Yukawa theory potential $e^{-\lambda mc/\hbar}/r$, giving $\lambda_{cutoff} \simeq \hbar/mc$. This gives for the gluon with bare mass zero (in the lagrangian), but physical mass $m(gluon) \neq 0$, the value $\lambda_{cutoff}(QCD) \simeq 0.3$ fm, which explains why QCD is only active within nuclei, although the bare mass $m = 0$ naively would give infinite reach as its coupling to the Higgs is zero. Despite what many thinks, this problem has not been solved [11].

For gravity, the same calculation leads to $\lambda_{cutoff}(gravity) \simeq 3 \times 10^8$ light-years, or 100 Mpc, which happens to coincide with the largest known structures in the universe, the cosmic voids [12]. The corresponding graviton mass is

$$m(graviton) \simeq 5 \times 10^{-32}\,\mathrm{eV}, \tag{7}$$

well in line with the experimental upper limits [13]. Another thing to keep in mind is that if/when gravity decouples, it will appear as if the universe accelerates when going from the coupled (decelerating) to the uncoupled (coasting) regime where distance $\geq \lambda_{cutoff}(gravity)$, perhaps making dark energy superfluous as explanation for cosmic "acceleration" [14, 15]. If masses really originate in this way it might be possible to include other interactions but the gravitational in an "equivalence principle", hence perhaps opening the door to a unified description of all interactions.

The relation $m(graviton) \neq 0$ has other peculiar effects: gravitational waves of different wavelengths (energies) would travel at different velocities, smearing them out, the longer the wavelength, the larger the effect. Also, not being strictly massless, gravitons (spin s=2) should have $2s + 1 = 5$ polarization states instead of the two conventionally assumed helicity states if massless. This might be why gravitational waves hitherto have escaped detection, as it would scramble their signature.

If we, just for the moment, tentatively reintroduce the perturbative running of coupling "constants" (renormalization group) we obtain $m(graviton) \to \infty$ as $r \to 0$ implying that (quantum) gravity gets a dynamical cutoff for small separations, as an increasingly more massive quantum is harder to exchange, effectively making the interaction of gravity disappear in that limit, perhaps showing a way out of the ultraviolet divergencies of quantum gravity in a way reminiscent of how massive vector bosons cured the Fermi theory.

We have not addressed the known replication of particles into three generations of seemingly identical, but more massive, variants, the most exactly studied from an experimental standpoint being the three charged leptons, *i.e.* (e, μ, τ), the electron and its heavier "cousins" the muon and tauon.*

A straightforward way would be to introduce some "generation charge" or quantum number, make *e.g.* a power-law ansatz and fit to the observed values of the charged leptons and deduce the masses of neutrinos and quarks in the higher generations. That would, however, not bring us any closer to a true understanding.

A more promising way could be to assume that the stable elementary particles of the first generation are exact soliton solutions to the relevant quantum field theory, or its dual [16], whereas unstable higher generation elementary particles would be solitary wave (particle-like, but not stable) solutions to the said quantum field theory. Unfortunately, there are no known exact 3+1 dimensional soliton solutions to quantum field theories, with non-trivial soliton scattering [16]. Another avenue would be to explore if Thom's "catastrophe theory" [17] (or other more general theories of bifurcation) applied to particle physics could spontaneously reproduce multiple generations, as it is known to include stable/unstable multiple solutions. Thom's theory states that all possible sudden jumps between the simplest attractors – points – are determined by the elementary catstrophes, and the equilibrium states of any dynamical system can in principle be described as attractors. As one attractor gives way for another the stability of the system may be preserved, but often it is not. It could be capable to generate masses spontaneously in a different and novel way compared to the Higgs mechanism. The different charges, *i.e.* coupling constants, could define the control surface, whereas the actual physical mass would define the behavior surface. Sudden bifurcations could signify decay of previously stable elementary particles.

To summarize, our simple and physically compelling assumption that particle masses are solely due to self-interactions: i) Directly and simply gives the correct mass hierarchy between neutrinos, electrons and quarks. ii) Reduces the number of *ad hoc* parameters in the standard model. iii) Qualitatively explains why the photon is the only massless fundamental particle, why QCD has short range, and why neutrinos are not strictly massless. iv) Gives testable predictions, *e.g.* regarding gravitons (gravitational waves).

*Are there additional generations? Data on the decay width of the Z indicate that there at least cannot be any additional light neutrinos. A fourth neutrino would have to be very massive $> m_Z/2 \simeq 45$ GeV. One might well ask if the generation structure is a true aspect of nature, or just a result of our incomplete understanding of the weak interaction [10].

Submitted on January 22, 2014 / Accepted on January 23, 2014

References

1. Glashow S. L. *Nucl. Phys.*, 1961, v. 22, 579.
2. Weinberg S. *Phys. Rev. Lett.*, 1967, v. 19, 1264.
3. Salam A. in Svartholm N., ed. Elementary Particle Physics: Relativistic Groups and Analyticity, Eight Nobel Symposium. Almqvist and Wiksell, 1968, p. 367.
4. Fritzsch H., Gell-Mann M., Leutwyler H. *Phys. Lett. B*, 1973, v. 47, 365.
5. Cahn R. N., Goldhaber G. The Experimental Foundations of Particle Physics, 2nd ed. Cambridge University Press, Cambridge, 2009.
6. Higgs P. *Phys. Rev. Lett.*, 1964, v. 13, 508.
7. Feynman R. P. *Phys. Rev.*, 1949, v. 76, 769.
8. Hansson J. *Can. J. Phys.*, 2002, v. 80, 1093. arXiv: hep-ph/0208137.
9. D'Souza I. A., Kalman C. S. Preons. World Scientific, Singapore, 1992.
10. Dugne J.-J., Fredriksson S., Hansson J. *Europhys. Lett.*, 2002, v. 60, 188. arXiv: hep-ph/0208135.
11. Clay Mathematics Institute Millennium Prize Problem: Yang-Mills, http://www.claymath.org/millennium/Yang-Mills-Theory/.
12. Lindner U. et al. *Astron. Astrophys.*, 1995, v. 301, 329.
13. Goldhaber A. S., Nieto M. M. *Rev. Mod. Phys.*, 2010, v. 82, 939.
14. Riess A. et al. *Astr. J.*, 1998, v. 116, 1009.
15. Perlmutter S. et al. *Ap. J.*, 1999, v. 517, 565.
16. Manton N.S. *Nonlinearity*, 2008, v. 21, T221.
17. Thom R. Stabilité Structurelle et Morphogenèse: Essai d'une Théorie Générale des Modèles. Benjamin, 1972. English trans. by Fowler D. H. Structural Stability and Morphogenesis: An Outline of a Theory of Models. Benjamin, 1975.

Extended Analysis of the Casimir Force

Bo Lehnert

Alfvén Laboratory, Royal Institute of Technology, SE-10044 Stockholm, Sweden. E-mail: Bo.Lehnert@ee.kth.se

There are several arguments for the conventional form of the Zero Point Energy frequency spectrum to be put in doubt. It has thus to be revised into that of a self-consistent system in statistical equilibrium where the total energy density and the equivalent pressure become finite. An extended form of the Casimir force is thereby proposed to be used as a tool for determining the local magnitude of the same pressure. This can be done in terms of measurements on the force between a pair polished plane plates consisting of different metals, the plates having very small or zero air gaps. This corresponds to the largest possible Casimir force. Even then, there may arise problems with other adhering forces, possibly to be clarified in further experiments.

1 Introduction

The vacuum is not merely an empty space. Due to quantum theory, there is a non-zero level of the ground state, the Zero Point Energy (ZPE) as described by Schiff [1] among others. An example of the related spectrum of vacuum fluctuations was given by Casimir [2], who predicted that two metal plates will attract each other when being separated by a sufficiently small air gap. This prediction was first confirmed experimentally by Lamoreaux [3].

In a number of investigations the author has called attention to the importance of ZPE in connection with fundamental physics, on both the microscopic and the macroscopic scales. This applies to revised quantum electrodynamics and its relation to massive elementary particle models [4–6], as well as to attempts of explaining the concepts of dark energy and dark matter of the expanding universe [7, 8].

This paper presents an extended analysis of the ZPE frequency spectrum and its effect on the Casimir force, thereby leading to proposed experimental investigations on the features of the same spectrum.

2 Frequency spectrum of the Zero Point Energy

The local Zero Point Energy density has to become derivable from the frequency spectrum of an ensemble of ZPE photons. Such a procedure has to be conducted in the same standard way as for statistical systems in general, as described by Terletskii [9] and Kennard [10] among others.

For a "gas" of ZPE photons the number of field oscillations per unit volume in the range $(\nu, \nu + \mathrm{d}\nu)$ becomes

$$\mathrm{d}n = \frac{8\pi}{c^3}\,\nu^2\,\mathrm{d}\nu. \tag{1}$$

This number can also be conceived to represent the various "rooms" to be populated by the photon frequency distribution.

In finding the corresponding self-consistent and fully determined contribution to the ZPE energy density, two points have to be taken into account:

- The quantized energy of every single photon is $E_0 = \frac{1}{2}h\nu$.
- The photon population of the frequency states has to be adapted to a statistical equilibrium, under the constraint of a finite and given total energy density. The latter corresponds to an average energy $\bar{E}_0 = \frac{1}{2}h\bar{\nu}$ per photon with a related average frequency $\bar{\nu}$.

Due to these points, the contribution to the energy density within the range $(\nu, \nu + \mathrm{d}\nu)$ becomes [7, 8]

$$\mathrm{d}u = \frac{4\pi h}{c^3}\,\nu^3 \exp\left(-\frac{\nu}{\bar{\nu}}\right). \tag{2}$$

Here the Boltzmann factor

$$P_B = \exp\left(-\frac{E_0}{\bar{E}_0}\right) = \exp\left(-\frac{\nu}{\bar{\nu}}\right) \tag{3}$$

is due to the probability of the various photon states in statistical equilibrium.

In the present isotropic state, the contribution to the pressure becomes $\mathrm{d}p = \mathrm{d}u/3$. The local ZPE pressure then has the total integrated value

$$p_0 = \frac{8\pi h\bar{\nu}^4}{c^3} \tag{4}$$

as obtained from relation (2).

In the earlier conventional analysis, the factor (3) has been missing, thus resulting in an infinite total ZPE energy density and pressure. Several investigators, such as Riess and Turner [11] as well as Heitler [12], have thrown doubt upon such an outcome. Attempts to circumambulate this irrelevant result by introducing cutoff frequencies either at the Planck length or at an arbitrary energy of 100 GeV, are hardly acceptable. This omission does not only debouch into a physically unacceptable result, but also represents an *undetermined* and not self-consistent statistical system [7, 8].

3 Experimental possibilities

The average frequency $\bar{\nu}$ appearing in the factor (3) is an important but so far not determined basic parameter. It may have a characteristic value in the environment of the Earth, or even of our galaxy. It should therefore be investigated if this para-

meter can be determined from experiments. This would require earlier experiments on the Casimir force to be extended. Two options are here proposed for such investigations, all using polished plane metal plates:

- Air gaps of a smaller width than those in earlier experiments, but being larger than the electromagnetic skin depth of the plates, would extend the measurable range. Thereby the insertion of insulating material of very small thickness may be tested.
- The largest possible Casimir force is expected to occur at a vanishing air gap. In this case the skin depth of the plates acts as an equivalent air gap. Even at this maximum Casimir force, other surface and sticking mechanisms such as by Van der Waals' forces may interfere with the measurements. To eliminate at least part of these difficulties, any magnetic alloy should be avoided as plate material in the first place. Further, as pointed out by N. Abramson [13] and G. Brodin [14], plates of different materials should be chosen to avoid microscopic matching of the metal structures. Possible choices of plate material are Ag, Cu, Au, Al, Mg, Mo, W, Zn, Ni, Cd, Sb, and Bi in order of decreasing electric conductivity.

As a device for measurement of the Casimir force, a weighting machine with two horizontal plates is proposed, in which the weight of the upper plate is outbalanced and a vertical Casimir force can be recorded.

4 The Casimir force

The Casimir force arises from the difference in pressure on the out- and insides of the metal plates. Whereas the full ZPE pressure acts at their outsides, there is a reduced pressure acting on their insides, due to the boundary condition which sorts out all frequencies below a limit $\hat{\nu}$. The latter corresponds to wavelengths larger than $\hat{\lambda} = c/\hat{\nu}$, as being further specified for the two options defined in Sec. 3. The net Casimir pressure thus becomes

$$\hat{p} = \int_0^\infty \mathrm{d}p - \int_{\hat{\nu}}^\infty \mathrm{d}p = \frac{4\pi h}{3c^3} \int_0^{\hat{\nu}} \nu^3 \exp\left(-\frac{\nu}{\bar{\nu}}\right) \mathrm{d}\nu \qquad (5)$$

due to the distribution (2). With $x = \nu/\bar{\nu}$ and $\hat{x} = \hat{\nu}/\bar{\nu}$ expression (5) obtains the form

$$\hat{p} = p_0 \, \Pi(\hat{x}) \qquad (6)$$

where p_0 is given by (4) and

$$\Pi = \int_0^{\hat{x}} x^3 \exp(-x) \, \mathrm{d}x = \\ = 1 - \left(1 + \hat{x} + \frac{1}{2}\hat{x}^2 + \frac{1}{6}\hat{x}^3\right) \exp(-\hat{x}) \, . \qquad (7)$$

4.1 Plates with an air gap

The first option concerns an air gap of the width a, being substantially larger than the skin depth of the plates at relevant frequencies. Then the frequencies smaller than $\hat{\nu} = c/2a$ and wavelengths larger than $\hat{\lambda} = 2a$ are excluded. In the limit of $\hat{x} \ll 1$, Π then approaches the value $\hat{x}^4/24$, and the net pressure becomes

$$\hat{p} \cong \frac{\pi h c}{48 a^4} \qquad (8)$$

being proportional to $1/a^4$ as earlier shown by Casimir [2].

For arbitrary values of $\hat{x} = c/2a\bar{\nu}$, the Casimir pressure (6) can then for various gap widths be studied as a function of $\bar{\nu}$. The set of obtained values of $\hat{p}$ then leads to information about the average frequency $\bar{\nu}$, within the limits of application of this option.

4.2 Plates with zero air gap

With the second option of a vanishing air gap, the sum of the skin depths at each plate plays the rôle of a total air gap. Using two plates of different metals having the electric conductivities σ_1 and σ_2, their skin depths at the frequency ν become [15]

$$(\delta_1, \delta_2) = \frac{1}{\sqrt{\pi \mu_0 \nu}} \left(\frac{1}{\sqrt{\sigma_1}} \, , \frac{1}{\sqrt{\sigma_2}} \right). \qquad (9)$$

The total skin depth can then be written as

$$\delta_1 + \delta_2 = \frac{2}{\sqrt{\pi \mu_0 \nu}} \frac{1}{\sqrt{\sigma_{12}}} \qquad (10)$$

where

$$\sigma_{12} = \frac{4 \, \sigma_1 \sigma_2}{\sigma_1 + \sigma_2 + 2\sqrt{\sigma_1 \sigma_2}}. \qquad (11)$$

In the limiting case where half a wavelength $\lambda/2 = c/2\nu$ is equal to the total skin depth (10), the corresponding frequency limit becomes

$$\hat{\nu} = \frac{\mu_0 \pi c^2 \sigma_{12}}{16} \, . \qquad (12)$$

Since λ varies as $1/\nu$ and $\delta_1 + \delta_2$ as $1/\sqrt{\nu}$, it is seen that all frequencies ν less than $\hat{\nu}$ are excluded by the boundary condition. Thus $\hat{\nu}$ represents the Casimir frequency limit, as in the analogous case of a nonzero air gap.

With p_0 given by (4), $\hat{p}$ and Π by (6) and (7), $\hat{\nu}$ by (12), and $\hat{x} = \hat{\nu}/\bar{\nu}$, the Casimir pressure $\hat{p}$ is obtained as a function of the average frequency $\bar{\nu}$ for a given effective conductivity (11) of a pair of plates. Examples are given by (Ag/Cu, Ni/Cd, Sb/Bi) for which $\sigma_{12} = (60.5, 14.1, 1.26) \times 10^6$ A/Vm and $\hat{\nu} = (134, 31.2, 2.79) \times 10^{16}$ s^{-1} and $\hat{\lambda} = (2.23, 9.60, 107) \times 10^{-10}$ m, respectively. The dependence of $\hat{p}$ on $\bar{\nu}$ for the three examples of metal plate combinations are demonstrated in Fig. 1. The left-hand part of the figure relates to large values of $\hat{x}$ for which $\hat{p}$ nearly includes the full pressure (4), and

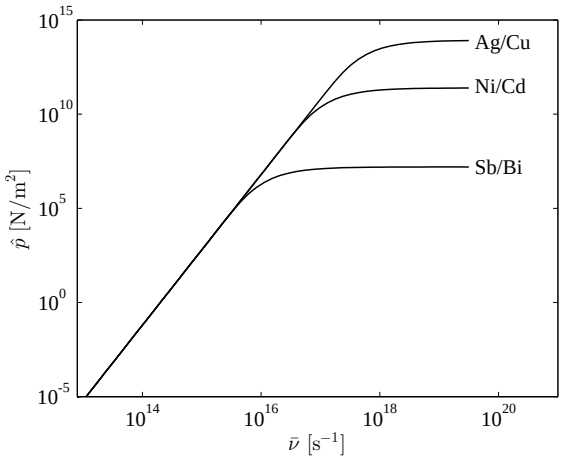

Fig. 1: Casimir pressure $\hat{p}$ as a function of the ZPE average frequency $\bar{\nu}$ for the three metal plate combinations Ag/Cu, Ni/Cd, and Sb/Bi.

for which there is a vanishing difference between the various plate combinations. The right-hand part of the same figure corresponds on the other hand to small $\hat{x}$ for which there is a difference due to the various values of resistivity and $\hat{\nu}$. This part leads to a pressure $\hat{p}$ having the asymptotic limit $(\pi h/3c^3)\,\hat{\nu}^4$ at large $\bar{\nu}$. To extend the range of resistivity dependent Casimir pressures in respect to $\bar{\nu}$, plates with even lower values of σ_{12} would have to be used. Provided that the Casimir force is the dominant one, the measured pressure $\hat{p}$ should thus be related to the same value of the average frequency $\bar{\nu}$, then being independent of the choice of metal combinations. This would, in its turn, lead to an identification of $\bar{\nu}$.

5 Conclusions

There are strong arguments for the frequency spectrum of the Zero Point Energy to be determined by means of a self-consistent system of statistical equilibrium in which there is a finite total pressure and a related finite average frequency. To investigate this state, an extended experimental analysis is proposed, based on the largest possible Casimir force which occurs on a pair of metal plates separated by a very small or even vanishing air gap. Provided that these forces become much stronger than those due to other possible adhering mechanisms, the proposed measurements may give an estimate of the average frequency defined in Section 2.

Submitted on January 30, 2014 / Accepted on February 7, 2014

References

1. Schiff L. I. Quantum Mechanics. McGraw-Hill Book Comp. Inc., New York-Toronto-London, 1949, Ch. IV, Sec. 13.
2. Casimir H. B. G. On the attraction between two perfectly conducting plates. *Proc. K. Ned. Akad. Wet.*, 1948, v. 51, 793–795.
3. Lamoreaux S. K. Demonstration of the Casimir force in the 0.6 to 6 μm Range. *Phys. Rev. Lett.*, 1997, v. 78, 5–8.
4. Lehnert B. Revised Quantum Electrodynamics. In Dvoeglazov V. V. (ed), Contemporary Fundamental Physics. Nova Science Publishers, Inc., New York, 2013.
5. Lehnert B. Potentialities of revised quantum electrodynamics. *Progress in Physics*, 2013, v. 4, 48–52.
6. Lehnert B. Mass-radius relations of Z and Higgs-like bosons. *Progress in Physics*, 2013, v. 10, 5–7.
7. Lehnert B. On dark energy and dark matter of the expanding universe. *Progress in Physics*, 2009, v. 2, 77–82.
8. Lehnert B. Dark energy and dark matter as due to zero point energy. *Journal of Plasma Physics*, 2013, v. 79, 324–334.
9. Terletskii Ya. P. Statistical Physics. North-Holland, Amsterdam and London, 1971, Ch. VI.
10. Kennard E. H. Kinetic Theory of Gases. McGraw-Hill Book Comp., Inc., First edition, New York and London, 1938, Sec. 226.
11. Riess A. G. and Turner M. S. From slowdown to speed-up. *Scientific American*, February 2004, 50–55.
12. Heitler W. The Quantum Theory of Radiation. Oxford: Clarendon Press, 1954, pp. 57 and 326.
13. Abramson N. Private communication 2012.
14. Brodin G. Private communication 2012.
15. Stratton J.A. Electromagnetic Theory. McGraw-Hill Book Comp., Inc., New York and London, 1941, p. 504.

Proton-Electron Mass Ratio: A Geometric Inference

Paulo R. Silva

Departamento de Física (Retired Associate Professor), Universidade Federal de Minas Gerais, Brazil
E-mail: prsilvafis@gmail.com

In this paper we propose that the inertial masses of the proton and of the electron can be associated to volumes of the unit cells of hyper-cubic lattices constructed in the momentum space. The sizes of the edges of these cells are given by the Planck's momentum in the case of the electron, and by a modified Planck's momentum in the case of the proton. We introduce a "conservation of information principle" in order to obtain the wave function which leads to this modified momentum. This modification is attributed to the curvature of the space-time, and in doing this, the concept of the entropy of a black hole has been considered. The obtained proton-electron mass ratio reproduces various results of the literature, and compares well with the experimental findings.

1 Introduction

The volumes of certain associated symmetric spaces have been used as a means to estimate the proton-electron mass ratio, besides the ratios among leptons and mesons masses [1–7]. Some of these papers [1–4] claim to present more consistent physical interpretations of the particles mass ratio, obtained through these geometric approaches. As was pointed out by González-Martin, Smilga [1,4] obtained a volume factor from the decomposition of $SO(3,3)$ with respect to the product group $SO(3,1) \times SO(2)$. He calculated this volume factor that when compared with the volume factor of the electron furnishes a proton-electron mass ratio very close to known experimental result. The same evaluation was done earlier by Wyler [7].

In this work we intend to pursue further on this subject, by associating the masses of the proton and of the electron to the volumes of unit cells in the momentum space, with each unit cell having its appropriate size. For appropriate size we mean that, the unit cell edge associated to the electron mass is given by a characteristic momentum of the Planck's scale. On the other hand the unit cell related to the proton mass is also evaluated with the aid of a Planck's scale momentum, but modified by the curvature of the space-time. The reason to establish such differences is that the electron is usually described through Quantum Electrodynamics (QED) [8], an abelian field theory. Meanwhile the proton is described by Quantum Chromodynamics (QCD) [9], a non-abelian field theory, and we propose that this feature introduces a curvature in space-time modifying the size of the cell of the momentum space.

2 A conjecture about the conservation of the information

If we consider a black hole of radius r, its entropy is given by the well known Bekenstein-Hawking [10–12] formula

$$S = \frac{A}{4} = \frac{\pi r^2}{L_{Pl}^2}, \tag{1}$$

where L_{Pl} is Planck's length.

Let us write a "law of the conservation of the information" in the form

$$S + I = C. \tag{2}$$

In (2), C is a constant. Now we propose to associate the quantity of information, I, to the logarithm of a density of probability Ψ^2, where Ψ is a wave function associated to this curved space-time. We have

$$\frac{\pi r^2}{L_{Pl}^2} + \ln(\Psi^2) = C. \tag{3}$$

Equation (3) leads to

$$\Psi = \Psi_0 \exp\left(-\frac{\pi r^2}{L_{Pl}^2}\right). \tag{4}$$

In order to better examine the content of Ψ it is convenient to interpret it as a ground-state wave function of a kind of one-dimensional harmonic oscillator. Inserting this function and its second derivative in a Schrödinger equation for a particle of mass M, we have

$$-\frac{\hbar^2}{2M}\left(\frac{\pi^2 r^2}{L_{Pl}^4}\right)\Psi + \frac{\hbar^2}{2M}\left(\frac{\pi}{L_{Pl}^2}\right)\Psi + V\Psi = \epsilon_0\Psi. \tag{5}$$

Making the identification of the "r-squared" and the "independent of r" terms, we have

$$\frac{1}{2}\frac{\hbar^2\pi^2}{ML_{Pl}^4} r^2 = \frac{1}{2} kr^2 = V(r) \tag{6}$$

and

$$\frac{\hbar^2\pi}{2ML_{Pl}^2} = \epsilon_0 = \frac{1}{2}\hbar\omega. \tag{7}$$

By taking

$$L_{Pl} = \frac{\hbar}{M_{Pl}} \quad \text{and} \quad M \equiv M_{Pl}, \tag{8}$$

we get

$$\hbar\omega = \pi M_{Pl}\, c^2 = <p> c \tag{9}$$

with

$$<p> = \pi M_{Pl}\, c. \tag{10}$$

We interpret (10) as the size of the unit cell in the curved momentum space. Equation (9) can be seen as the difference in energy levels in the curved space, namely $\hbar\omega$ being related to the emission (absorption) of a boson of momentum $<p>$.

3 Estimate of the proton-electron mass ratio

As was pointed out by Wesson [13], Einstein's Equivalence Principle (EEP) may be a direct consequence of an extra dimension. Yet according to Wesson, a null path in five space-time dimensions (5-D) can describe a massive particle which usually lives in four dimensions. This null path conditions in 5-D can encompass both the gravitational mass of this particle (related to its Schwarzschild radius) as well its inertial mass (related to its Compton length).

Partially inspired in Wesson work [13], we will assume that particle masses are tied to some type of unit cell in a five-dimensional momentum space lattice. First let us consider the electron. The field theory which deals with the electron is the (abelian) QED [8]. We imagine that the amount of inertial mass of the electron (m_e) is proportional to the five-dimensional volume of the unit cell in the momentum space lattice, which size is given by the Planck's characteristic momentum, namely

$$p = M_{Pl}\, c, \tag{11}$$

and

$$V_5 = p^5 = (M_{Pl}\, c)^5 . \tag{12}$$

Therefore we write

$$m_e = K V_5 = K\,(M_{Pl}\, c)^5 . \tag{13}$$

On the other hand the proton is a hadron which structure is described by QCD [9, 14], a non-abelian field theory. QCD has in common with General Relativity (GR), the fact that both are known to be non-linear theories. It seems that in evaluating the proton mass, a curved space-time must be considered. This leads to a modified size of the unit cell in the momentum space lattice. Looking at the wave function given by (4) and the structure of energy levels implied by it, we have obtained $<p>$ given by (10). But the curvature of a space seems not to be displayed by a mathematical object such as a volume. Then we propose that the inertial mass of the proton m_p is proportional to a five-surface area in the curved momentum space lattice, this surface area being a derivative from a six-volume. Therefore we write

$$<V_6> = <p>^6 \tag{14}$$

$$<S_5> = \frac{\mathrm{d}<V_6>}{\mathrm{d}<p>} = 6<p>^5 \tag{15}$$

and

$$m_p = K<S_5> = K\,6\pi^5\,(M_{Pl}\, c)^5 . \tag{16}$$

In writing (16) we have used (10), and considered that the proportionality constant K is the same as that used in determining the electron mass. By comparing (13) and (16), we finally obtain

$$\frac{m_p}{m_e} = 6\pi^5 \approx 1836.12. \tag{17}$$

The ratio given by (17) has been previously obtained by various authors, and compares relatively well with the experimental values (please see [1,3,4] and references cited in those papers).

Submitted on January 21, 2014 / Accepted on February 6, 2014

References

1. González-Martin G. arXiv: physics/0009066.
2. González-Martin G. arXiv: physics/0405094.
3. González-Martin G. *Revista Mexicana de Fisica*, 2003, v. 49 (3), 118.
4. Smilga W. arXiv: gen-ph/0505040v3.
5. Lenz F. *Phys. Rev.*, 1951, v. 82, 554.
6. Good J. *Phys. Lett. A*, 1970, v. 33, 383.
7. Wyler A. *C. R. Acad. Sc. Paris*, 1971, v. 217A, 186.
8. Ryder L. H. Quantum Field Theory. Cambridge Univ. Press, Cambridge, 1992.
9. Wilczek F. *Phys. Today*, 2000 (August), 22.
10. Bekenstein J. D. *Phys. Rev.D*, 1973, v. 7, 2333.
11. Hawking S. *Comm. Math. Phys.*, 1975, v. 43, 199.
12. Damour T. arXiv: hep-th/0401160.
13. Wesson P. S. arXiv: gen-ph/1301.0033v1.
14. Moriyasu K. An Elementary Primer For Gauge Theory. World Scientific, Singapore, 1983.

Memory of Living Beings and Its Three Characteristic Times

Paulo R. Silva

Departamento de Física (Retired Associate Professor), ICEx, Universidade Federal de Minas Gerais, Brazil
E-mail: prsilvafis@gmail.com

In this study we first evaluate the time between collisions related to the transport properties in liquid water, provided by the protons motion tied to the hydrogen bonds. As water is an essential substance for the establishment of life in the living beings, we take this time as the basic unit to measure some kinds of retention time related to their memory. Besides this, integration is an important feature associated to the operation of the memory. Then we consider two possible ways of doing integration and an average between them. One of these characteristic times, the Darwin time, is given by adding over the N basic units which forms the memory. The other possibility, the recent time, is obtained by considering a kind of time-like random walk running over the N basic units. Finally we perform a geometric average between these two times and call it generations' time. As a means to estimate these characteristic times, we take the number of protons contained in a volume of water compatible with the dimensions of the portion of the brain responsible by its memory.

1 Introduction

It seems that water is fundamental to the flourishing of life [1], and the hydrogen-bond kinetics [2] plays an important role in the establishment of the transport properties of this liquid. Besides this, living beings which exhibit the property of to replicate, must have this feature encoded in its memory. In electronic computers, electrical currents are the agents responsible for writing or deleting the information stored in its memory. In this paper we propose that, in the living beings case, the protonic currents do this job. In order to accomplish this we will treat protonic currents in close analogy with the electrical currents in metals.

First we will evaluate the averaged time between collisions for protonic currents and after we will use this time in an integration sense, in order to find characteristic times of persistency of the information registered in the living beings memories. By integration sense we mean that we are looking for physical properties which depend on the whole system, a kind of cooperative effect, or an emergent property of the collective of particles.

2 Electrical conductivity through protons

Drude formula for the electrical conductivity of metals can be written as

$$\sigma = \frac{e^2 n \tau}{M}\,, \tag{1}$$

where e is the quantum of electric charge, n is the number of charge carriers per unit of volume, τ is the average time between collisions and M is the mass of the charge carriers.

Besides this in reference [3], starting from Landauer's paradigm: conduction is transmission [4], the relation for the electrical conductivity can be put in the form

$$\sigma = \frac{e^2}{\pi \hbar \ell_0}\,. \tag{2}$$

where ℓ_0 is the size of the channel of conduction. In the case of the charge carrier being the proton, the maximum conductivity is reached when the length, ℓ_0, becomes equal to the reduced Compton wavelength of it, namely

$$\ell_0 = \frac{\hbar}{Mc}\,. \tag{3}$$

Inserting equation (3) into equation (2) we get

$$\sigma_{max} = \frac{e^2 M c}{\pi \hbar^2}\,. \tag{4}$$

Making the identification between the two relations for the electrical conductivity, namely equating equation (1) to equation (4), and solving for τ, we obtain for the maximum time between collisions the expression

$$\tau_{max} = \tau = \frac{M^2 c}{n \pi \hbar^2}\,. \tag{5}$$

It would be worth to evaluate numerically equation (5). In order to do this we consider that water molecules in the liquid state are relatively closed packed. Therefore by taking $n = 10^{29}\,\mathrm{m}^{-3}$, which seems to be an acceptable number for n, we get

$$\tau = 2.7 \times 10^{-7}\ \mathrm{s}. \tag{6}$$

This time interval is seven orders of magnitude greater than the time between collisions of electrons in metallic copper at room temperature [5].

3 Hydrogen bond and the transport properties of liquid water

As far we know, protonic currents have not been directly measured in water. Indeed, equation (5) for the maximum time between collisions, does not show explicit dependency on the quantum of electric charge e.

Meanwhile, from equation (27) of reference [5], we have

$$\lambda_{\mathrm{F}}^2 = \lambda_{\mathrm{C}}\,\ell\,. \tag{7}$$

In equation (7), λ_{F}, λ_{C} and ℓ, are respectively the Fermi and Compton wavelengths and the mean free path of the particle responsible by the transport property in water. Besides this, Luzar and Chandler [2] pointed out that: "In the hydrogen — bond definition employed by them, two water molecules separated by less than 3.5Å can be either bond or not bonded, depending upon their relative orientations. At large separations, a bond cannot be formed." This information comes from the first coordination shell of water, as measured by its oxygen-oxygen radial distribution function. We will idealize a lattice of water molecules, and by considering its Fermi length $\lambda_{\mathrm{F}} = 3.5$Å, and by taking λ_{C} equal to the reduced Compton length of the proton, we obtain from equation (7)

$$\ell = 6.2 \times 10^{-4}\ \mathrm{m}. \tag{8}$$

Equation (8) is an estimate of the proton mean free path in water. If we write

$$\ell = V_{\mathrm{F}}\tau \tag{9}$$

where V_{F} is a kind of Fermi velocity of the system and solving for V_{F}, we find after using equations (6) and (8)

$$V_{\mathrm{F}} \approx 2300\ \mathrm{m/s}. \tag{10}$$

We observe that this value of V_{F} is comparable with the speed of sound in water, approximately 1500 m/s. Therefore this time between collisions estimated for the proton motion performing the hydrogen bond in water seems to make some sense.

4 Three characteristic times tied to the living beings

Recently Max Tegmark [6] published a paper entitled *Consciousness as a State of Matter*. Tegmark was inspired in a work by Giulio Tononi [7]: *Consciousness as Integrated Information: A Provisional Manifesto*. According to Tegmark [6], Tononi [7] stated that for an information processing system to be conscious, it needs to have two distinct properties:

1. Have the ability to store a long amount of information;
2. This information must be integrated into unified whole.

Besides this, as was pointed out by Tegmark [6]: "Natural selection suggests that self-reproducing information processing systems will evolve integration if it is useful for them, regardless of whether they are conscious or not". In this work we are interested in look at the integrated effects with respect to time intervals, taking in account the great number N of basic units which compose the whole. By whole, we consider for instance, a substantial part of the brain of a living being responsible by its memory. We assume that the characteristic times are measured in terms of units of time-base. This unit will be taking as the time between collisions of the protons motion, related to the transport properties of water and associated to the hydrogen-bond dynamics.

4.1 Integrated time: first possibility

Let us to take a time-like string of N unit cells or basic units. We suppose that the time elapsed, τ_{R}, for the information sweep the whole string can be computed by considering a kind of Brownian motion on this time-like string. Then we can write

$$\tau_{\mathrm{R}} = N^{\frac{1}{2}}\tau. \tag{11}$$

Eighteen grams of liquid water occupies a volume of approximately 18 cm^3 and contains $2N_A$ protons, where N_A stands for Avogrado number. We assume that this volume corresponds to a portion of the human brain compatible with the size of the region of memory storage. As a means to estimate τ_{R}, let us put numbers in (11) and we get

$$\tau_{\mathrm{R}} = (2N_A)^{\frac{1}{2}}\,\tau \approx 3 \times 10^5\ \mathrm{s}. \tag{12}$$

The time interval, given by equation (12), corresponds approximately to the duration of 3.5 days and perhaps can be associated to the recent memory of the human brain. If the volume of the memory's device is ten times smaller, namely 1.8 cm^3, the value of τ_{R} is reduced to approximately one day.

As a means of comparison, we cite a statement quoted in a paper by S. Mapa and H. E. Borges [8] that a type of memory which they call working memory, may persist by one or more hours. Meanwhile, with chemical aids this time can be extended, as we can find in the words of Yassa and collaborators [9]: "We report for the first time a specific effect of caffeine on reducing forgetting over 24 hours".

4.2 Integrated time: second possibility

Another possibility to consider for the integrated time is assuming that the overall time is the sum over the basic time units. Thinking in this way it is possible to write

$$\tau_{\mathrm{D}} = N\tau\,. \tag{13}$$

If we take $(2N_A)/10$ protons of 1.8 grams of water, we obtain for τ_{D},

$$\tau_{\mathrm{D}} \approx 3.2 \times 10^{16} \approx 10^9\ \mathrm{years}. \tag{14}$$

We will call τ_{D} the Darwin's time. This choice can be based in the following reasoning. According to Joyce [10]: "The oldest rocks that provide clues to life's distant past are 3.6×10^9 years old and by that time cellular life seems already to be established!" Another interesting paper about the origins of life can be found in reference [11].

4.3 Third characteristic time

The two characteristic times we have discussed before were associated by us to the recent memory time τ_{R} (order of magnitude of one day) and the Darwin's time τ_{D} (order of magnitude of one billion of years), this last one related to the establishment of life on earth. We judge interesting to consider an-

other characteristic time corresponding to the geometric average of the two times we just described. We write

$$\tau_{\mathrm{G}} = (\tau_{\mathrm{D}}\tau_{\mathrm{R}})^{\frac{1}{2}} = N^{\frac{3}{4}}\,\tau\,. \tag{15}$$

Inserting $N = 1.2\times10^{23}$, the number of protons contained in $1.8\,\mathrm{cm}^3$ of water and the unit of time interval $\tau = 2.7\times10^{-7}$ s in equation (15), we obtain for the generations' time τ_{D} the value

$$\tau_{\mathrm{G}} = 1700\,\mathrm{years}. \tag{16}$$

If we estimate a mean lifetime of the human beings as 70 years, the above number corresponds to approximately 24 generations.

5 Analogy with the polymer physics

Two characteristic times we have described in this paper can be thought in analogy with polymer physics [12]. In four dimensions, the scaling relation of polymers reproduces that of a single random walk.

If we think about a time-like string of time-length τ_{D}, composed by "monomers" having the duration of a unit-time τ, we have after N steps the relation

$$\tau_{\mathrm{R}} = (\tau_{\mathrm{D}}\tau)^{\frac{1}{2}} = N^{\frac{1}{2}}\tau\,. \tag{17}$$

We remember that τ_{D} is given by equation (13). Therefore the Darwin's time τ_{D} corresponds to the time-length of the string and the recent time τ_{R} looks similar to the end to end distance (equivalent to the gyration radius of polymers).

6 Concluding remarks

This work has been developed through two steps. In the first one, an averaged time τ between collisions was calculated, taking in account the proton current associated to the hydrogen bond in liquid water. As the human body, in particular its brain, is constituted in great extension by this liquid, it seems that any physical process occurring in it must consider the relevancy of water in supporting this task. Perhaps the above reasoning could be extended to all living beings. The falsifiability of the calculated τ was verified by obtaining a kind of Fermi velocity which is comparable to the sound velocity in liquid water.

In the second step we considered an important property of memory, namely its integrability. By taking a number N of hydrogen bonds contained in a volume of water representative of the memory device of the living beings, we was able to associate two characteristic times to them. The integrability given by simple addition of unit-base time gives the Darwin time which grows linearly with N. Another kind of integration, a time-like random walk, leads to the recent memory time which grows with the square root of N. An intermediate time interval given by the geometric average of the last two ones was also evaluated and we call it generation's time.

Although this work may sound very speculative, we think that it perhaps could inspire other more robust research on the present subject.

Submitted on February 9, 2014 / Accepted on February 13, 2014

References

1. Atteberry J. Why is water vital to life? 10 August 2010. http://science.howstuffworks.com/environmental/earth/geophysics/water-vital-to-life.html.
2. Luzar A., and Chandler D. Hydrogen-bond kinetics in liquid water. *Nature*, v. 379, 4 January 1996, 55–57.
3. Silva P. R., Sampaio M., Nassif C., Nemes M. C. *Phys. Lett. A*, v. 358, 2006, 358–362.
4. Landauer R. *IBMJ Res. Dev.*, 1957, issue 1, 223.
5. Silva P.R. Electrical conductivity of metals: a new look at this subject. viXra: 1209.0071 (2012).
6. Tegmark M. Consciousness as a state of matter. arXiv: 1401.1219.
7. Tononi G. Consciousness as integrated information: a provisional manifesto. *Biol. Bull.*, 2008, 215–216. http://www.biobull.org/content/215/3/216.full.
8. Mapa S. and Borges H. E. Modelagem de um mecanismo para formação e evocação de memórias em criaturas artificiais. http://www.dca.fee.unicamp.br/~gudwin/courses/IA889/2011/IA889-05.pdf
9. Borota D., Murray E., Kiceli G., Chang A., Watabe J. M., Ly M., Toscano J. P., Yassa M. A. Post-study caffeine administration enhances memory consolidation in humans. *Nature Neuroscience*, 2014, v. 17, 201–203.
10. Joyce G. F. RNA evolution and the origin of life. *Nature*, 16 March 1989, v. 338, 217–224. http://www.its.caltech.edu/~bch176/Joyce1989.pdf
11. Damineli A. and Damineli D. S. C. Origens da vida. *Estudos Avançados*, 2007, v. 21(59), 263–284. http://dx.doi.org /10.1590/S0103-40142007000100022
12. De Gennes P.-G. Scaling Concepts in Polymer Physics. Cornell University Press, Ithaca (N.Y.), 1979.

New Experiments Call for a Continuous Absorption Alternative to Quantum Mechanics – The Unquantum Effect

Eric S. Reiter

251 Nelson Avenue, 94044 Pacifica, CA, USA. E-mail: eric@unquantum.net

A famous beam-split coincidence test of the photon model was performed with γ-rays instead of visible light. A similar test was performed to split α-rays. In both tests, coincidence rates greatly exceed chance, leading to an *unquantum* effect. In contradiction to quantum theory and the photon model, these new results are strong evidence of the long abandoned accumulation hypothesis, also known as the loading theory. Attention is drawn to assumptions applied to past key experiments that led to quantum mechanics. The history of the loading theory is outlined, and a few key experiment equations are derived, now free of wave-particle duality. Quantum theory usually works because there is a subtle difference between quantized and thresholded absorption.

1 Introduction

Since Einstein's photoelectric work of 1905, quantum mechanics (QM) has endured despite its bizarre implications because no strong experimental evidence has been put forth to refute it. Such new evidence is presented in detail here.

By QM and the photon model, a singly emitted photon of energy $h\nu_{\mathrm{L}}$ must not trigger two coincident detections in a beam-split coincidence test (see p. 50 in [1] and p. 39 in [2]) where h is Planck's constant of action, and ν_{L} is frequency of the electromagnetic wave. Beam-split coincidence tests of past have seemingly confirmed QM by measuring only an accidental chance coincidence rate [3–6].

Here, new beam-split coincidence experiments use γ-rays instead of visible light. The detectors employed have high "energy" resolution, whereby their pulse-height is proportional to ν_{L}. The γ-ray detection-pulses were within a full-height window, indicating we are not dealing with frequency down-conversion.

To measure such an *unquantum* effect implies that a fraction of pre-loaded energy was present in the detector molecules preceding the event of an incoming classical pulse of radiant energy. It is called the *accumulation hypothesis* or the *loading theory* [7–12] (see p. 47 in [12]). The pre-loaded energy came from previous absorption that did not yet fill up to a threshold. The unquantum tests give us a choice: we either give up an always-applicable *particle-energy conservation*, or give up *energy conservation* altogether. We uphold energy conservation.

A beam-split coincidence test compares an expected chance coincidence rate R_c to a measured experimental coincidence rate R_e. Prior tests [3–6] all gave $R_e/R_c = 1$. Past authors admitted that exceeding unity would contradict QM. These unquantum experiments are the only tests known to reveal $R_e/R_c > 1$. This clearly contradicts the one-to-one "Born rule" probability prediction of QM.

It is counterintuitive to attempt to contradict the photon model with what was thought to be the most particle-like form of light, γ-rays. Prior tests have only pitted QM against an overly classical model that did not consider a pre-loaded state. A beam-split coincidence test with γ-rays is fair to both the loading theory and photon theory. The loading theory takes h as a maximum. This idea of action allowed below h is algebraically equivalent to "Planck's second theory" of 1911 [9, 10, 14, 15]. There, Planck took action as a property of matter, not light (see p. 136 in [10]). The unquantum effect implies that it was a false assumption to think h is due to a property of light. The loading theory assumes light is quantized at energy $h\nu_{\mathrm{L}}$ only at the instant of emission, but thereafter spreads classically.

Similar new beam-split tests with α-rays, contradicting QM with $R_e/R_c > 1$, are also described herein. This is important because both matter and light display wave-particle duality, and its resolution requires experiment and theory for both.

2 Gamma-ray beam-split tests

In a test of unambiguous distinction between QM and the loading theory, the detection mechanism must adequately handle both time and energy in a beam-split coincidence test with two detectors, as shown in the following analysis. Surprisingly, discussions of pulse "energy" (height) resolution have not been addressed in past tests [3–6] which were performed with visible light, and one test with x-rays. Referring to Fig. 1 we will analyze a photomultiplier tube (PMT) pulse-height response to monochromatic visible light [16]. A single channel analyzer (SCA) is a filter instrument that outputs a window of pulse heights ΔE_{window} to be measured; LL is lower level and UL is upper level (italic symbols denote notation in figures). If we set LL to less than half E_{mean}, one could argue we favored the loading theory, because a down-conversion might take place that would record coincidences in both detectors. Also, if LL were set too low, one could argue we were recording false coincidences due to noise. If we set LL higher than half E_{mean}, one could argue we were

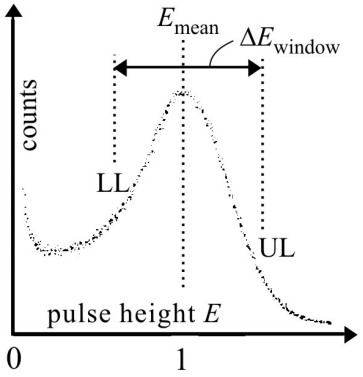

Fig. 1: PMT pulse-height response. Data according to [16].

Fig. 2: Two γ-ray detectors in tandem geometry; a demonstrator unit. Detector #1 was used with other components for data shown.

unfair to the loading theory by eliminating too many pulses that would have caused coincidences. Therefore a fair test requires high pulse-height resolution: $E_{mean} \gg \Delta E_{window}$. This criterion is not possible with a PMT or any visible light detector, but is easily met with γ-rays and scintillation detectors.

A high photoelectric effect detector-efficiency for the chosen γ-ray frequency was judged to enhance the unquantum effect, and this proved true. The single 88 keV γ-ray emitted in spontaneous decay from cadmium-109 (^{109}Cd), and detected with NaI(Tl) scintillators fit this criterion (see p. 717 [17]) and worked well. All radioisotopes used were low-level license-exempt.

A γ test of July 5, 2004 (see Fig. 6 in [18]) will be described in detail, and others briefly. After spontaneous decay by electron capture, ^{109}Cd becomes stable ^{109}Ag. ^{109}Cd also emits an x-ray, far below *LL*. We know that only one γ is emitted at a time, from a coincidence test with the γ source placed between two facing detectors that cover close to 4π solid angle (see p. 693 [19]). That test only revealed the chance rate, measured by

$$R_c = R_1 R_2 \tau , \qquad (1)$$

where R_1 and R_2 are the singles rates from each detector, and τ is the chosen time window within which coincident events are counted.

The test was performed with two detectors like those shown in Fig. 2, each being an NaI(Tl) crystal coupled to a PMT. The ^{109}Cd source was inside a tin collimator placed directly in front of detector #1, a custom made 4 mm thick 40×40 mm crystal. Directly behind detector #1 was detector #2, a 1.5″ Bicron NaI-PMT. We call this thin-and-thick detector arrangement tandem geometry. This test was performed inside a lead shield [20] that lowered the background rate 1/31. Referring to Fig. 3, components for each of the two detector channels are an Ortec 460 shaping amplifier, an Ortec 551 SCA, and an HP 5334 counter. For each detector channel, singles rates R_1 and R_2 were measured by calculating (counter pulses)/(test duration). A four channel Lecroy LT344 digital storage oscilloscope (DSO) with histogram software, monitored the analog pulses from each shaping amplifier on *Ch*1 (channel 1) and *Ch*2, and from the timing pulse outputs from each SCA on *Ch*3 and *Ch*4. Stored images of each triggered analog pulse assured that the number of misshaped pulses was well below 1%. Misshaped pulses can occur from pulse overlap and cosmic rays. This DSO can update pulse-height E and time difference Δt histograms after each triggered sweep. To assure exceeding particle-energy conservation, *LL* on each SCA window was set to $\sim 2/3$ of the ^{109}Cd γ characteristic pulse-height.

Data for this test is mostly from Fig. 4, a screen capture from the DSO. A control test with no source present is Δt histogram trace *B* of 16 counts/40.1 ks = 0.0004/s, a background rate to be subtracted. With τ taken as 185 ns, the chance rate from Eq. 1 was (291/s)(30/s)(185 ns) = R_c = 0.0016/s. From trace *A* and numbers on Fig. 4, R_e = 295/5.5 ks − 0.0004/s = 0.053/s. The unquantum effect was R_e/R_c = 33.5 times greater than chance. The described test is not some special case. Much critical scrutiny [18, 20] was taken to eliminate possible sources of artifact, including: faulty instruments, contamination by ^{113}Cd in the ^{109}Cd, fluorescence effects, cosmic rays, possibility of discovering stimulated emission, pile-up errors, and PMT artifacts. Hundreds of similar tests and repeats of various form have successfully defied QM. These tests include those with different sources (^{57}Co, ^{241}Am, pair-annihilation γ from ^{22}Na [21], ^{54}Mn, ^{137}Cs) and different detectors (NaI, high purity germanium, bismuth germinate, CsI), different geometries, and different collimator materials.

^{109}Cd was prepared in two chemical states of matter (see Fig. 11 in [18]). A salt state was prepared by evaporating an isotope solution. A metal state was prepared by electroplating the isotope in solution onto the end of a platinum wire. The unquantum effect from the salt state was 5 times greater than

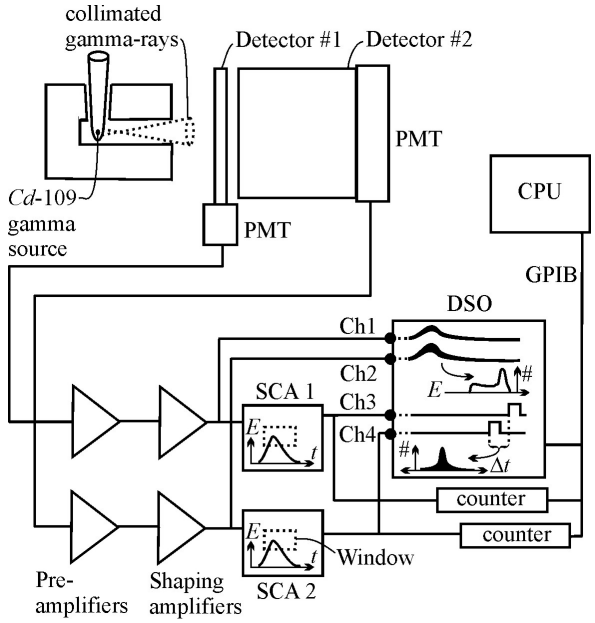

Fig. 3: γ-ray coincidence experiment.

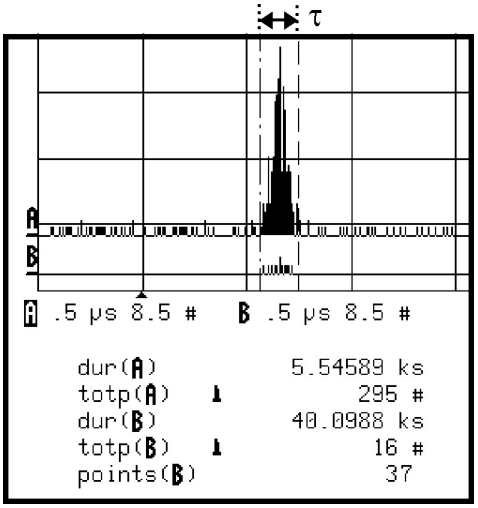

Fig. 4: γ-ray Δt from DSO.

from the metal state. This discovery measures how chemistry affects nuclear electron capture in isotope decay. We theorize that γ from the salt-crystaline source are more coherent and that the unquantum effect is enhanced by coherent waves. The singles spectrum did not measurably change with this chemical state change, so this sensitivity is due to the unquantum effect. A similar effect was reported [22] but was not nearly as sensitive or simple.

The unquantum effect is sensitive to distance (see Fig. 8–9 in [18]). A longer γ wavelength from ^{241}Am shows an enhanced unquantum effect when placed closer to the detectors, while a shorter γ wavelength from ^{137}Cs shows an enhanced effect when placed farther from the detector. Therefore, we can see how the spreading cone of a classical γ defines an area that matches the size of the microscopic scatterer (electron). We can measure how the short spatial and temporal qualities of a classical spreading γ wave-packet trigger the unquantum effect.

In addition to tandem geometry, a beam-split geometry was explored successfully. Different materials were tested to split an energy-fraction of a classical γ to one side, while the remaining ray passed through (see Fig. 12 in [18]). This beam-split geometry was developed into a spectroscopy whereby the pulse-height spectrum of the second detector was expanded. A non-shifted spectrum-peak indicates elastic Rayleigh scattering. A shifted spectrum-peak indicates non-elastic Compton scattering.

In beam-split geometry, crystals of silicon and germanium were explored with an apertured γ path to obtain angle resolution (see Fig. 13 in [18]). The unquantum effect varied with crystal orientation to reveal a new form of crystallography. This was not Bragg reflection from atomic planes, but rather from periodicity smaller than inter-atomic distance, perhaps electron-orbital structure.

The unquantum effect is sensitive to temperature of the beam-splitter (see Fig. 18 in [18]). A liquid nitrogen cooled slab of aluminum delivered a 50% greater unquantum effect, as expected.

Magnetic effects were explored with coincident deflected pulse-height analysis (see Fig. 14–16 in [18]) in beam-split geometry. A ferrite scatterer in a magnetic gap revealed enhanced Rayleigh scattering, indicating a stiff scatterer, as one would expect. A diamagnetic scatterer in a magnetic gap revealed enhanced Compton scattering, indicating a flexible scatterer, as expected.

The unquantum effect's increase/decrease response to several physical variables in the direction that made physical sense solidifies its fundamental validity. Each of the above mentioned modes of unquantum measurement represents a useful exciting discovery.

There is a simple way to measure the unquantum effect with a single NaI-PMT detector and a pulse-height analyzer [20]. Measure the ^{109}Cd sum-peak's count rate within a preset ΔE window that is set at twice 88 keV, and compare to chance. The result approached chance $\times 2$.

Our most impressive γ-split test [21] used ^{22}Na emitting a positron that annihilates into two 511 keV γ. The decay also emits a stronger γ that was caught in a third detector. In this triple-coincidence test $R_c = R_1 R_2 R_3 \tau_{12} \tau_{23}$. Only one from each pair of annihilation γ-rays were then captured by two detectors in tandem. Here $R_e/R_c = 963$. Energy $= h\nu$ is still true as a threshold value, but these experiments say there are no photons.

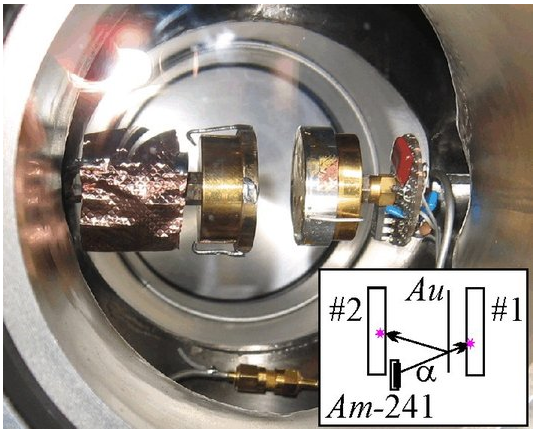

Fig. 5: α-split test in vacuum chamber.

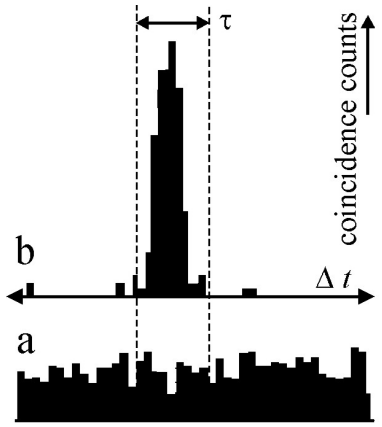

Fig. 6: α-ray Δt plots.

3 Alpha-ray beam-split tests

^{241}Am in spontaneous decay emits a single 5.5 MeV α-ray and a 59.6 keV γ. An α is a helium nucleus. This sounds like a particle, but consider a helium nuclear matter-wave. If the wave was probabilistic, the particle would go one way or another, and coincidence rates would only approximate chance. I performed hundreds of various tests in four vacuum chamber rebuilds. Two silicon Ortec surface barrier detectors with adequate pulse-height resolution were employed in a circuit nearly identical to Fig. 3. Fig. 5 shows the detectors and pre-amplifiers in the vacuum chamber. These tests were performed under computer CPU control by a program written in QUICKBASIC to interact with the DSO through a GPIB interface. Both SCA *LL* settings were at 1/3 of the characteristic α pulse-height, because it was found that an α-split usually maintains particle-energy conservation. The coincidence time-window was $\tau = 100$ ns. The Δt histograms of Fig. 6 were from DSO screen captures.

Data of Fig. 6-a was a two hour control test with the two detectors at right angles to each other and the ^{241}Am centrally located. Only the chance rate was measured, assuring that only one α was emitted at a time. This arrangement is adequate, and 4π solid angle capture is not practical with α. Any sign of a peak is a quick way to see if chance is exceeded. Background tests of up to 48 hours with no source gave a zero coincidence count.

Data of Fig. 6-b (Nov. 13, 2006) was from the arrangement of Fig. 5 using two layers of 24 carat gold leaf over the front of detector #1. Mounted on the rim of detector #2 were ^{241}Am sources, shaded to not affect detector #2. Every analog detector pulse in coincidence was perfectly shaped. $R_c = 9.8{\times}10^{-6}$/s, and $R_e/R_c = 105$ times greater than chance.

From collision experiments, the α requires $\sim$ 7 MeV per nucleon to break into components, and even more for gold [17]. It would take 14 MeV to create two deuterons. The only energy available is from the α's 5.5 MeV kinetic energy. So

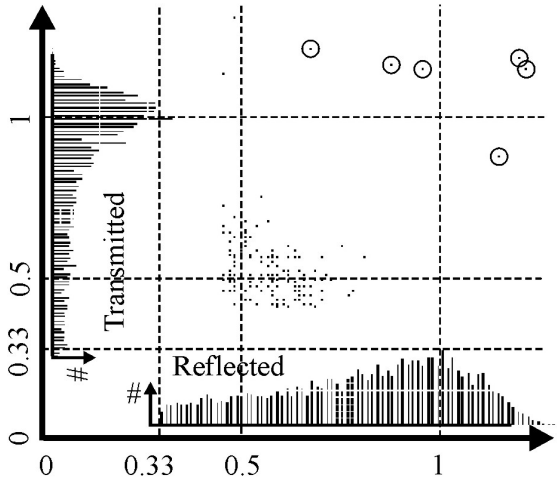

Fig. 7: Coincident α pulse-height pairs,

for any model of nuclear splitting there is not enough energy to cause a conventional nuclear split. Also plotted from the CPU program and data from the test of Fig. 6-b is data replotted in Fig. 7. Fig. 7 depicts pulse heights plotted as dots on a two dimensional graph to show coincident pulse heights from both detectors. The transmitted and reflected pulse-height singles spectra were carefully pasted into the figure. We can see that most of the a pulses (dots) are near the half-height marks; α usually splits into two lower kinetic-energy He matter-waves. Six dots, circled, clearly exceeded particle-energy conservation. Counting just these 6, we still exceed chance: $R_e/R_c = 3.97$. This is a sensational contradiction of QM because it circumvents the argument that a particle-like split, such as splitting into two deuterons, is somehow still at play.

In search for alternative explanations, we found none and conclude: an α matter-wave can split and continuous absorption can fill a pre-loaded state of He up to a detection thresh-

old. Also, the α-split test demonstrates how the loading theory applies to historical interference and diffraction tests with electrons, neutrons, and atoms [23, 24]. Several other materials were tested in transmission and reflection geometries to reveal the usefulness of this matter-wave unquantum effect in material science [21]. It is not necessary to use gold to exceed chance, but many materials tested just gave chance.

4 History of the loading theory and its misinterpretation

A believable report of such disruptive experimental results requires an accompanying historical and theoretical analysis.

Lenard [7, 8] recognized a pre-loaded state in the photoelectric (PE) effect with his trigger hypothesis. Most physicists ignored this idea in favor of Einstein's light quanta [25] because the PE equation worked. Planck (see Eq. 14 in [9], and p. 161 in [10]) explored a loading theory in a derivation of his black body law that recognized continuous absorption and explosive emission. Sommerfeld and Debye [11] explored an electron speeding up in a spiral around a nucleus during resonant light absorption. Millikan (see p. 253 in [13] described the loading theory, complete with its pre-loaded state in 1947, but assumed that its workings were "terribly difficult to conceive." In the author's extensive search, physics literature thereafter only treats a crippled version of the loading theory with no consideration of a pre-loaded state.

Most physics textbooks (e.g. [26], p. 79) and literature (e.g. [27]) routinely use photoelectric response time as evidence that the loading theory is not workable. Effectively, students are taught to think there is no such thing as a pre-loaded state. Using a known light intensity, they calculate the time an atom-sized absorber needs to soak up enough energy to emit an electron. One finds a surprisingly long accumulation time (the longest response time). They claim no such long response time is observed, and often quote $\sim$ 1 ns, the shortest response time from the 1928 work of Lawrence and Beams [28] (L&B). Such arguments unfairly compare a shortest experimental response time with a longest calculated response time. An absorber pre-loaded to near threshold explains the shortest response times. The longest response time from L&B was $\sim$ 60 ns. L&B did not report their light intensity, so it is not fair to compare their results to an arbitrary calculation. Energy conservation must be upheld, so an appropriate calculation is to measure the longest response time and the light intensity, assume the loading theory starting from an unloaded state, and calculate the effective size of the loading complex. The loading theory was the first and obvious model considered for our earliest experiments in modern physics. There is no excuse for the misrepresentation outlined here.

5 A workable loading theory

For brevity, the theory is elaborated for the charge matter-wave. If we develop three principles, we will find they explain both the quantum and unquantum experiments [29]:

1. de Broglie's wavelength equation is modified to the wavelength of a beat or standing-wave envelope-function of Ψ;
2. Planck's constant h, electron charge e, and mass constants like the electron mass m_e are maximum thresholds whereby emission is quantized but absorption is continuous and thresholded;
3. Ratios h/e, e/m, h/m, in our equations are conserved as the matter-wave expands and thins-out.

In de Broglie's derivation of his famous wavelength equation (see. p. 3 in [30])

$$\lambda_\Psi = \frac{h}{m_e v_p}\,, \tag{2}$$

he devised a frequency equation

$$h\nu_\Psi = m_e c^2, \tag{3}$$

and a velocity equation

$$v_p V_\Psi = c^2. \tag{4}$$

For equations (2–4), subscript Ψ is for either a matter-wave or a probabilistic wave, λ_Ψ is the phase wavelength, ν_Ψ the phase frequency, v_p the particle velocity, V_Ψ the phase velocity, and m_e the electron mass. Equations (3) and (4) remain widely accepted, but have serious problems. Equation (3) is only true when using ν_{L} instead of ν_Ψ to calculate a mass equivalent. If we measure v_p, λ_Ψ, and m_e for matter diffraction, equation (3) fails. Our experimental equations use h associated with kinetic energy, or momentum, not mass-equivalent energy.

As for equation (4), one might attempt to extract it from the Lorentz transformation equation of time by dimensional analysis, but its derivation independent of equations (2) or (3) has not been found by the author. Nevertheless, it describes an infinite V_Ψ in any particle's rest frame. Many physicists use equation (4) to justify the probability interpretation of QM, (see p. 89 in [31]) but this leads to "spooky action at a distance" we are all well aware of.

A much more reasonable frequency equation is the PE effect equation $h\nu_{\text{L}} = {}^1\!/_2\, m_e v_p^2$, with the work function not yet encountered. It is very reasonable to understand that something about charge is oscillating at the frequency of its emitted light, but just how to replace ν_{L} with a charge frequency requires insight. Recall the Balmer or Rydberg equation of the hydrogen spectrum in terms of frequency in its simplest form: $\nu_{\text{L}} = \nu_{\Psi 2} - \nu_{\Psi 1}$. Here ν_Ψ is frequency of a non-probabilistic Ψ matter-wave. The hydrogen atom is telling us that the relationship between ν_{L} and ν_Ψ is about difference-frequencies and beats. Consider that this difference-frequency property is fundamental to free charge as well as atomically bound charge. Beats, constructed from superimposing two sine waves are understood from a trigonometric identity to equal

an averaged Ψ wave modulated by a modulator wave M, as graphed in Fig. 8. If we take M as the coupling of light to charge we see that there are two beats per modulator wave, and we can write a relationship between light frequency and the frequency of charge beats: $2\nu_{\text{L}} = \nu_g$. Group velocity is commonly substituted for particle velocity, so $v_p = v_g$. Substituting the last two equations into the PE equation makes $h\nu_g = m_e v_g^2$. Groups are periodic, so we apply $\nu_g = v_g/\lambda_g$ to derive a wavelength equation (principle 1):

$$\lambda_g = \frac{h}{m_e v_g}\,. \tag{5}$$

Notice that both the PE equation and equation (5) have h/m_e. Recall several equations applicable to so-called "wave properties of particles": Lorentz force, PE, Compton effect, Aharonov-Bohm effect, others. They all have ratios like e/m, h/m, h/e. Examining $h/m_e \equiv Q_{h/m}$, if action is less than h and mass is less than m_e and the proportion is conserved, we would not be able to tell if those values went below our thresholds (h, m, e) while the charge-wave spreads out and diffracts (principles 2 & 3). Therefore we can write equation (5) as $\lambda_g = Q_{h/m}/v_g$ and the PE equation as $\nu_{\text{L}} = {}^1\!/_2\, Q_{m/h} v_g{}^2$. At threshold, $m_{group} = m_e$ and at sub-threshold we use Q ratios to emphasize wave nature (Q for quotient). To understand the PE effect without photons, visualize the pre-loaded state in the $Q_{m/h}$ ratio. Energy loads up to threshold and an electron is emitted explosively (principle 2); thereafter, the charge-wave can spread classically.

The Compton effect is often claimed to require QM treatment. A classical treatment is in Compton and Allison's book (see p. 232 in [12]) based upon a Bragg grating of envelopes from standing de Broglie waves. However, the envelopes were weak. If charge structures were inherently composed of beats of length d, it would naturally create a plausible Bragg grating. Use the Bragg diffraction equation $\lambda_{\text{L}} = 2d\sin(\phi/2)$, where ϕ is deflection angle. Substitute for d, λ_g from equation (5). Solve for v_g and insert into the Doppler shift equation $\Delta\lambda_{\text{L}}/\lambda_{\text{L}} = (v_g/c)\sin(\phi/2)$. Simplify using the trigonometric identity $\sin^2\theta = [1 - \cos(2\theta)]/2$ and $Q_{h/m}$ to yield

$$\Delta\lambda_{\text{L}} = \frac{Q_{h/m}}{c}(1 - \cos(\phi)),$$

the Compton effect equation.

Also related to the Compton effect are popular accounts of the test by Bothe and Geiger. The measured coincidence rate was not a one-to-one particle-like effect as often claimed, but rather the coincidence rate was $\sim 1/11$ [32].

What about quantized charge experiments? Measurements of e are performed upon ensembles of many atoms, such as in the Millikan oil drop experiment, and earlier by J. J. Thompson. Granted, electron detectors go click, but that is the same threshold effect demonstrated by the unquantum α-split experiments. From evidence of charge diffraction alone, it was a poor assumption to think charge was always quantized at e. Charge, capable of spreading out as a wave with a fixed e/m_e ratio for any unit of volume, loading up, and detected at threshold e, would remain consistent with our observations. Furthermore, the electron need not be relatively small. Chemists performing Electron Spin Resonance measurements often model the electron to be as large as a benzene ring. A QM electron would predict a smeared-out ESR spectrum.

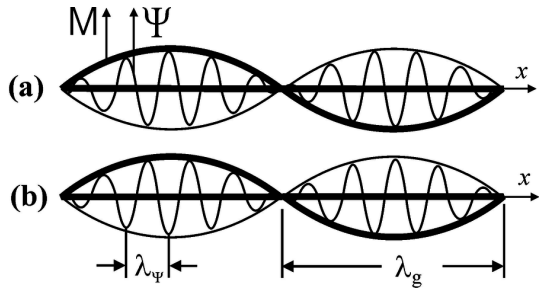

Fig. 8: Illustration of the concept of matter and antimatter. (a) Two positron beats. (b) Two electron beats.

The following is a list of famous experiments and principles re-analyzed with this newly developed Loading Theory (LT) by the author [29]: PE effect, Compton effect, shot noise, black body theory, spin, elementary charge quantization, charge & atom diffraction, uncertainty principle, exclusion principle, Bothe-Geiger experiment, Compton-Simon experiment, and the nature of antimatter, as envisioned in Fig. 8. The LT visualizes these fundamental issues, now free of wave-particle duality.

The LT supported by the unquantum effect easily resolves the enigma of the double-slit experiment. The wave of light or matter would load-up, and show itself as a click at a threshold.

These realizations lead to matter having two states: (1) a contained wave in a particle state, and (2) a spreading matter-wave that is not a particle at all, yet carries the wave-form matching a loading-up particle. One may protest by quoting experiments in support of QM, such as giant molecule diffraction, EPR tests, and quantum cryptography. My analysis of major flaws in such tests, and elaboration of topics outlined here, are freely viewable from my posted essays and at `www.unquantum.net`.

Submitted on October 11, 2013 / Accepted on February 23, 2014

References

1. Bohr N. Atomic physics and human knowledge. John Wiley and Sons Inc, New York, 1958.
2. Heisenberg W. The physical principles of the quantum theory. Dover Publications, Dover, 1930.
3. Givens M. P. An experimental study of the quantum nature of x-rays. *Philosophical Magazine*, 1946, v. 37, 335–346.
4. Brannen E., Ferguson H. The question of correlation between photons in coherent light rays. *Nature*, 1956, v. 4531, 481–482.

5. Clauser J. F. Experimental distinction between the quantum and classical field theoretic predictions for the photoelectric effect. *Physical Review D*, 1974, v. 9, 853–860.
6. Grainger P., Roger G., Aspect A. A new light on single photon interferences. *Annals of the New York Academy of Sciences*, 1986, v. 480, 98–107.
7. Lenard P. On cathode rays. Nobel lecture, *Nobel Lectures, Physics 1901-1921*, Elsevier Publishing Company, Amsterdam, 1967.
8. Lenard P. Ueber die lichtelektrische Wirkung. *Annalen der Physik*, 1902, v. 313(5), 149–198.
9. Planck M. Eine neue Strahlungshypothese. *Verhandlungen der Deutschen Physikalischen Gesellschaft*, 1911, v. 13, 138–148. Reprinted in: *Physikalische Abhandlungen und Vorträge*, Carl Schütte & Co, Berlin, 1958, v. 2, 249–259.
10. Planck M. The theory of heat radiation. Masius, M. (transl.) P. Blakiston's Son & Co., Philadelphia, 1914.
11. Debye P., Sommerfeld A. Theorie des lichtelektrischen Effektes vom Standpunkt des Wirkungsquantums. *Annalen der Physik*, 1913, v. 41, 872–930.
12. Compton A., Allison S. K. X-rays in theory and experiment. Van Nostrand, New York, 1935.
13. Millikan R.A. Electrons (+ and −) protons photons neutrons mesotrons and cosmic rays. University of Chicago Press, 1947.
14. Kuhn T. S. Black-body theory and the quantum discontinuity, 1894–1912. Oxford University Press, 1978, (see p. 235–264).
15. Whittaker E. A history of the theories of aether and electricity: the modern theories 1900–1926. Thomas Nelson and Sons, London, Edinburg, 1953, (see p. 103)
16. Flyckt S.-O., Mamonier C. Photomultiplier tubes principles and applications. Philips Photonics, Brive, France, 2002.
17. Evans R. The atomic nucleus. Tata McGraw Hill Publishing Company Limited, Bombay, New Delhi, 1955.
18. Reiter E. S. Photon violation spectroscopy. viXra: 1203.0094.
19. Knoll G. Radiation detection and measurement. John Wiley and Sons, Inc., New York, 1979.
20. Reiter E. S. A serious challenge to quantization. viXra: 1203.0092.
21. Reiter E. S. Particle violation spectroscopy. viXra: 1204.0032.
22. Kraushaar J. J., Wilson E. D., Bainbridge K. T. Comparison of the values of the disintegration constant of Be^7 in Be, BeO, and BeF_2. *Physical Review*, 1953, v. 90, 610–614.
23. Estermann I., Frisch R., Stern O. Monochromasierung der de Broglie-Wellen von Molekularstrahlen. *Zeitschrift fuer Physik*, 1932, v. A73, 348–365.
24. Berman P. R. Atom interferometry. Academic Press, San Diego, London, Boston, New York, Sydney, Tokyo, Toronto, 1997.
25. Einstein A. On a heuristic point of view concerning the production and transformation of light (title translated). *Annalen der Physik*, 1905, v. 17, 132–148.
26. Eisberg R. Fundamentals of modern physics. John Wiley and Sons, Inc., New York, 1961.
27. Gluck P., Saering B. No time lag in the photoelectric effect. *The Physics Teacher*, 2010, v. 48, 285–286.
28. Lawrence E., Beams J. The element of time in the photoelectric effect. *Physical Review*, 1928, v. 32, 478–485.
29. Reiter E. S. An understanding of the particle-like property of light and charge. viXra: 1203.0077.
30. de Broglie L. An introduction to the study of wave mechanics. E. P. Dutton, New York, 1930.
31. Born M. Atomic physics, fifth edition. Hafner Publishing Co., New York, 1951.
32. Shankland R. S. An apparent failure of the photon theory of scattering. *Physical Review*, 1936, v. 49, 8–13.

Staggering Phenomenon in Gamma Transitional Energies over Spin for Negative Parity States of Octupole Vibrational Nuclear Bands

A.M. Khalaf[1] and F.A. Altalhi[2]

[1]Physics Department, Faculty of Science, Al-Azhar University, Cairo, Egypt. E-mail: ali_khalaf43@hotmail.com
[2]Department of Science, Tabuk University, Ministry of Higher Education, Kingdom of Saudi Arabia. E-mail: Faltahi@hotmail.com

The negative parity states of octupole vibrational bands in Tungsten and Osmium nuclei have perturbed structure. To explore the $\Delta I = 1$ staggering, we plotted the gamma transitional energy over spin (EGOS) versus I^2. Such a plot exhibit large deviation from a linear $I(I+1)$ dependence $E(I) = A[I(I+1)]+B[I(I+1)]^2$ and effectively splits into two different curves for odd and even spin states and a staggering pattern is found. The odd-spin members $I^\pi = 1^-, 3^-, 5^-, \ldots$ were displaced relatively to the even-spin members $I^\pi = 2^-, 4^-, 6^-, \ldots$ i.e. the odd levels do not lie at the energies predicted by the pure rotator fit to the even levels, but all of them lie systematically above or all of them lie systematically below the predicted energies because the odd-spin states can be aligned completely, while the even-spin states can only be aligned partially. Also the $\Delta I = 1$ staggering effect has been clearly investigated by examining the usual backbeding plot.

1 Introduction

The properties of nuclear rotational bands built on octupole degrees of freedom have been extensively studied within various microscopic as will as macroscopic model approaches in nuclear structure [1–6]. It is will known that heavy nuclei have low-lying $K^\pi = 0^-$ octupole deformed bands [7,8]. Theoretical works of such bands have been presented in framework of cranked random phase approximation (RPA) [9, 10], the collective model [5], the interacting boson model (IBM) [3, 11], the variable moment of inertia (VMI) model [12] and the alpha particle cluster model [4, 13]. The IBM and the exotic cluster models address the existence of negative parity bands with $K^\pi \neq 0^-$.

Several staggering effects are known in nuclear spectroscopy. The $\Delta I = 2$ staggering has been observed and interpreted in superdeformed (SD) nuclei [14–22], where the levels with $I = I_0 + 2, I_0 + 6, I_0 + 10, \ldots$ are displaced relatively to the levels with $I = I_0, I_0 + 4, I_0 + 8, \ldots$, i.e. the level with angular momentum I is displaced relatively to its neighbors with angular momentum $I \pm 2$. There is another kind of staggering happening in SD odd-A nuclei, the $\Delta I = 1$ signature splitting in signature partners pairs [23].

The $\Delta I = 1$ Staggering in odd normal deformed (ND) nuclei is familiar for a long time [24–28], where the rotational bands with $K = 1/2$ separate into signature partners, i.e. the levels with $I = 3/2, 7/2, 11/2, \ldots$ are displaced relatively to the levels with $I = 1/2, 5/2, 9/2, \ldots$. In this paper, we will investigate another type of $\Delta I = 1$ energy staggering occurring in the negative parity octupole bands of even-even nuclei, where the levels with odd spin $I^\pi = 1^-, 3^-, 5^-, \ldots$ are displaced relatively to the levels with even spin $I^\pi = 2^-, 4^-, 6^-, \ldots$. This is more strikingly revealed when one makes the usual backbending plot of the energies in which the kinematic moment of inertia is plotted against the square of rotational frequency. The negative parity octupole band breaks into even and odd-spin bands with, however, very little backbending tendency.

2 Outline of the Theory of ΔI = 1 Energy Staggering

To analyze the $\Delta I = 1$ energy staggering in collective bands, several tests have been considered in the literature. In our analysis, the basic staggering parameter is the gamma transitional energy over spin (EGOS=$E_\gamma(I)/I$) of the transitional energies in a $\Delta I = 1$, where E(I) is the energy of the state of the spin I, and $E_\gamma(I)$ denotes the dipole transition energy

$$E_\gamma(I) = E(I) - E(I-1). \quad (1)$$

The level energies in a band can be more realistic parameterize by two-term rotational formula as a reference

$$E(I) = A[I(I+1)] + B[I(I+1)]^2. \quad (2)$$

The first two-term represents the perfect purely collective rigid rotational energy, where A denotes the inertial parameter $A = \hbar/2J$ (where J is the kinematic moment of inertia). The introduction of the second term is based on the assumption that, on rotation, the moment of inertia of the nucleus increases as does the quadratic function of the square of the angular velocity of rotation of the nucleus.

It is interesting to discuss the energy levels by plotting EGOS against spin. This is not helpful to identify the structure of the nucleus, but also to see clearly changes as a function of spin. For pure rotator, the energies of the yrast states are:

$$E(I) = A[I(I+1)]. \quad (3)$$

Then the $E2$ γ-ray energies are given by

$$E_\gamma(I) = A[4I - 2] \quad (4)$$

which yield

$$EGOS = A\left(4 - \frac{2}{I}\right). \quad (5)$$

Table 1: The adopted best model parameters A and B for our selected octupole vibrational bands.

	^{178}W	^{180}W	^{176}Os	^{178}Os	^{180}Os	^{182}Os
A (keV)	13.637	13.027	9.665	10.083	11.796	9.491
B (eV)	-13.821	-8.517	-2.223	-3.032	-8.607	0.140

In units of A, EGOS evolves from 3 for $I = 2$ up to 4 for high I, and so gradually increasing and asymptotic function of I.

EGOS for our proposed reference formula (2) is given by

$$EGOS = 2A + 4BI^2. \tag{6}$$

The EGOS when plotted against I^2, it represent a straight line of intercept 2A and slope 4B. Practically, the plot splits into two different curves for the odd and even spin states respectively. To see fine variation in the plot (EGOS & I^2), we use the staggering parameter

$$e(I) = EGOS - \left(2A + 4BI^2\right)_{\text{ref}} \tag{7}$$

where the unknown A and B are determined by minimizing the function F

$$F(I, A, B) = \sum_I |e(I)|^2. \tag{8}$$

The summation over spin in equation (8) is taken in step of $\Delta I = 1$. The function F has a minimum value when all its partial derivatives with respect to A and B vanish ($\partial F/\partial A = 0, \partial F/\partial B = 0$), this leads to

$$2nA + 4\sum_I I^2 B = \sum_I EGOS(I) \tag{9}$$

$$2\sum_I I^2 A + 4\sum_I I^4 B = \sum_I I^2 EGOS(I) \tag{10}$$

where n is the number of data points.

The behavior of the octupole band is most clearly illustrated by a conventional backbending plot. For each $\Delta I = 2$ value, the effective nuclear kinematic moment of inertia is plotted versus the square of the rotational frequency. If we consider the variation of the kinematic moment of inertia $J^{(1)}$ with angular momentum I, we can write

$$\frac{2J^{(1)}}{\hbar^2} = \frac{4I - 2}{E(I) - E(I-2)}. \tag{11}$$

Lets us define the rotational frequency $\hbar\omega$ as a derivative of the energy E(I) with respect to the angular momentum $[I(I+1)]^{1/2}$,

$$\hbar\omega = \frac{dE}{d[I(I+1)]^{1/2}} \tag{12}$$

usually we adopt the relation

$$(\hbar\omega)^2 = \frac{4(I^2 - I + 1)}{(2J^{(1)}/\hbar^2)^2}. \tag{13}$$

3 Numerical Calculation and Discusion

Our selected octupole bands are namely: ^{178}W, ^{180}W, ^{176}Os, ^{178}Os, ^{180}Os and ^{182}Os. The optimized model parameters A and B for each nucleus have been adjusted by using a compuer simulation search program to fit the calculated theoretical energies $E^{cal}(I_i)$, with the corresponding experimental ones $E^{exp}(I_i)$. The procedure of fitting is repeated for several trail values A and B to minimize the standard quantity χ which represent the root mean square deviation

$$\chi = \left[\frac{1}{N}\sum_{i=1}^{N}\left(\frac{E^{exp}(I_i) - E^{Cal}(I_i)}{\triangle E^{exp}(I_i)}\right)^2\right]^{1/2}$$

where N is the number of data points and $\Delta E^{exp}(I_i)$ are the experimental errors. The best optimized parameters are listed in table (1). The negative parity octupole bands have several interesting characteristics, the most obvious of which is the staggering effect. In this paper the $\Delta I = 1$ staggering is evident on a plot of staggering parameter $e(I)$ against I^2 and illustrated in figure (1), the band effectively splits into an odd- and even-spin sequence with a slight favoring in energy for the odd-spin states. In terms of an alignment of the angular momentum of the octupole vibration, the odd energy favoring can be understood since the odd-spin states can be aligned completely ($I \sim R + 3$, where $R = 0, 2, 4, \ldots$ is the collective rotation), while the even spins can only be aligned partially ($I \sim R + 2$). As expected from a good rotor model, the γ-ray transition energy $E_\gamma(I)$ increases with increasing the angular momentum I. It is found in some rotational deformed nuclei that the transition energy decreases with increasing I, this anomalous behavior is called nuclear backbending. In order to represent this backbending, one prefers to plot twice the kinematic moment of inertia $2J^{(1)}/\hbar^2$ versus the square of the rotational frequency $(\hbar\omega)^2$. Figure (2) shows the backbending plot for our selected octupole bands. It is seen that the bands are essentially separate into odd and even spin sequences which shows the effects of rotation alignment. The increase in Coriolis effects is due to the lowering of the Fermi level, then these effects depress the odd spin states relative to the even spin states. When the Coriolis effects are large compered with the octupole correlations effected through the residual interaction, it becomes inappropriate to identify these bands as octupole bands (decoupled two quasiparticle bands). These are bands in which the intrinsic spin has been aligned with the rotational spin through the decoupling action of the Coriolis force.

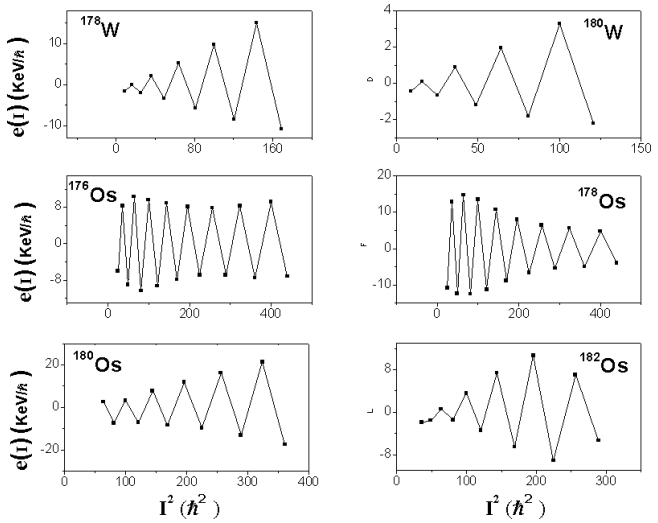

Fig. 1: The odd-even $\Delta I = 1$ energy staggering parameters $e(I)$ versus I^2 for negative parity states of octupole vibrational bands in doubly even nuclei ^{178,180}W and ^{176,178,180,182}Os.

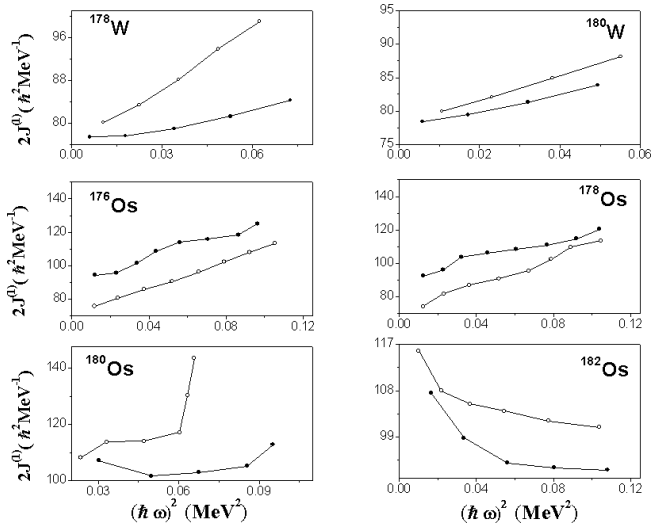

Fig. 2: Plot of twice Kinematic moment of inertia $2J^{(1)}$ against the square of the rotational frequency $(\hbar\omega)^2$ for the negative parity bands in ^{178,180}W and ^{176,178,180,182}Os isotopes.

4 Conclusion

In negative parity octupole bands of even-even W/Os nuclei, the levels with odd spins $I^\pi = 1^-, 3^-, 5^-, ...$ are displaced relatively to the levels with even spins $I^\pi = 2^-, 4^-, 6^-, ...$ The effect is called $\Delta I = 1$ staggering and its magnitude is clearly larger than the experimental errors. The phase and amplitude of the splitting is due to rotation particle Corialis coupling. Our proposed two terms formula provided us with information about the effective moment of inertia.

Submitted on February 11, 2014 / Accepted on February 23, 2014

References

1. Ahmed I. and Butler B.M. Octupole Shapes in Nuclei *Annual Review of Nuclear and Particle Science*, 1993, v. 43, 71–814.
2. Denisov V.Yu. and Dzyublik A.Ya. Collective states of even-even and odd nuclei with $\beta_2, \beta_3, ..., \beta_N$ deformations. *Nuclear Physics*, 1995, v. A589 17–57.
3. Zamfir N.V. and Kusnezov D. Octupole Correlations in the Transitional octinides and the spdf interacting boson Model. *Physical Review*, 2001, v. C63 054306–054315 and Octupole Correlations in U and Pu Nuclei. *Physical Review*, 2001, v. C67 014305–014313.
4. Shneidman T.M., et al. Cluster interpretation of parity splitting in alternating parity bands. *Physics Letters*, 2002, v. B526 322–328, and Cluster interpretation of properties of alternating parity bands in heavy nuclei. *Physical Review*, 2003, v. C67 014313–014325.
5. Minkov N., et al. Parity shift and beat staggering structure of octupole bands in a collective model for quadrupole–octupole-deformed nuclei. *Journal of Physics G: Nuclear and Particle Physics*, 2006, v. 32 497–510.
6. Hinde D. and Dasgupta M. Insights into the dynamics of fusion forming heavy elements. *Nuclear Physics*, 2007, v. A787 176–183.
7. Butler P.A. and Nazarewicz W. Intrinsic reflection asymmetry in atomic nuclei. *Review of Modern Physics*, 1996, v. 68 349–421.
8. Stefan Frauendorf. Spontaneous symmetry breaking in rotating nuclei. *Review of Modern Physics*, 2001, v. 73 463–514.
9. Ward D. et al. Rotational bands in ^{238}U. *Nuclear Physics*, 1996, v. A600 88–110.
10. Hackman G. High-spin properties of octupole bands in ^{240}Pu and ^{248}Cm. *Physical Review*, 1998, v. C57 R1056–R1059.
11. Cottle P.D. and Zamfir N.V. Octupole states in deformed actinide nuclei with the interacting boson approximation. *Physical Review*, 1998, v. C58 1500–1514.
12. Lenis D. and Dennis Bonatsos. Parameter-free solution of the Bohr Hamiltonian for actinides critical in the octupole mode. *Physics Letters*, 2006, v. B633 474–478.
13. Buck B., Merchant A.C. and Perez S.M. Negative parity bands in even–even isotopes of Ra, Th, U and Pu. *Journal of Physics G: Nuclear and Particle Physics*, 2008, v. 35 085101–085102.
14. Flibotte S., et al. $\Delta I = 4$ bifurcation in a superdeformed band: Evidence for a C_4 symmetry band. *Physical Review Letters*, 1993, v. 71 4299–4302.
15. Cederwall B, et al. New features of superdeformed bands in ^{194}Hg. *Physica Scripta*, 1994, v. 72 3150–3153.
16. Haslip1 D.S., Flibotte1 S. and de France G. $\Delta I = 4$ Bifurcation in Identical Superdeformed Bands. *Physical Review Letters*, 1997, v. 78 3447–3450.
17. Hamamoto I. and Mottleson B. Superdeformed rotational bands in the presence of $_4$4Y deformation. *Physics Letters*, 1994, v. B333 294–298.
18. Pavlichenkov I.M. and Flibotte S. C_4 symmetry and bifurcation in superdeformed bands. *Physical Review*, 1995, v. C51 R460–R464.
19. Khalaf A.M., Taha M.M., and Kotb M. Studies of Superdeformation in Gadolinium Nuclei Using Three-Parameters Rotational Formula. *Progress in Physics*, 2012, v. 8 (4), 39–44.
20. Khalaf A.M. and Sirag M.M. Analysis of $\Delta I = 2$ Staggering in Nuclear Superdeformed Rotational Bands. *Egypt Journal of Physics*, 2004, v. 35 (2), 359–375.
21. Sirag M.M. Reexamination of $\Delta I = 2$ Energy Staggering in Nuclear Superdeformed Rotational Bands. *Egypt Journal of Physics*, 2007, v. 38 (1), 1–14.
22. Madiha D. Okasha. ΔI=2 Nuclear Staggering in Superdeformed Rotational Bands. *Progress in Physics*, 2014, v. 10 (1), 41–44.

23. Khalaf A.M., et al. ΔI = 1 Signature Splitting in Signature Partners of Odd Mass Superdeformed Nuclei. *Progress in Physics*, 2013, v. 9 (3), 39–43.

24. Stephens F.S. Spin alignment in superdeformed rotational bands. *Nuclear Physics*, 1990, v. A520 c91–c104.

25. Toki H. and Faessler A. Asymmetric rotor model for decoupled bands in transitional odd-mass nuclei. *Nuclear Physics*, 1975, v. A253 231–252.

26. Khalaf A.M. High Spin Properties in Deformed Nuclei Using Weak Coupling Model. *Indian Journal of pure and Applied Physics*, 1986, v. 24 469–471.

27. Khalaf A.M. Nuclear Backbending and Evidence for Particle Core Coupling in Even-Even Nuclei. *Indian Journal of pure and Applied Physics*, 1986, v. 24 530–535.

28. Khalaf A.M. and Hegazi A.N. Theoretical Investigation of Potential Spectra for Axially Symetric Nuclei. *Proceedings of the Mathematical and Physical Society of Egypt*, 1984, v. 57 (2), 95–104.

A Model for the Expansion of the Universe

Nilton Penha Silva
Departmento de Física (Retired Professor), Universidade Federal de Minas Gerais, Belo Horizonte, MG, Brazil
Email: nilton.penha@gmail.com

One introduces an ansatz for the expansion factor $a(t) = e^{(H(t)t-H_0T_0)/\beta}$ for our Universe in the spirit of the FLRW model; β is a constant to be determined. Considering that the ingredients acting on the Universe expansion ($t > 4\times10^{12}\ s \approx 1.3\times10^{-5}\ Gyr$) are mainly matter (baryons plus dark matter) and dark energy, one uses the current measured values of Hubble constant H_0, the Universe current age T_0, matter density parameter $\Omega_m(T_0)$ and dark energy parameter $\Omega_\Lambda(T_0)$ together with the Friedmann equations to find $\beta = 0.5804$ and that our Universe may have had a negative expansion acceleration up to the age $T_\star = 3.214\ Gyr$ (*matter era*) and positive after that (*dark energy era*), leading to an eternal expansion. An interaction between matter and dark energy is found to exist. The deceleration $q(t)$ has been found to be $q(T_\star) = 0$ and $q(T_0) = -0.570$.

1 Introduction

The Cosmological Principle states that the Universe is spatially homogeneous and isotropic on sufficiently large scale [1–4] and [7]. This is expressed by the Friedmann spacetime metric:

$$ds^2 = \mathfrak{R}^2(t)\,d\psi^2+\mathfrak{R}^2(t)f_k^2(\psi)\left(d\theta^2 + sin^2\theta\,d\phi^2\right)-c^2dt^2, \quad (1)$$

where ψ, θ and ϕ are comoving space coordinates ($0 \le \psi \le \pi$, $for\ closed\ Universe$, $0 \le \psi \le \infty$, $for\ open\ and\ flat\ Universe$, $0 \le \theta \le \pi$, $0 \le \phi \le 2\pi$), t is the proper time shown by any observer clock in the comoving system. $\mathfrak{R}(t)$ is the scale factor in units of distance; actually $\mathfrak{R}(t)$ is the *radius of curvature* of the Universe. The proper time t may be identified with the cosmic time. In terms of the usual expansion factor

$$a(t) = \frac{\mathfrak{R}(t)}{\mathfrak{R}(T_0)}, \quad (2)$$

being T_0 the current age of the Universe, equation (1) becomes

$$\begin{aligned} ds^2 = {} & \mathfrak{R}^2(T_0)\,a^2(t) \\ & \left(d\psi^2 + f_k^2(\psi)\left(d\theta^2 + sin^2\theta\,d\phi^2\right)\right) - c^2dt^2, \end{aligned} \quad (3)$$

$f_k^2(\psi)$ assumes the following expressions:

$$f_k^2(\psi)\begin{cases} f_1^2(\psi) = sin^2\psi & \text{(closed Universe)} \\ f_0^2(\psi) = \psi^2 & \text{(flat Universe)} \\ f_{-1}^2(\psi) = sinh^2\psi & \text{(open Universe)} \end{cases} \quad (4)$$

The expansion process one will be considering here is the one started by the time of $4\times10^{12}\ s \approx 1.3\times10^{-5}\ Gyr$ when the so called *matter era* began. Right before that, the Universe went through the so called *radiation era*. In this paper one considers only the role of the matter (baryonic and non-baryonic) and the dark energy.

2 Einstein's field equations

Let one uses Einstein's Field Equations [5], with the inclusion of the Λ "cosmological constant" term.

$$G_{\mu\nu} = R_{\mu\nu} - \frac{1}{2}g_{\mu\nu}\,R = \frac{8\pi G}{c^4}\left(T_{\mu\nu} + T^\Lambda_{\mu\nu}\right) \quad (5)$$

where $g_{\mu\nu}$ is the metric tensor, $R_{\mu\nu}$ is the Ricci tensor, R is the Ricci scalar curvature, $T_{\mu\nu}$ is the energy-momentum tensor, and, $T^\Lambda_{\mu\nu}$ the dark-energy-momentum tensor,

$$T^\Lambda_{\mu\nu} = \rho_\Lambda c^2 g_{\mu\nu}, \quad (6)$$

$$\rho_\Lambda = \frac{\Lambda c^2}{8\pi G}; \quad (7)$$

Λ is the "cosmological constant", which will be here allowed to vary with time. The metric tensor for the metric above, equation (3), is

$$(g_{\mu\nu}) = \begin{pmatrix} \mathfrak{R}^2(t) & 0 & 0 & 0 \\ 0 & \mathfrak{R}^2(t)f_k^2(\psi) & 0 & 0 \\ 0 & 0 & \mathfrak{R}^2(t)f_k^2(\psi)sin^2\theta & 0 \\ 0 & 0 & 0 & -c^2 \end{pmatrix} \quad (8)$$

where

$$\mathfrak{R}(t) = \mathfrak{R}(T_0)\,a(t). \quad (9)$$

The Ricci tensor is given by

$$R_{\mu\nu} = \partial_\lambda\Gamma^\lambda_{\mu\nu} - \partial_\nu\Gamma^\lambda_{\mu\lambda} + \Gamma^\eta_{\mu\nu}\Gamma^\lambda_{\eta\lambda} - \Gamma^\eta_{\mu\lambda}\Gamma^\lambda_{\eta\nu} \quad (10)$$

where the Christoffel symbols $\Gamma^\lambda_{\mu\nu}$ are

$$\Gamma^\lambda_{\mu\nu} = \frac{1}{2}g^{\lambda\sigma}\left(\partial_\mu g_{\sigma\nu} + \partial_\nu g_{\sigma\mu} - \partial_\sigma g_{\mu\nu}\right). \quad (11)$$

The Ricci scalar curvature is given by

$$R = g^{\mu\nu}R_{\mu\nu}\,, \quad (12)$$

and the energy-momentum tensor is

$$T_{\mu\nu} = \left(\rho_m + \frac{1}{c^2}p_m\right)u_\mu u_\nu + p_m g_{\mu\nu}\,, \tag{13}$$

where ρ_m is the matter density and p_m is the matter pressure, both only time dependent. By making straightforward calculations, one gets

$$\begin{aligned} R &= 6\left(\frac{k}{\Re^2(T_0)a^2(t)} + \frac{1}{c^2}\left(\left(\frac{\dot{a}(t)}{a(t)}\right)^2 + \frac{\ddot{a}(t)}{a(t)}\right)\right) \\ &= 6\left(K(t) + \frac{1}{c^2}\left(\left(\frac{\dot{a}(t)}{a(t)}\right)^2 + \frac{\ddot{a}(t)}{a(t)}\right)\right). \end{aligned} \tag{14}$$

Here $K(t)$ is Gaussian curvature at cosmic time t:

$$K(t) = \frac{k}{\Re^2(t)} = \frac{k}{\Re^2(T_0)\,a^2(t)}. \tag{15}$$

The Einstein's field equations are

$$\begin{aligned} &G_{ii} = \frac{8\pi G}{c^4}\left(T_{ii} + T^{\Lambda}_{ii}\right) \;\leftrightarrow \\ &-\left(c^2K(t) + \left(\frac{\dot{a}(t)}{a(t)}\right)^2 + 2\frac{\ddot{a}(t)}{a(t)}\right) = 8\pi G\left(\frac{1}{c^2}\,p_m - \rho_\Lambda\right) \end{aligned} \tag{16}$$

and

$$\begin{aligned} &G_{tt} = \frac{8\pi G}{c^4}\left(T_{tt} + T^{\Lambda}_{tt}\right) \;\leftrightarrow \\ &3\left(c^2K(t) + \left(\frac{\dot{a}(t)}{a(t)}\right)^2\right) = 8\pi G\,(\rho_m + \rho_\Lambda) \end{aligned} \tag{17}$$

where $i = (\psi, \theta, \phi)$; all off-diagonal terms are null. The equation of state for dark energy is

$$p_\Lambda = -\rho_\Lambda c^2. \tag{18}$$

Simple manipulation of equations above leads to

$$\frac{\ddot{a}(t)}{a(t)} = -\frac{4\pi G}{3}\left(\rho_m + 3\frac{1}{c^2}p_m - 2\rho_\Lambda\right), \tag{19}$$

$$\left(\frac{\dot{a}(t)}{a(t)}\right)^2 + c^2K(t) = \frac{8\pi G}{3}\,(\rho_m + \rho_\Lambda)\,. \tag{20}$$

Equations (19-20) are known as Friedmann equations. Having in account that

$$\frac{\dot{a}(t)}{a(t)} = H(t), \tag{21}$$

$$\frac{\ddot{a}(t)}{a(t)} = \dot{H}(t) + H^2(t), \tag{22}$$

where $H(t)$ is time dependent Hubble parameter, and that pressure $p_m = 0$ (matter is treated as dust), one has

$$\dot{H}(t) + H^2(t) = \frac{8\pi G}{3}\left(-\frac{1}{2}\,\rho_m + \rho_\Lambda\right), \tag{23}$$

$$c^2K(t) + H^2(t) = \frac{8\pi G}{3}\,(\rho_m + \rho_\Lambda)\,, \tag{24}$$

or

$$\frac{\dot{H}(t)}{H^2(t)} + 1 = \frac{1}{\rho_{crit}}\left(-\frac{1}{2}\,\rho_m + \rho_\Lambda\right), \tag{25}$$

$$\frac{c^2K(t)}{H^2(t)} + 1 = \frac{1}{\rho_{crit}}\,(\rho_m + \rho_\Lambda)\,, \tag{26}$$

where

$$\rho_{crit} = \frac{3H^2(t)}{8\pi G} \tag{27}$$

is the so called critical density. From equations (25-26) one obtains, after simple algebra,

$$\rho_m = \frac{1}{4\pi G}\left(c^2K(t) - \dot{H}(t)\right), \tag{28}$$

$$\rho_\Lambda = \frac{1}{4\pi G}\left(\frac{1}{2}\,c^2K(t) + \frac{3}{2}H^2(t) + \dot{H}(t)\right), \tag{29}$$

or,

$$\Omega_m = \left(\frac{2}{3}\frac{c^2K(t)}{H^2(t)} - \frac{2}{3}\frac{\dot{H}(t)}{H^2(t)}\right), \tag{30}$$

$$\Omega_\Lambda = \left(\frac{1}{3}\frac{c^2K(t)}{H^2(t)} + \frac{2}{3}\frac{\dot{H}(t)}{H^2(t)} + 1\right), \tag{31}$$

where $\Omega_m = \rho_m/\rho_{crit}$ and $\Omega_\Lambda = \rho_\Lambda/\rho_{crit}$ are, respectively, the cosmological matter and dark energy density parameters.

The Ricci scalar curvature stands as

$$R = 6\left(K(t) + \frac{1}{c^2}\left(2H^2(t) + \dot{H}(t)\right)\right). \tag{32}$$

3 The ansatz

Now let one introduces the following ansatz for the expansion factor:

$$a(t) = e^{(H(t)t\,-\,H_0T_0)/\beta} \tag{33}$$

where T_0 is the current age of the Universe, $H_0 = H(T_0)$ is the Hubble constant, and β is a constant parameter to be determined. From equations (21-23) one obtains

$$H(t) = H_0\left(\frac{t}{T_0}\right)^{\beta-1} \tag{34}$$

$$\dot{H}(t) = H(t)\frac{1}{t}\,(\beta - 1)\,. \tag{35}$$

By inserting equations (34-35) into equation (25) one has:

$$\frac{\beta - 1}{H_0 t}\left(\frac{t}{T_0}\right)^{1-\beta} + 1 = \frac{1}{\rho_{crit}}\left(-\frac{1}{2}\,\rho_m + \rho_\Lambda\right) \tag{36}$$

$$\frac{\beta - 1}{H_0T_0}\left(\frac{t}{T_0}\right)^{-\beta} = -\frac{1}{2}\,\Omega_m + \Omega_\Lambda - 1 \tag{37}$$

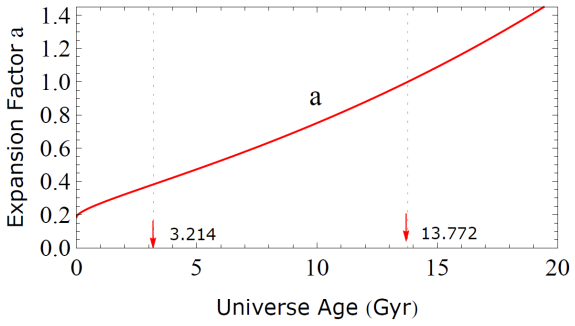

Fig. 1: $a(t) = e^{\frac{1}{\beta}\left(\left(\frac{t}{T_0}\right)^{\beta}-1\right)H_0T_0}$

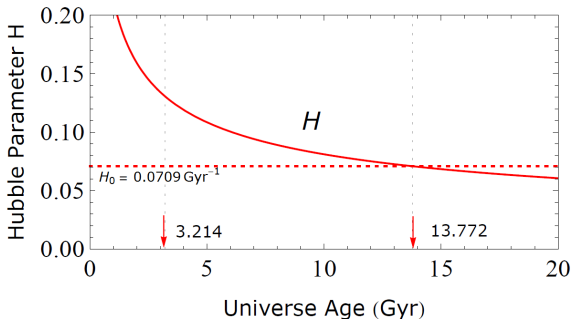

Fig. 2: $H(t) = H_0\left(\frac{t}{T_0}\right)^{\beta-1}$

Since β is assumed to be a constant, and, that $\Omega_m(T_0)$, $\Omega_\Lambda(T_0)$ and $H(T_0) = H_0$ are measured quantities, one has for $t = T_0$,

$$\frac{\beta-1}{H_0T_0} = -\frac{1}{2}\,\Omega_m(T_0) + \Omega_\Lambda(T_0) - 1 \tag{38}$$

which solved for β gives

$$\beta = 1 + H_0T_0\left(-\frac{1}{2}\Omega_m(T_0) + \Omega_\Lambda(T_0) - 1\right) = 0.5804. \tag{39}$$

where

$$H_0 = 69.32\ kms^{-1}Mpc^{-1} = 0.0709\ Gyr^{-1},$$

$$T_0 = 13.772\ Gyr,$$

$\Omega_m(T_0) = 0.2865$ and $\Omega_\Lambda(T_0) = 0.7135$ [6].

The plot of the expansion acceleration

$$\ddot{a}(t) = \left(\dot{H}(t) + H^2(t)\right)a(t) \tag{40}$$

as function of t = *age of the Universe* reveals that for $t < T_\star$, the acceleration is *negative* and for $t > T_\star$, the acceleration is *positive*. See Figure (4). This means that when the Universe is younger than $T_\star$, the regular gravitation overcomes dark energy, and after $T_\star$, dark energy overcomes gravitation. The result is an eternal positive accelerated expansion after $T_\star = 3.214\ Gyr$. See ahead.

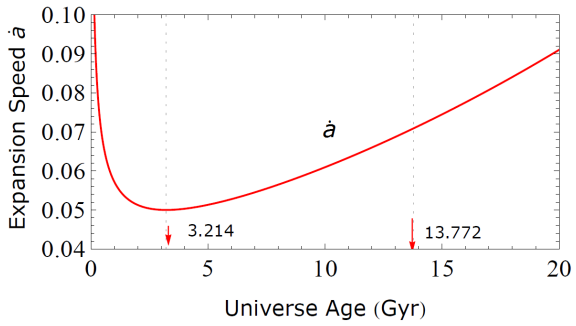

Fig. 3: $\dot{a}(t) = a(t)\,H_0\left(\frac{t}{T_0}\right)^{\beta-1}$

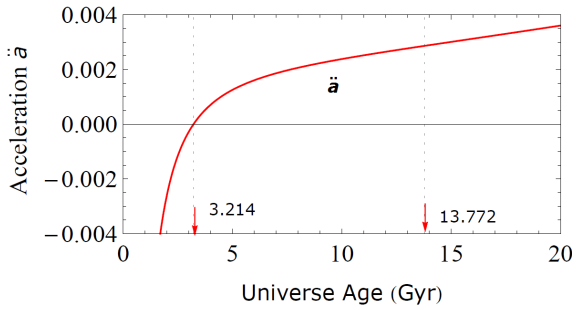

Fig. 4: $\ddot{a}(t) = a(t)\left(H_0\left(\frac{t}{T_0}\right)^{\beta} - (1-\beta)\,\frac{1}{t}\right)H_0\left(\frac{t}{T_0}\right)^{\beta-1}$

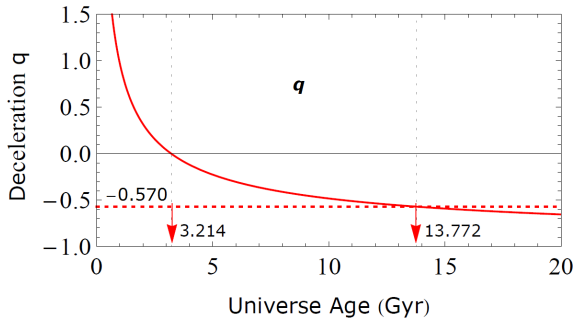

Fig. 5: $q(t) = -\left(1 + \frac{1}{H_0T_0}\,(\beta-1)\left(\frac{t}{T_0}\right)^{-\beta}\right)$

In fact, by setting equation (40) to zero and just solving it for t,

$$H(t)\frac{1}{t}(\beta-1) + H^2(t) = 0, \tag{41}$$

one gets

$$t = T_\star = T_0\left(\frac{1-\beta}{H_0T_0}\right)^{\frac{1}{\beta}} = 3.214\ Gyr\,. \tag{42}$$

From equation (26), one writes

$$\frac{c^2k}{\Re^2(t)H^2(t)} = \Omega_m + \Omega_\Lambda - 1. \tag{43}$$

The known recently measured values of $\Omega_m(T_0)$ and $\Omega_\Lambda(T_0)$ [6] do not allow one to say, from above equation, that the

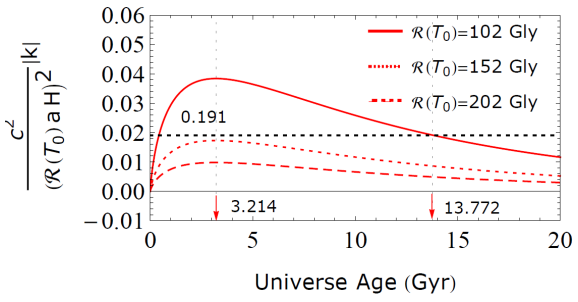

Fig. 6: Left hand side of equation (43) is plotted for some values of $\Re(T_0)$. At the current Universe age $T_0 = 13.772\,Gyr$, the right side of the referred equation has the margin of error equal to ±0.0191.

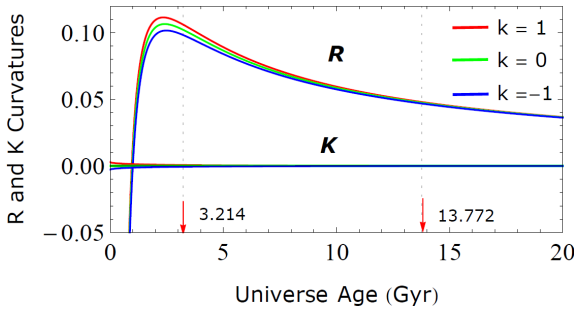

Fig. 7: Gaussian curvature $K(t) = \frac{k}{\left(\Re(T_0)a(t)\right)^2}$ and Ricci scalar curvature $R(t) = 6\left(K(t) + \frac{1}{c^2}H(t)\left(2H(t) + \frac{1}{t}(\beta-1)\right)\right)$.

Universe is clearly flat ($k = 0$). The referred measured values have a margin of error:

$$\Omega_\Lambda(T_0) = 0.7135 \begin{cases} +0.0095 \\ -0.0096 \end{cases}$$

$$\Omega_m(T_0) = 0.2865 \begin{cases} +0.0096 \\ -0.0095 \end{cases}$$

Considering also the margin of errors of the other measured parameters [6], one cannot distinguish between $k = 1$, -1 or 0. The match between both sides of equations (43) requires that, the today's curvature radius of the Universe be $\Re(T_0) > 100\,Gly$, in the context of this paper. See Figure (6).

The so called deceleration parameter is

$$\begin{aligned} q(t) &= -\frac{\ddot{a}(t)a(t)}{\dot{a}^2(t)} = -\left(\frac{\dot{H}(t)}{H^2(t)} + 1\right) \\ &= -\left(1 + \frac{\beta-1}{H_0T_0}\left(\frac{t}{T_0}\right)^{-\beta}\right) \end{aligned} \tag{44}$$

which, at current Universe age is $q(T_0) = -0.570$. See Figure (5).

The expansion scalar factor $a(t)$, Hubble parameter $H(t)$, expansion speed $\dot{a}(t)$, expansion acceleration $\ddot{a}(t)$, and the deceleration parameter $q(t)$ are plotted in Figures (1-5).

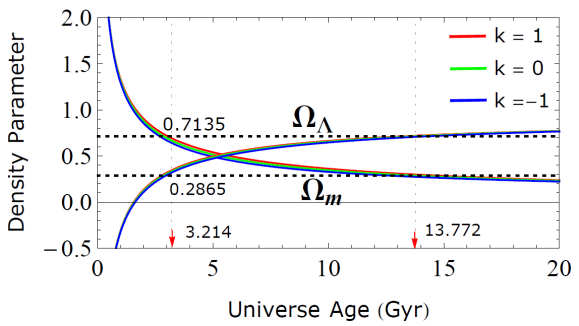

Fig. 8: Matter and dark energy density parameters for $k = 1, 0, -1$: $\Omega_m(t) = \frac{2}{3H^2(t)}\left(c^2K(t) - (\beta-1)\frac{H(t)}{t}\right)$; $\Omega_\Lambda(t) = \frac{1}{3H^2(t)}\left(c^2K(t) + 2(\beta-1)\frac{H(t)}{t} + 3H^2(t)\right)$. The radius of curvature is taken as $\Re(T_0) = 102\,Gly$.

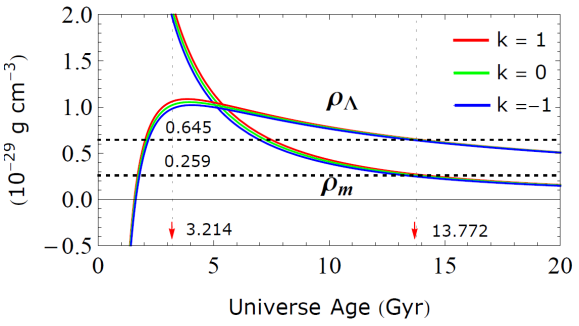

Fig. 9: Matter and dark energy densities for $k = 1, 0, -1$:
$\rho_m(t) = \frac{2}{8\pi G}\left(c^2K(t) - (\beta-1)\frac{H(t)}{t}\right)$;
$\rho_\Lambda(t) = \frac{1}{8\pi G}\left(c^2K(t) + 2(\beta-1)\frac{H(t)}{t} + 3H^2(t)\right)$.
The radius of curvature is taken as $\Re(T_0) = 102\,Gly$.

The sequence of Figures (7-10) shows the Gaussian $K(t)$ and R curvatures, matter density parameter $\Omega_m(t)$, dark energy density parameter $\Omega_\Lambda(t)$, matter density $\rho_m(t)$, dark energy density $\rho_\Lambda(t)$ and cosmological dark energy $\Lambda(t)$.

The time derivatives of $\rho_\Lambda(t)$ and $\rho_m(t)$ reveal interesting detail of the model in question:

$$\dot{\rho}_m + 3H\left(\rho_m + \frac{1}{c^2}p_m\right) = \dot{\rho}_m + 3H\rho_m = -Q \tag{45}$$

$$\dot{\rho}_\Lambda + 3H\left(\rho_\Lambda + \frac{1}{c^2}p_\Lambda\right) = \dot{\rho}_\Lambda = Q \tag{46}$$

$$Q = 2H\left(\frac{1}{t^2}(\beta-2)(\beta-1) + 3\dot{H} - c^2K\right) \tag{47}$$

where $p_m = 0$ and $p_\Lambda = -\rho_\Lambda c^2$. This implies that

$$\dot{\rho}_m + \dot{\rho}_\Lambda = -3H\rho_m. \tag{48}$$

The two perfect fluids interact with each other. In Figure (11) one shows the plots for $\dot{\rho}_m$, $\dot{\rho}_\Lambda$ and $\dot{\rho}_m + \dot{\rho}_\Lambda$ as functions of cosmic time.

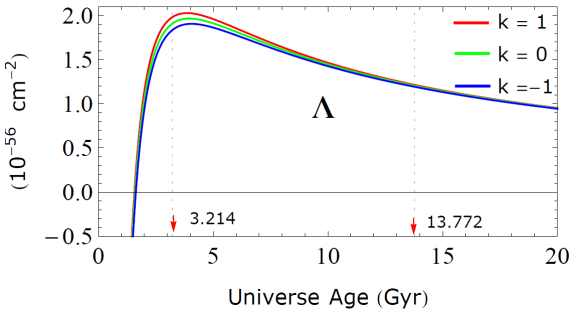

Fig. 10: Dark energy $\Lambda(t)$, in units of cm^{-2} for $k = 1, 0, -1$. $\Lambda(t) = \frac{1}{c^2} 8\pi G \rho_\Lambda(t)$. The radius of curvature is taken as $\Re(T_0) = 102\, Gly$. The result for $\Lambda(t)$ satisfies the following inequality: $|\Lambda| < 10^{-42} cm^{-2}$ [4].

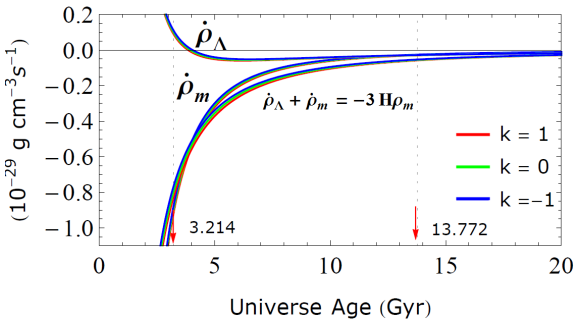

Fig. 11: Time derivatives of ρ_Λ, ρ_m and of the sum $\rho_\Lambda + \rho_m$ for $k = 1, 0, -1$. The radius of curvature is taken as $\Re(T_0) = 102\, Gly$.

4 Conclusion

The expression for the expansion factor $a(t) = e^{\frac{H_0 T_0}{\beta}\left(\left(\frac{t}{T_0}\right)^\beta - 1\right)}$, where $\beta = 0.5804$, constitutes a model for the expansion of the Universe for $t > 4 \times 10^{12} s \approx 1.3 \times 10^{-5} Gyr$ in which gravity dominates up to the Universe age of $T_* = 3.214\, Gyr$ and after that dark energy overcomes gravity and that persists forever. The acceleration of expansion is negative in the first part (*matter era*) and positive after that (*dark energy era*). The mathematical expressions for dark energy and matter densities indicate a clear interaction between the two perfect fluids (dark energy and matter). The classical deceleration parameter $q(t)$ is found to have the value $q(T_0) = -0.570$ for the current Universe age and the current radius of curvature should be $\Re(T_0) > 100\, Gly$.

Submitted on March 2, 2014 / Accepted on March 4, 2014

References

1. Raine, D. An Introduction to the Science Of Cosmology. Institute of Physics Publishing Ltd, 2001.
2. Peacock, J.A. Cosmological Physics. Cambridge University Press, 1999.
3. Harrison, E.R. Cosmology: The Science of the Universe. Cambridge University Press, 2nd ed. 2000.
4. Islam J.N. An Introduction to Mathematical Cosmology. Cambridge University Press. 2002.
5. Baryshev, Y.V. Expanding space: The root of conceptual problems of the cosmological physics. arXiv: gr-qc/0810.0153. 2008
6. Bennett, C.L. et al. Nine-Year Wilkinson Microwave Anisotropy Probe (WMAP) Observations: Final Maps and Results. arXiv: astro-ph.CO. 2013.
7. Ellis, G.F.R. et al. Relativistic Cosmology. Cambridge University Press, 2012.

Binding Energy and Equilibrium of Compact Objects

Massimo Germano

Department of Basic and Applied Sciences for Engineering (SBAI), University of Rome "La Sapienza", Via Antonio Scarpa 14 00162, Rome, Italy. E-mail: massimo.germano@uniroma1.it

The theoretical analysis of the existence of a limit mass for compact astronomic objects requires the solution of the Einstein's equations of general relativity together with an appropriate equation of state. Analytical solutions exist in some special cases like the spherically symmetric static object without energy sources that is here considered. Solutions, i.e. the spacetime metrics, can have a singular mathematical form (the so called Schwarzschild metric due to Hilbert) or a nonsingular form (original work of Schwarzschild). The former predicts a limit mass and, consequently, the existence of black holes above this limit. Here it is shown that, the original Schwarzschild metric permits compact objects, without mass limit, having reasonable values for central density and pressure. The lack of a limit mass is also demonstrated analytically just imposing reasonable conditions on the energy-matter density, of positivity and decreasing with radius. Finally the ratio between proper mass and total mass tends to 2 for high values of mass so that the binding energy reaches the limit m (total mass seen by a distant observer). As it is known the negative binding energy reduces the gravitational mass of the object; the limit of m for the binding energy provides a mechanism for stable equilibrium of any amount of mass to contrast the gravitational collapse.

1 Introduction to nonsingular Schwarzschild metric

The fate of extremely compact objects in the universe is ruled by the particular solutions of the Einstein's equations. As it is true that no all the mathematical theorems and statements have a corresponding meaning in the physical world, at the same time there is not a general rule, other than the verification by means of experimental and observational data, to establish, a priori, which mathematical solution must be discarded and which must be accepted.

In the case of the basic static model for compact objects, in the theory up to date the collapse is ruled by a specific solution (called Schwarzschild solution but not given explicitly by Schwarzschild, coming from the Hilbert's interpretation instead) that contains mathematical and thus physical singularities leading to a mass limit for ordinary compact objects and to the consequent black hole hypothesis (generalization to rotating or charged objects contains as well the features of singularity and horizon surface and it is not necessary in this context).

However, a different interpretation of the solution (nonsingular), particularly the original Schwarzschild solution, cannot be excluded if the completely different consequences (the nonexistence of mass limit and thus of black holes) are not yet demonstrated to be inconsistent with observational data.

1.1 Possible solutions to the static problem

Karl Schwarzschild in 1916 [1, eq. 14, page 194] gave an exact solution in vacuum to Einstein's field equation determining the line element for systems with static spherical symmetry (in units such that $c = G = 1$):

$$ds^2 = \left(1-\frac{\alpha}{R(r)}\right)dt^2 - \frac{dR(r)^2}{1-\frac{\alpha}{R(r)}} - R(r)^2\left(d\theta^2 + \sin^2\theta\, d\phi^2\right), \quad (1)$$

where α is a constant depending on the value of the mass, that can be obtained from the newtonian limit, and

$$R(r) = (r^3 + \sigma)^{1/3} \quad (2)$$

where σ (indicated with ρ in the original article) is a second constant to be determined and r is the same radial variable of the spherically symmetric Minkowski spacetime. Mathematically, there are two possible solutions that satisfy Einstein's field equation in vacuum ($R_{\mu\nu} = 0$): one is given by the class of infinite values of $R(r)$ such that [2, 3]

$$R(r) = (|r - r_0|^n + \alpha^n)^{1/n} \quad (3)$$

with arbitrary r_0 and $r \neq r_0$, the other is given by setting

$$R(r) = r. \quad (4)$$

It is worth to note that all the solutions of the class (3) can be obtained one from another by means of a simple coordinate transformation as must be in general relativity, while the solution (4) cannot be obtained from (3) and viceversa with a simple coordinate transformation. So, since the actual solution must be of course unique, the actual solution must be chosen among the form (3) and the form (4). At this stage, the only request that $R_{\mu\nu} = 0$ cannot discriminate about these solutions, additional considerations must be examined: in the

following it will be shown that, since $R(r)$ is related to the Gaussian curvature, it cannot be set equal to the radial coordinate r as in (4) because this brings to unphysical consequences.

The choices made, for example, by Schwarzschild [1] ($r_0 = 0$, $r > r_0$, $n = 3$), by Brillouin [4] ($r_0 = 0$, $r > r_0$, $n = 1$) and by Droste [5] ($r_0 = \alpha$, $r > r_0$, $n = 1$) belong to the class of solutions of the first kind (3); all the solutions of this class share the same constant α in the denominator (or, like in the Droste's solution, the additional condition for validity that $r > \alpha$) that prevents the metric to become singular and to change signature so that they could be called a class of "nonsingular" solutions.

The other possibility is the "singular" solution (4), due to the contribution by Hilbert [6], leading to the so called "Schwarzschild Solution", that from now on will be called Schwarzschild-Hilbert or "singular" solution, that sets $n = 1$, $r_0 = \alpha$ in (3), so that $\sigma = 0$ in (2) i.e. $R = r$; this is similar to the Droste's solution but with no limitation on r so that $0 \leqslant r \leqslant \infty$. The line element in this case is the well known Schwarzschild (-Hilbert) metric

$$ds^2 = \left(1 - \frac{\alpha}{r}\right)dt^2 - \frac{dr^2}{1 - \dfrac{\alpha}{r}} - r^2\left(d\theta^2 + \sin^2\theta\, d\phi^2\right), \qquad (5)$$

where r is (supposed to be) the usual radial coordinates (but it is actually related to the Gaussian curvature as it will be shown later) running from zero to infinity and α is determined from the Newtonian potential in the limit $r \to \infty$, so that $\alpha = 2m$ where m is the mass in geometrized units while its complete expression would be $m = GM/c^2$.

The consequences of the line element (5) are well known, among them the existence of an "event horizon", a not removable singularity in $r = 0$, the change in the sign of the g_{00} and g_{11} elements of the metric when $0 \leqslant r \leqslant 2m$ and the existence of a mass limit for equilibrium of massive neutron cores [7] and the consequent black hole hypothesis.

There is an open question about if there is an actual difference between all these solutions, leading to different physical consequences. An example of this discussion can be find on references [2, 3, 8, 9].

The present article will not enter deep into the question, instead it must be intended as a contribute for understanding the possible physical consequences, on compact objects, applying the nonsingular metric (1 and 2).

1.2 Some characteristics of the Schwarzschild metric

This article, will start from a "nonsingular" solution, the one given by K. Schwarzschild [1] (1 and 2) (from now on, simply, Schwarzschild solution), that set (eq. 13 in [1])

$$\sigma = \alpha^3 = 8m^3 \qquad (6)$$

so that the line element of the Schwarzschild Solution (1), using the coordinate r, becomes

$$ds^2 = \left(1 - \frac{\alpha}{(r^3+\sigma)^{1/3}}\right)dt^2 - \frac{r^4(r^3+\sigma)^{-4/3}}{1 - \dfrac{\alpha}{(r^3+\sigma)^{1/3}}}dr^2 - \\ - (r^3+\sigma)^{2/3}\left(d\theta^2 + \sin^2\theta d\phi^2\right), \qquad (7)$$

where σ has been explicitly left in order to compare all the subsequent formulas for this Schwarzschild metric (7) to the ones derived from the Schwarzschild-Hilbert metric (5), by simply setting $\sigma = 0$.

A first glance at the metric (7) indicates that there is no singularity at $r = 2m$, no "event horizon" and no change of sign (and of nature of the light cone) in the g_{00} and g_{11} elements of the metric. The "problem" has been moved to the origin $r = 0$ with the choice $\sigma = \alpha^3$. Moreover, the behavior of Schwarzschild metric, at the origin, is totally different from the one of Schwarzschild-Hilbert metric: in this latter, indeed, the presence of r in the denominator produces a mathematical, and consequently physical, not removable singularity, in the former there is just a smooth vanishing of the g_{00} and g_{11} metric elements, since in Schwarzschild metric (7)

$$\lim_{r\to 0} g_{00} = 0; \qquad \lim_{r\to 0} g_{11} = 0. \qquad (8)$$

It worths to note that the expression of the "time" element g_{00} in the limit $r \to 0$ is analogous to the limit $r \to 2m$ of the same element in metric (5), so that there is a coordinate time (time measured by a distant observer) going to infinite while a radially ingoing object would approach $r = 0$.

Both singular (4) and nonsingular (3) class of solutions give similar results in the weak field limit, that is the limit where all the experimental proofs for general relativity are performed. For example, Schwarzschild, applied his metric (7) to solve the problem of the observed anomaly in the perihelion of Mercury. He found the exact solution ([1] eq.18 p.195) and noticed that the approximate Einstein's solution is the exact one by substituting the Einstein radial coordinate r with $(r^3+\alpha^3)^{1/3} = r(1+\alpha^3/r^3)^{1/3}$; since the term within parenthesis differs from 1 by a quantity of the order of 10^{-12}, the actual level of precision of the measurements cannot make a distinction between the two kind of metrics. Quite a different behavior appears in the strong field limit as it will be shown later.

1.3 Different nature of r and different centers of spherical symmetry for the two kind of metrics

The further analysis to discriminate among these two kind of metrics involves the nature of the r coordinate that represents two very different quantities in the two metrics. In effect can be demonstrated that, in the Schwarzschild metric (1), r is the usual radial coordinate analogue of the coordinate in

Minkowski space and $r = 0$ is the actual center of the configuration with a finite curvature: in the derivation of metric (1), Schwarzschild never changes the nature of r (see [1] eq.7) that corresponds to the radial coordinate of the Minkowski space. $r = 0$ corresponds to the center of the distribution and this is demonstrated if one looks at a curvature invariant, the Kretschmann scalar, that is maximized at $r = 0$ as it is required. In effect, considering the nonsingular Schwarzschild solution, its expression is

$$R_{kr} = R_{\mu\nu\lambda\xi}R^{\mu\nu\lambda\xi} = \frac{12\alpha^2}{\left(r^3+\alpha^3\right)^2} \tag{9}$$

that has a maximum finite value in $r = 0$ of $R_{kr}(0) = 12/\alpha^4$.

At the same time, the Gaussian Curvature is defined by

$$K_S = \frac{R_{1212}}{g} = \frac{1}{R^2} = \frac{1}{(r^3+\alpha^3)^{2/3}} \tag{10}$$

so that for $r = 0 \Rightarrow K_S = 1/\alpha^2$ so K_S is finite at the center.

On the other side, the r of the Schwarzschild-hilbert metric (5) it is not the radial coordinate neither a distance at all but it is, actually, the square of the inverse of the Gaussian curvature of a spherically symmetric geodesic surface in the spatial section of the spacetime manifold because

$$K_{SH} = \frac{R_{1212}}{g} = \frac{1}{r^2}\,. \tag{11}$$

Where are the centers of spherical distribution for the two kind of metric? The answer to this question can be given by the quantity that represents the *proper distance* $R_p(r) = \int g_{11}dr$.

In the Schwarzschild-Hilbert case (5),

$$\begin{aligned} R_p(r) &= \int g_{11}dr = \int \frac{1}{\sqrt{1-\dfrac{\alpha}{r}}}\,dr = \\ &= \sqrt{r}\,\sqrt{r-\alpha} + \alpha\ln\left[2\left(\sqrt{r}+\sqrt{r-\alpha}\right)\right] + C \end{aligned} \tag{12}$$

where C is a constant. The center r_c of the distribution is found setting the proper distance equal to zero ($R_p(r_c) = 0$) that happens for $r_c = \alpha$ and $C = -\alpha\ln\left(2\sqrt{\alpha}\right)$. Finally the expression for the proper distance is [2, 3]

$$R_p(r) = \sqrt{r}\,\sqrt{r-\alpha} + \alpha\ln\left(\frac{\sqrt{r}+\sqrt{r-\alpha}}{\sqrt{\alpha}}\right). \tag{13}$$

So, in the Schwarzschild-Hilbert metric $\alpha \equiv 2m < r \leqslant \infty$, while the range of the proper distance is $0 \leqslant R_p \leqslant \infty$, there is no meaning for $r \leqslant 2m$ coherently with its nature connected with the Gaussian curvature and the center of the distribution is $r_c = 2m$.

This means that, if is given a Minkowski spacetime, where $\mathbf{E}^3$ is its Euclidean space, the center of the spherical symmetry is $r_c = 0$ and r coincides with the proper distance R_p and with the radius of Gaussian curvature R_G, $r = R_p = R_G$, considering the metric manifold $\mathbf{M}^3$, that is the spatial part of Schwarzschild-Hilbert spacetime, then the central point $R_p(r_c) = 0$ corresponds to the point $r_c = 2m$ in $\mathbf{E}^3$ that is any point on a spherical surface centered in $r = 0$ with radius $r = 2m$. Only in this way there is a one to one correspondence between all points of $\mathbf{E}^3$ and $\mathbf{M}^3$.

In the Schwarzschild case (7) instead,

$$\begin{aligned} R_p(r) &= \int g_{11}dr = \int \sqrt{\frac{r^4\left(r^3+\alpha^3\right)^{-\frac{4}{3}}}{1-\dfrac{\alpha}{\left(r^3+\alpha^3\right)^{\frac{1}{3}}}}}\,dr = \\ &= \left(r^3+\alpha^3\right)^{-\frac{1}{3}} \times \sqrt{\left(r^3+\alpha^3\right)^{\frac{4}{3}} - \alpha\left(r^3+\alpha^3\right)} + \\ &+ \alpha\ln\left[2\left(r^3+\alpha^3\right)^{\frac{1}{6}} + 2\sqrt{\left(r^3+\alpha^3\right)^{\frac{1}{3}} - \alpha}\right] + C. \end{aligned} \tag{14}$$

The center of the distribution r_c if found setting $R_p(r_c) = 0$ that is for $r_c = 0$ and $C = -\alpha\ln\left(2\sqrt{\alpha}\right)$ so that the expression for the proper distance is

$$\begin{aligned} R_p(r) &= \left(r^3+\alpha^3\right)^{-\frac{1}{3}}\sqrt{\left(r^3+\alpha^3\right)^{\frac{4}{3}} - \alpha\left(r^3+\alpha^3\right)} + \\ &+ \alpha\ln\left[\frac{\left(r^3+\alpha^3\right)^{\frac{1}{6}} + \sqrt{\left(r^3+\alpha^3\right)^{\frac{1}{3}} - \alpha}}{\sqrt{\alpha}}\right]. \end{aligned} \tag{15}$$

In conclusion, in Schwarzschild metric (1) r is the actual radial coordinate that goes from 0 to ∞ (whole manifold) and $r = 0$ is recognized to be the center where the Kretschmann scalar is maximized (9) and the Gaussian Curvature $K_S(r) = 1/R(r)^2$ is finite since it goes from $K_S(0) = 1/\alpha^2$ to $K_S(\infty) = 0$. In Schwarzschild-Hilbert metric, (5) instead, r has nothing to do with the radial coordinate or distance but it is actually related to the Gaussian curvature $K_{SH} = 1/r^2$ and it is defined only from $2m$ to ∞ as recognized by Droste [5].

2 Metric inside matter and equilibrium equations

Let's consider a mass of degenerate matter (without source of energy [10]) in a finite volume, the full treatment consists in solving Einstein's equations (equilibrium equations) together with an appropriate equation of state for the matter. There are well known studies dedicated to the analysis of equilibrium in the strong field limit, for massive compact objects in the environment of the singular Schwarzschild-Hilbert metric, where neutron massive cores of neutron stars have been considered, imposing different equations of state for the neutron matter.

Anyway, all these different equations of state, from the pioneer and fundamental work of Oppenheimer and Volkoff [7] to the more realistic models [11] [12], share an important common characteristic: all these models, applied to the singular metric (5), predict some theoretical upper limit to a

mass in equilibrium due to the intrinsic relativistic effect of the metric itself, and a consequent final collapse above this limit. The difference between these approaches regards the value of the limit that can change from 0.7 solar masses in the Oppenheimer-Volkoff (O-V) model to few solar masses in the other models [13]. Above these limits nothing can stop the object from the final collapse inside its "Schwarzschild" radius $2m$ and then, because of the changing of sign, up to a not avoidable final singularity, where curvature reaches an infinite value and the known physics meets its limits.

In this article, one of these models will be considered, in particular the O-V model in the environment of the nonsingular Schwarzschild metric (7) in the form valid inside the matter. The O-V model is not quite realistic because it considers the neutrons as a Fermi gas; however, no matter which model is considered, all the models predict a limit to the mass because of the singular metric, while it will be shown that in a nonsingular metric even the O-V model, that otherwise gives the sharper limit to the mass (≈ 0.7 of solar mass), does not show it, instead it gives the equilibrium radius for any value of the mass.

The procedure will follow the original one given by Oppenheimer and Volkoff so that the results can be directly compared. The difference will be that the nonsingular Schwarzschild metric inside matter will be applied instead of the singular one and the equations derived from the latter can be obtained from the former setting $\sigma = 0$.

Let's consider the static metric (7) with spherical symmetry, valid in empty space and set the g_{00} and g_{11} elements in the general exponential form:

$$ds^2 = e^{\nu(r)}dt^2 - e^{\lambda(r)}dr^2 - \left(r^3+\sigma\right)^{2/3}\left(d\theta^2+\sin^2\theta d\phi^2\right). \quad (16)$$

Solving Einstein's equations (see Appendix A) the metric inside the matter is found:

$$ds^2 = \left(1-\frac{2m(r)}{\left(r^3+8m^3\right)^{1/3}}\right)dt^2 - \frac{r^4\left(r^3+8m^3\right)^{-4/3}}{1-\dfrac{2m(r)}{\left(r^3+8m^3\right)^{1/3}}}\,dr^2 - \left(r^3+8m^3\right)^{2/3}\left(d\theta^2+\sin^2\theta d\phi^2\right). \quad (17)$$

The system of equilibrium equations becomes:

$$\left.\begin{aligned}\frac{dp(r)}{dr} &= -\frac{(p(r)+\varrho(r))\left[m(r)+4\pi\left(r^3+\sigma\right)p(r)\right]}{\dfrac{\left(r^3+\sigma\right)^{4/3}}{r^2}\left[1-\dfrac{2m(r)}{\left(r^3+\sigma\right)^{1/3}}\right]}\\ \frac{dm(r)}{dr} &= 4\pi\varrho(r)r^2\end{aligned}\right\}. \quad (18)$$

where $\sigma = 8m^3$ and

$$m(r) = \frac{1}{2}\left(r^3+8m^3\right)^{1/3}\left(1-e^{-\lambda}\frac{r^4}{\left(r^3+8m^3\right)^{4/3}}\right).$$

If one sets $\sigma = 0$ in the first equation of (18), then the Tolman-Oppenheimer-Volkoff equation (A-4) can be obtained; equations (18) together with an equation of state $\varrho = \varrho(p)$ constitute the system to be integrated.

3 Equation of state and numerical integration

Following the procedure by Oppenheimer and Volkoff [7], the matter is considered to consist of particles with rest mass μ_0 obeying Fermi statistics, neglecting thermal energy and forces between them; the equation of state can be put in the parametric form

$$\varrho = K\left(\sinh(t) - t\right),$$

$$p = \frac{1}{3}K\left(\sinh(t) - 8\sinh(t/2) + 3t\right),$$

where $K = \pi\mu_0^4c^5(4h^3$ and $t = 4\log(\hat{p}/\mu_0c + [1+(\hat{p}/\mu_0c)^2]^{1/2})$ where $\hat{p}$ is the maximum momentum in the Fermi distribution related to the proper particle density $N/V = 8\pi\hat{p}^3/(3h^3)$.

Setting $K = 1/4\pi$ the units of length a and of mass b are fixed such that, for neutron gas,

$$a = \frac{1}{\pi}\left(\frac{h}{\mu_0c}\right)^{2/3}\frac{c}{(\mu_0G)^{1/2}} = 1.36\times10^6\text{cm} \quad (19)$$

and $b = c^2a/G = 1.83\times10^{34}$g.

Finally the system of adimensional equations, renaming the adimensional mass $m(r) \equiv u(r)$, to be integrated are

$$\left.\begin{aligned}\frac{du}{dr} &= r^2\left(\sinh(t)-t\right)\\ \frac{dt}{dr} &= -\frac{4(\sinh(t)-2\sinh(t/2))}{\dfrac{r^3+8m^3}{r^2}\left[\left(r^3+8m^3\right)^{1/3}-2u\right]}\times\\ &\times\frac{\left[\frac{1}{3}\left(r^3+8m^3\right)(\sinh(t)+8\sinh(t/2)+3t)+u\right]}{\cosh(t)-4\cosh(t/2)+3}\end{aligned}\right\}. \quad (20)$$

This system is the analogous of the system integrated by Oppenheimer and Volkoff ([7], Eqs. 18 and 19) which can be obtained setting $\sigma \equiv \alpha^3 \equiv 8m^3 = 0$.

The procedure followed by Oppenheimer and Volkoff first fixes the value t_0 for the parameter t when $r = 0$ (determining central energy density and pressure), then the equations in [7] are numerically integrated for several finite values of t_0. Another boundary condition can be obtained setting of $u(0) \equiv u_0 = 0$. The equations are integrated till a value of $r = r_b$ for which t (and consequently the pressure) drops to 0, representing the border radius of the matter distribution; the corresponding value $u(r_b) = m$ is then, the value of the mass that can stay in equilibrium with a radius r_b and the imposed central density.

In the original paper (O-V) the first 4 results for t_0 equal to 1, 2, 3 and 4 are reported in a table (table I in [7], reported

Table 1: Comparison with Oppenheimer Volkoff table [7]; numbers not in parenthesis are in units a and b defined in (19).

	$m(M_s)$	$t_0(\varrho_0(10^{14}\mathrm{g/cm^3}))$	r_b (km)
O-V	0.033 (0.30)	1.000 (1.014)	1.550 (21.1)
Eqs. (20)	0.033 (0.30)	1.006 (1.033)	1.506 (20.49)
O-V	0.066 (0.60)	2.000 (9.418)	0.980 (13.33)
Eqs. (20)	0.066 (0.60)	1.835 (6.923)	1.001 (13.61)
O-V	0.078 (0.71)	3.000 (40.62)	0.700 (9.52)
Eqs. (20)	0.078 (0.71)	2.166 (12.376)	0.861 (11.71)

here in table 1) together with an asymptotic value: the characteristics of the results is that, starting from $t_0 = 1$, the mass is increasing for increasing t_0 (the central density) but soon, for $t_0 = 3$, the mass reaches its maximum value calculated to be $M_{max} = 0.71$ solar masses.

Increasing further t_0, causes a decreasing of values for the mass (see [7], Fig. 1) so, for $m < M_{max}$ there are two values for central density but only the lower value must be considered to describe stable neutron stars; the maximum mass is thus considered the maximum possible mass for a stable equilibrium configuration of neutron stars with a Fermi equation of state as obtained by Oppenheimer and Volkoff. Different equations of state give different values of the maximum mass (till some units of solar masses) but anyway, as it will be seen later, a limit exists and is due to the use of the singular metric.

In our case, the equations to be integrated (20) came from the Schwarzschild nonsingular metric (17) so results can be quite different: in particular, there is an additional parameter that is the constant mass m, as seen by a distant observer. The integration procedure must then be modified: first, the parameter m is set and a prove of integration is performed starting from a low value of the central parameter t_0; integration on r ends at $r = r_b$, the border radius, where $t(r_b) = 0$ (null pressure): if the starting value t_0 is set too low, then the resulting mass would be $u(r_b) < m$. If this would be the case, then it would be necessary to increase t_0 to the minimum value such that $u(r_b) = m$. This minimum value t_0 together with m fixed and r_b found, will be the correct values for central density and pressure, mass and radius of the configuration in stable equilibrium.

For low values of the mass, i.e. for weak gravitational fields, results are expected to be similar to those of O-V while for increasing mass values the nonsingular metric should lead to results very different from those resulting from the singular one. In table I, the results are compared with the first three values of O-V table. It can be noted that for the lower mass (0.30 M_s), almost the same values are obtained for central density and radius, while on increasing the mass, the two approaches diverge and the nonsingular one leads to a "softer" equilibrium, with lower central density and greater radius, with respect to the O-V calculation.

If the mass is further increased, the two metrics behave in a complete different way: the O-V equations show a decreasing mass and a mass above the maximum found limit $0.71M_s$ cannot be sustained in equilibrium. On conversely, the nonsingular Schwarzschild metric will permit equilibrium for increasing masses and will not have a limit mass. The central density indeed will meet a maximum limit and, then, will decrease for increasing masses. At the same time the radius, instead of continuously decreasing for increasing masses as in O-V case, will show a minimum to keep the equilibrium configuration.

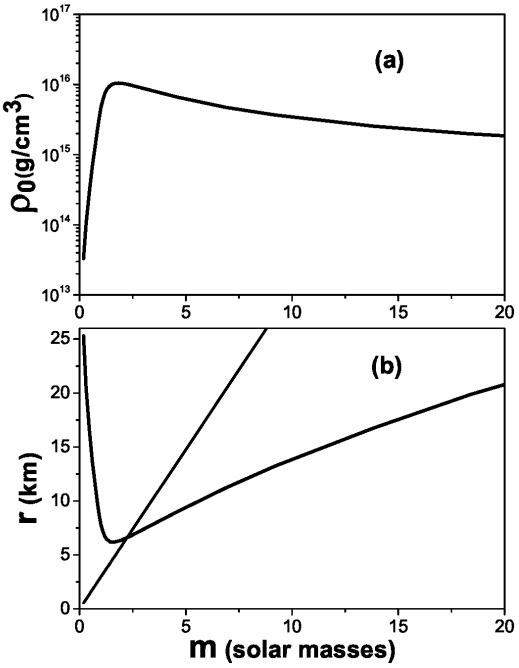

Fig. 1: Central density and equilibrium radius vs. mass: (a) central density shows a maximum; (b) equilibrium radius shows a minimum, straight line represents the so called Schwarzschild radius for that mass.

Let's first consider the behavior of various parameters for low masses: in Fig. 1 values of central density ρ_0 and radius r_b for low masses (up to 20 solar masses) are plotted; turning zones are clearly visible before the value of 2 solar masses in which the central density reaches a maximum and the radius a minimum. In particular, the central density reaches the maximum value of $1.048 \times 10^{16}\mathrm{g\ cm^{-3}}$ at 1.84 solar masses while the radius reaches the minimum value of 6.172 km at 1.47 solar masses. It can be noted, in Fig. 1(b), that, in this zone, the equilibrium radius of the mass is below the value $r_b < 2m$ where $2m$ here is the constant in the denominator of the nonsingular metric and not a limit like the so called "Schwarzschild" radius for the singular metric.

The behavior of ρ_0 and r_b is, thus, totally different from the results obtained by Oppenheimer and Volkoff for the equilibrium with the singular metric; an interpretation for this behavior could derive from recalling the concept of proper mass

M^p, linked to the concept of gravitational binding energy E_B: the total mass m, i.e. the mass seen by a distant observer, is defined by $m = \int_0^{r_b} 4\pi\varrho(r)r^2dr$ but if one integrates the energy-density ϱ over the proper "local" volume, the proper mass M^p of the system can be defined.

The proper volume element $d\tau$ is defined from $d\tau^2 = g_{ij}dx^i dx^j$ where $i, j = 1, 2, 3$ are only spatial coordinates. The proper volume from the O-V singular metric (5) then is $d\tau_S = 4\pi r^2(1 - 2m/r)^{-1/2}dr$ and the proper volume from the actual Schwarzschild nonsingular metric (7) $d\tau_N S = 4\pi r^2(1 - 2m/(r^3 + \sigma)^{1/3})^{-1/2}dr$; coherently can be defined respectively as two proper masses M^P:

$$M_S^P = \int_0^{r_b} \varrho 4\pi r^2(1 - 2m/r)^{-1/2}dr \qquad (21)$$

and

$$M_{NS}^P = \int_0^{r_b} \varrho 4\pi r^2(1 - 2m/(r^3 + \sigma)^{1/3})^{-1/2}dr. \qquad (22)$$

The physical meaning of proper mass is connected with the difference $M^P - m = E_B$ where E_B is the gravitational binding energy ([14] p. 126). In Fig. 2 the completely different behavior of the binding energy is shown, in the cases of singular solution and nonsingular solution: in the first case, the binding energy increases dramatically (together with the increasing of the central density to unphysical values) and above the maximum mass limit of about 0.7 solar masses the function becomes multivalued.

On the other side, in the nonsingular case, the binding energy increases smoothly with increasing mass and does not indicate any mass limit. In Fig. 2 only low mass values are reported but it will be shown later that, in the nonsingular case, the binding energy for higher mass values increases linearly with the mass and, considering that the ratio M^P/m in Fig. 3 tends $\to 2$, the binding energy tends to the value m of the rest mass.

Central (ϱ_0) and average $\varrho_{AV} \equiv M/(\frac{4}{3}\pi r_b^3)$ densities have a similar behavior: starting from values of $\varrho_0(0.184M_s) = 3.29 \times 10^{13} g/cm^3$ and $\varrho_{AV}(0.184M_s) = 5.40 \times 10^{12} g/cm^3$, reaching the maximum values of $\varrho_0(1.84M_s) = 1.0476 \times 10^{16} g/cm^3$ and $\varrho_{AV}(2.30M_s) = 3.688 \times 10^{15} g/cm^3$ and finally reaching the values for the last considered mass, $\varrho_0(3.68 \times 10^6 M_s) = 1.243 \times 10^{10} g/cm^3$ and $\varrho_{AV}(3.68 \times 10^6 M_s) = 8.687 \times 10^9 g/cm^3$.

Behavior evidences the presence of a maximum for both the densities and a decreasing for increasing masses: the central density converges to the average density values which decrease because volume grows with radius with an higher power than the mass.

Integration of the system (20) admits solution with an equilibrium radius for any amount of mass: in Fig. 3, higher values of mass are considered till, as an example, a value around 4 million of solar masses as it is supposed to be concentrated in the Milky Way's center.

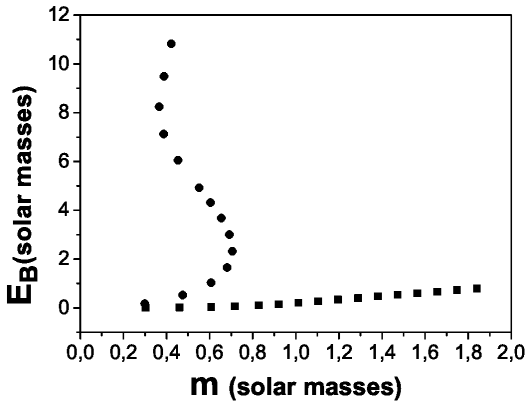

Fig. 2: Gravitational binding energy vs. mass: comparison between Oppenheimer-Volkoff results [7] (multivalued line with circles) and this article results (squares).

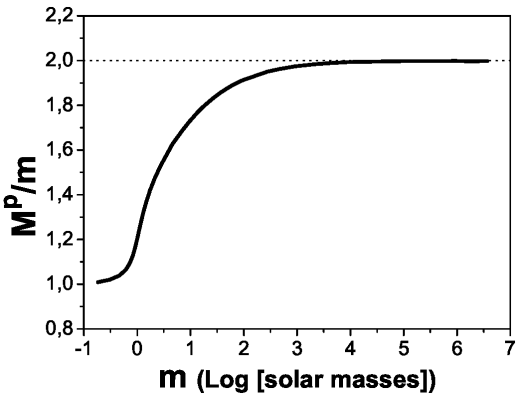

Fig. 3: Ratio between proper mass and mass vs. mass logarithm: limit tends to value 2 corresponding to an efficiency of 100% of mass conversion in gravitational binding energy

Together with the density decreasing with mass, there is another peculiar behavior, the one referred to the ratio of proper mass on mass: in Fig. 3 it is shown that this ratio tends to the value 2, meaning that there ia a 100% efficiency in converting mass into binding energy. The total mass of the compact object includes both the rest-mass energy and the negative binding energy so that the mass of the collapsed object is smaller than the sum of the component particles [15]. For neutron stars this mass deficit can be as large as 25% [16] but here it increases till 100% above 1 thousand of solar masses (depending on the equation of state) and this can be the mechanism to support stable equilibrium for such objects.

4 Inequality for nonexistance of a limit mass

Numerical results show that there is not a mass limit for equilibrium. This result can be seen also analytically trying to find an upper limit for the mass, independently from the specific equation of state. This limit exists in the case of singular

metric and it is possible to see that this limit does not exist in the case of nonsingular metric following the procedure expressed, for example, by R.M. Wald [14, p. 130].

A first less sharp limit exists for the singular metric as necessary condition for the metric to be static: a metric is said to be static if it is stationary and, in addition, exists a spacelike hypersurface Σ (orthogonal to the timelike Killing vector field ξ^α); in order for Σ to be spacelike the necessary condition for staticity is that the radial element of the metric g_{11} would be greater than zero (in the following calculation, it will be used the Wald notation of $g_{11} \equiv h(r)$ and $g_{00} \equiv f(r)$, with the Suffix S to indicate the expression from the singular metric and NS for the nonsingular one).

So for the two metrics (5) and (7) it will be

$$h_S(r) = \left(1 - \frac{2m(r)}{r}\right)^{-1} \tag{23}$$

and

$$h_{NS}(r) = r^4\left(r^3 + \sigma\right)^{-4/3}\left(1 - \frac{2m(r)}{(r^3+\sigma)^{1/3}}\right)^{-1}. \tag{24}$$

The necessary condition for stability implies that, for a given mass M and equilbrium radius r_b, $h(r_b) > 0$ so, it clearly requires a limit for M only in the singular case, that is $M < r_b/2$ (eq. 6.2.32 in [14]) while, in the nonsingular case, $h_{NS}(r_b) > 0$ is always satisfied for any value of M and r_b (considering that $\sigma \equiv 8M^3$).

This limit for M (for the singular metric) can be sharpened using the condition $g_{00} \equiv f(r) \geqslant 0$ that imposes the Killing field ξ^α to be timelike everywhere. The term $f(r)$ has the form, for the singular and nonsingular metric, respectively

$$\left.\begin{aligned} f_S(r) &= \left(1 - \frac{2m(r)}{r}\right) \\ f_{NS}(r) &= \left(1 - \frac{2m(r)}{(r^3+\sigma)^{1/3}}\right) \end{aligned}\right\}. \tag{25}$$

Since $f(r)$ must be greater than zero everywhere, it could seem that it would be necessary to know the specific equation of state for matter but, actually, the only conditions that must be assumed are very basic i.e. the density must be such that $\varrho \geqslant 0$ and $d\varrho/dr \leqslant 0$ while there is no need for whatsoever assumption about pressure P.

Applying these conditions, the following inequalities are obtained (see Appendix B): in the singular case it is found an upper mass limit

$$M \leqslant \frac{4}{9}\, r_b\,, \tag{26}$$

in the nonsingular case, instead, the following inequality is found:

$$1 - \left(\frac{8M^3}{r_b^3 + 8M^3}\right)^{\frac{1}{3}} \geqslant \frac{1}{9}\left(1 - \frac{8M^3}{r_b^3 + 8M^3}\right). \tag{27}$$

Since it is always true that $0 \leqslant 8M^3/(r_b^3 + 8M^3) \leqslant 1$, the inequality for the nonsingular case (27), i.e. the condition of stability, is always satisfied for any values of both M and r_b so that there is no upper limit for the mass, to have equilibrium, whatever would be the, reasonable, equation of state.

5 Conclusions

In conclusion, the application of the class of nonsingular static spherically symmetric metrics (particularly the Schwarzschild solution [1]) to the problem of hydrostatic equilibrium gives completely different solutions from those of the singular case. In this latter, there is a mass limit (whose value depends from the specific state equation) for dense cores of degenerate matter: above this limit, nothing can stop the configuration from a final gravitational collapse with formation of event horizon and inner physical singularity. In the case of nonsingular metric (that does not include the possibility of an event horizon) instead, the equilibrium is always reached whatever would be the amount of mass.

The application with a Fermi gas state equation, as in the Oppenheimer-Volkoff work [7], shows that central density has the same behavior, for increasing mass, than average density i.e. a maximum (with reasonable physical value), before reaching the 2 solar masses and then a decreasing. The equilibrium radius of the system shows a minimum before the 2 solar masses then grows with increasing masses but remaining well below the so called "Schwarzschild radius" for that mass which, in the nonsingular metric environment, is not the dimension of an event horizon but only a parameter connecting the general relativistic metric with the newtonian one. Proper mass of the system tends to the limit of twice the mass. This means that the negative binding energy tends to the limit of m counterbalancing the gravitational mass m. This is a mechanism that can stop gravitational collapsing and that can sustain stable equilibrium.

Considering experimental observations, weak field experiments give same results, within errors, for the singular and nonsingular metrics, while for strong fields, the nonsingular metric admits stable configuration of greater amount of mass while singular metrics admits black hole formation. Few observational, indirect, evidences for black holes existence have been performed in years but it seems that an alternative hypothesis of very compact degenerate matter configurations, permitted by nonsingular metrics, could be compatible with observations: let's consider, for example, a single nonrotating compact object of 9.2 solar masses (m=1 in units of (19)), in the singular metric, it would be a black hole, no matter of which state equation is used, and a "Schwarzschild radius" $r_s = 27.17$ km would define the horizon event whose surface would have an infinite gravitational redshift and would surround a pointlike singularity.

The application of nonsingular metric (with a Fermi equation of state) instead, would give a very compact object, of

radius $r_b = 13.23$km, made by ordinary (degenerate) matter with a central density $\varrho_0 = 13.23 \times 10^{15} g/cm^3$; the density value is not far from the ordinary nuclear density, moreover a more realistic state equation would keep density value within reasonable physical limit.

Gravitational redshift factor $f = \sqrt{-g_{11}}$ (the ratio between wavelength observed at infinity and wavelength emitted at distance r) at the surface of the matter configuration would be $f = 1.165$. This redshift would correspond, in the black hole case, to a redshift of a photon emitted ad distance $r = r_s f^2/(f^2 - 1) = 3.8 r_s$. This difference, theoretically, could be observable but total luminosity would be so faint not to permit direct observations while indirect observations due to, for example, the accretion disk surrounding these compact objects, would be very similar. The existence of compact massive (several solar masses) objects could justify why observed emissions from individuated neutron stars and black hole candidates are so similar [17] despite the totally different characteristics of a hard surface and an event horizon.

Recent observations involving magnetic fields of quasars also put in doubt the existence of inner super-massive black holes [18]. It must be remarked that at the state of the art there is still no observational proof of a black hole event horizon [19].

Lack of single compact objects of very great mass it is due more to mechanism of formation of such object than to some mass limit, anyway in the galactic's centers there is gravitational evidence for compact objects of millions of solar masses. Let's resume how it would be such an object in the nonsingular model with a Fermi gas state equation (others EOS would not change the qualitative features): considering an object 3.6 millions of solar masses, it would have a radius of about $58,000$ km that is the half percent of its estimated "Schwarzschild radius" in the black hole hypothesis, a central density $\varrho_0 = 1.24 \times 10^{10} g/cm^3$ and a central pressure $P_0 = 7.3 \times 10^{16}$ Pa both smoothly decreasing outward.

Sagittarius A, the radio point source associated with the dark mass located at the center of the Milky Way, is the best studied black hole candidate to date, but till now has not be possible to verify or to exclude the presence of a horizon [20]. The horizon existence has been inferred because a surface emission, to remain undetected, would require large radiative efficiencies, greater than 99.6% [21] anyway, this is actually the phenomenon predicted by the application of nonsingular metric, because, as seen in Fig. 3, the limit value of 2 for the ratio M^P/M means an efficiency limit of about 100%. This could be justified, actually, by a not exotic object having a hard surface, emissions and gravitational effects compatible with observations, and that could be permitted because the contribution of the negative binding energy.

Submitted on February 16, 2014 / Accepted on February 24, 2014

References

1. Schwarzschild K. Über das Gravitationsfeld eines Massenpunktes nach der Einsteinschen Theorie (On the Gravitational Field of a Mass Point According to Einstein's Theory), *Sitzungsber. Preuss. Akad. Wiss., Phys. Math. Kl.*, 1916, v. 1916a, 189–196.
2. Crothers S.J. The Schwarzschild solution and its implications for gravitational waves: Part I. *SPESIF-2009* (Space, Propulsion and Energy Sciences International Forum 2009), Huntsville, AL, Von Braun Center, February 24-27, 2009; http://viXra.org/abs/1405.0326
3. Crothers S.J. The Schwarzschild solution and its implications for gravitational waves: Part II. *SPESIF-2009* (Space, Propulsion and Energy Sciences International Forum 2009), Huntsville, AL, Von Braun Center, February 24-27, 2009; http://viXra.org/abs/1405.0325
4. Brillouin M. The singular points of Einstein's universe. *J. Phys. Radium*, 1923, v. 23, 43–46.
5. Droste J. The field of a single centre in Einstein's theory. *Ned. Acad. Wet.*, 1917, v. 19, 197–215.
6. Hilbert D. Die Grundlagen der Phisik. *Nachr. Ges. Wis. Göttingen Math. Phys. Kl.*, 1915, 395–407.
7. Oppenheimer J.R., Volkoff G.M. On massive neutron cores. *Phys. Rev.*, 1939, v. 55, 374–381.
8. Abrams L.S. Black holes: the legacy of Hilbert's error. *Can. J. Phys.*, 1989, v. 67, 919–934.
9. Stavroulakis N. On a paper by J. Smaller and B. Temple. *Ann. Fond. de Broglie*, 2002, v. 27(3), 511–519.
10. Landau L. On the theory of stars. *Physik. Zeits. Sowjetunion*, 1932, v. 1, 285–288.
11. Rhoades C.E., Ruffini R. Maximum mass of a neutron star. *Phys. Rev. Lett.*, 1974, v. 32, 324–327.
12. Srinivasan G. The maximum mass of neutron stars. *Bull. Astr. Soc. India.*, 2002, v. 30, 523–547.
13. Hartle J.B., Sabbadini A.G. The equation of state and bounds on the mass of nonrotating neutron star. *Astrophys. J.*, 1977, v. 213, 831–835.
14. Wald R.M. General Relativity. The University of Chicago Press, Chicago, 1984.
15. Alécian E., Morsink S.M. The effect of neutron star gravitational binding energy on gravitational radiation-driven mass-transfer binaries. *Astrophys. J.*, 2004, v. 614, 914–921.
16. Cook G.B., Shapiro S.L., Teukolsky S.A. Rapidly rotating neutron stars in general relativity realistic equation of state. *Astrophis. J.*, 1994, v. 424, 823–845.
17. Ed. Maccarone J., Fender R. P., Ho L.C. From X-ray Binaries to Quasars: Black Holes on all Mass Scales. Springer, the Netherlands, 2005.
18. Schild R.E., Leiter D.J. Black hole or MECO? decided by a thin luminous ring structure deep within Quasar Q0957+561. *J. of Cosmology*, 2010, v. 6, 1400–1437.
19. Abramowicz M.A., Kluzniak W., Lasota, J.P. No observational proof of black hole event-horizon. *Astronomy and Astrophysics*, 2002, v. 396, L31–L34.
20. Broderick A.E., Narayan R. On the Nature of the Compact Dark Mass at the Galactic Center. *Astrophys. J.*, 2006, v. 638 (1), L21–L24.
21. Broderick A.E., Loeb A., Narayan R. The event horizon of Sagitarius A. *Astrophys. J.*, 2009, v. 701, 1357–1366.
22. Tolman R.C. Relativity Thermodynamics and Cosmology. University Press, Oxford, 1934.

Appendix A

The only non vanishing components of the Einstein Tensor G are G^0_0, G^1_1 and $G^2_2 = G^3_3$. Considering a matter that supports no transverse stresses and has no mass motion then the energy momentum components are [22] $T^1_1 = T^2_2 = T^3_3 = -p$ and $T^0_0 = \varrho$ where p is the pressure and ϱ is the macroscopic energy density measured in proper coordinates. So Einstein's equations are

$$G^0_0 = 8\pi T^0_0 = 8\pi\varrho = e^{-\lambda}\left[\frac{\lambda' r^2}{r^3+\sigma} - \frac{r^4}{(r^3+\sigma)^2} - \right.$$
$$\left. - \frac{4r\sigma}{(r^3+\sigma)^2}\right] + \frac{1}{(r^3+\sigma)^{2/3}} \qquad \text{(T00)}$$

$$G^1_1 = 8\pi T^1_1 = 8\pi p = e^{-\lambda}\left[\frac{\nu' r^2}{r^3+\sigma} + \frac{r^4}{(r^3+\sigma)^2}\right] -$$
$$- \frac{1}{(r^3+\sigma)^{2/3}} \qquad \text{(T11)}$$

$$G^2_2 = 8\pi T^2_2 = e^{-\lambda}\left[\frac{(\nu'-\lambda')r^2}{2(r^3+\sigma)} - \frac{\lambda'\nu'}{4} + \frac{\nu'^2}{4} + \right.$$
$$\left. + \frac{2r\sigma}{(r^3+\sigma)^2} + \frac{\nu''}{2}\right] + \frac{1}{(r^3+\sigma)^{2/3}} \qquad \text{(T22)}$$

where p, ϱ, λ and ν are functions of r and the primes indicates a differentiation with respect to r. Since $T^1_1 = T^2_2$ then $(T^1_1 - T^2_2)\times 2/r = 0$ and from equations (T00) it is easy to verify that

$$\frac{d}{dr}\left(-T^1_1\right) + \left(T^0_0 - T^1_1\right)\frac{\nu'}{2} = \left(T^1_1 - T^2_2\right)\frac{2}{r} = 0 \qquad \text{(A-1)}$$

so that this latter equation can be read

$$\frac{dp}{dr} = -\frac{p+\varrho}{2}\,\nu'. \qquad \text{(A-2)}$$

Equations (T00), (T11) and (A-2) constitute the system of equations to be solved and correspond to the ones in Oppenheimer Volkoff article [7, Eqs. 4,3 and 5] if σ is set equal to 0; an opportune equation of state $\varrho = \varrho(p)$ must also be included in the system.

Eliminating ν' in (T11) and (A-2), the hydrostatic equilibrium equation in exponential form is

$$\frac{dp}{dr} = -\frac{p+\varrho}{2}\times$$
$$\times\left[8\pi p\, e^{\lambda}\frac{(r^3+\sigma)}{r^2} + e^{\lambda}\frac{(r^3+\sigma)^{1/3}}{r^2} - \frac{r^2}{(r^3+\sigma)}\right]. \qquad \text{(A-3)}$$

If it is set $\sigma = 0$ and the singular metric (5) (inside the matter) is considered where $e^{\lambda(r)} = (1-2m(r)/r)^{-1}$ (and consequently $m(r) = \frac{1}{2}r(1-e^{-\lambda})$) then the Tolman-Oppenheimer-Volkoff equilibrium equation is obtained

$$\frac{dp}{dr} = -\frac{(p(r)+\varrho(r))\left[m(r)+4\pi r^3 p(r)\right]}{r^2\left(1-\dfrac{2m(r)}{r}\right)}. \qquad \text{(A-4)}$$

In our case (A-3) instead, it is possible to give the correct physical meaning to $m(r)$ setting, for the nonsingular metric inside the matter,

$$e^{\lambda(r)} = \frac{(r^3+\sigma)^{-4/3}}{1-\dfrac{2m(r)}{(r^3+\sigma)^{1/3}}}\, r^4; \qquad \text{(A-5)}$$

in effect, at the border $r = r_b$ there will be continuity with the metric in vacuum (7) and (6) so that

$$e^{\lambda(r_b)} = e^{\lambda} = \frac{r^4(r^3+8m^3)^{-4/3}}{1-\dfrac{2m}{(r^3+8m^3)^{1/3}}}$$

and $m(r_b)$ will assume its value m as seen by an external observer

$$m(r_b) = \frac{1}{2}\left(r_b^3+8m^3\right)^{1/3}\left(1-e^{-\lambda}\frac{r_b^4}{\left(r_b^3+8m^3\right)^{4/3}}\right) = m. \qquad \text{(A-6)}$$

Finally the Schwarzschild metric inside the matter (in continuity with (7) where it is set $\alpha = 2m(r)$ and $\sigma = 8m^3$ so that $\sigma = \alpha^3$ outside the matter) will be

$$ds^2 = \left(1-\frac{2m(r)}{(r^3+8m^3)^{1/3}}\right)dt^2 -$$
$$- \frac{r^4\left(r^3+8m^3\right)^{-4/3}}{1-\dfrac{2m(r)}{(r^3+8m^3)^{1/3}}}\,dr^2 - \qquad \text{(A-7)}$$
$$- \left(r^3+8m^3\right)^{2/3}\left(d\theta^2+\sin^2\theta d\phi^2\right).$$

So, with $e^{\lambda(r)}$ given by (A-5), the equilibrium equation (A-3) (that is the merging of the two Einstein's equations (T11) and (A-2)) and the other Einstein's equation (T00) will become respectively

$$\left.\begin{aligned}\frac{dp(r)}{dr} &= -\frac{(p(r)+\varrho(r))\left[m(r)+4\pi(r^3+\sigma)p(r)\right]}{\dfrac{\left(r^3+\sigma\right)^{4/3}}{r^2}\left[1-\dfrac{2m(r)}{(r^3+\sigma)^{1/3}}\right]}\\ \frac{dm(r)}{dr} &= 4\pi\varrho(r)r^2\end{aligned}\right\}, \qquad \text{(A-8)}$$

where $\sigma = 8m^3$.

Appendix B

Pressure P can be eliminated from Einstein's equations considering that $G^1_1 - G^2_2 = 0$, this, together with the definition of $h(r)$ (23) leads to the following equation for the singular metric (using the notation by Wald, eq. 6.2.34 in [14])

$$\frac{d}{dr}\left[r^{-1}h_S(r)^{-1/2}\frac{df_S^{1/2}(r)}{dr}\right] = \\ = \left[f_S(r)h_S(r)\right]^{1/2}\frac{d}{dr}\left[\frac{m(r)}{r^3}\right] \tag{B-1}$$

while, for the nonsingular metric

$$\frac{d}{dr}\left[(r^3+\sigma)^{-1/3}h_{NS}(r)^{-1/2}\frac{df_{NS}(r)^{1/2}}{dr}\right] = \\ = \frac{(r^3+\sigma)^{2/3}}{r^2}\left[f_{NS}(r)h_{NS}(r)\right]^{1/2}\frac{d}{dr}\left[\frac{m(r)}{r^3+\sigma}\right]. \tag{B-2}$$

The right sides for both equations are proportional to the derivative with respect to r of the average density, so because the condition $d\varrho/dr \leqslant 0$, the left sides must be both less or equivalent to 0. Integrating the inequalities for the left sides, inward from the border r_b to a generic radius r we obtain

$$\frac{1}{rh_S^{1/2}(r)}\frac{df_S(r)^{1/2}}{dr} \geqslant \frac{M}{r_b^3}, \tag{B-3}$$

$$\frac{1}{(r^3+\sigma)^{1/3}h_{NS}^{1/2}(r)}\frac{df_{NS}^{1/2}(r)}{dr} \geqslant \frac{M}{r_b^3+\sigma}. \tag{B-4}$$

These inequalities can be integrated again inward from r_b to 0. The condition $d\varrho/dr \leqslant 0$ implies that $m(r)$ cannot be smaller than the value it would have for a uniform density star so, for the singular case, $m(r) \geqslant Mr^3/r_b^3$ and, for the nonsingular one, $m(r) \geqslant M(r^3+\sigma)/(r_b^3+\sigma)$, so that inequalities (B-3 and B-4) become: for the singular case (Wald, eq. 6.2.39)

$$f_S^{1/2}(0) \leqslant \frac{3}{2}\left(1-\frac{2M}{r_b}\right)^{1/2} - \frac{1}{2} \tag{B-5}$$

and for the nonsingular case

$$f_{NS}^{1/2}(0) \leqslant \frac{3}{2}\left(1-\frac{2M}{(r_b^3+\sigma)^{1/3}}\right)^{1/2} - \frac{1}{2}\left(1-\frac{2M\sigma^{2/3}}{r_b^3+\sigma}\right) \tag{B-6}$$

(as usual for $\sigma = 0$ the two cases are equivalent). Finally, the condition $f^{1/2}(0) \geqslant 0$ implies that, for the singular case, the necessary condition for staticity involves a maximum limit for the mass: from (B-5)

$$M \leqslant \frac{4}{9}\, r_b\,. \tag{B-7}$$

For the nonsingular case instead, the stability condition implies, from (B-6) and inserting the value $\sigma \equiv 8m^3$, the inequality

$$1-\left(\frac{8M^3}{r_b^3+8M^3}\right)^{\frac{1}{3}} \geqslant \frac{1}{9}\left(1-\frac{8M^3}{r_b^3+8M^3}\right). \tag{B-8}$$

Addendum to "Phenomenological Derivation of the Schrödinger Equation"

Fernando Ogiba
E-mail: Ogiba@cpovo.net

This addendum to the article [1] is crucial for understanding how the complex effective action, despite its derivation based on classical concepts, prevents quantal particles to move along extreme action trajectories. The reason relates to homogenous, isotropic and unpredictable impulses received from the environment. These random impulses allied to natural obedience to the dynamical principle imply that such particles are permanently and randomly passing from an extreme action trajectory to another; all of them belonging to the ensemble given by the stochastic Hamilton-Jacobi-Bohm equation. Also, to correct a wrong interpretation concerning energy conservation, it is shown that the remaining energy due to these permanent particle-medium interactions (absorption-emission phenomena) is the so-called quantum potential.

1 Introduction

The central subject of the article [1] is: Quantal particles (such as electrons), due to its interactions with the environment, move in accordance with the complex effective action

$$S_{eff} = S + i\frac{\hbar}{2}\ln P \tag{1}$$

which was obtained following the classical Hamilton's dynamical principle but considering the motion as a whole, that is, taking averages. The resulting canonical equations coincide with those extracted from the Schrödinger equation writing $\psi = \sqrt{P}\exp(iS/\hbar)$, namely:

$$\frac{\partial S}{\partial t} + \frac{\nabla S \cdot \nabla S}{2m} + V + Q = 0 \tag{2}$$

and

$$\frac{\partial P}{\partial t} + \nabla \cdot \left(P\frac{\nabla S}{m}\right) = 0\,, \tag{3}$$

where

$$Q = \frac{\hbar^2}{8m}\frac{\nabla P \cdot \nabla P}{P^2} - \frac{\hbar^2}{4m}\frac{\nabla \cdot \nabla P}{P} \tag{4}$$

is the quantum potential which, visibly, is the remaining energy of two distinct concurrent phenomena.

The main motivation for writing this addendum concerns the result

$$\int P\left(i\frac{\hbar}{2}\frac{1}{P}\frac{\partial P}{\partial t}\right)d^3r = 0 \tag{5}$$

which is not the expression of energy conservation, as argued in connection with Eg. 23 of the article. In true, the null value of this average means that the involved energy (the enclosed quantity) does not remain in the particle; it is radiation, as will be shown. In doing this, it is necessary to explain how Q — as an energy resulting from the particle-medium interactions — agrees with the energy conservation required by the so-called quantum equilibrium.

Also, in the mentioned article the meaning of the effective action (1) is not so clear. It was derived supposing a particle over a possible trajectory; what, in view of the results, must be true. On the other hand, a continuous trajectory of elementary particles is an experimentally discredited concept. So, there must be a link between these two opposing points of view. In true, there is, as will be seen. Indeed, it will be shown that quantal particles occupies, sequentially and instantly, just one point over different trajectories which are randomically chosen in the ensemble (2). This means that quantal particles don't move along extreme action trajectories but occupy trajectories (permited by the dynamical principle) just for a moment.

The interacting medium — primarily responsible for quantum effects — is the zero-point field (ZPF) which, according to the classical description of the Casimir's experiment, is viewed as a homogeneous and isotropic distribution of electromagnetic waves pervading all space. As the phases of these waves are randomically distributed in the range $[0, 2\pi]$, then electrical charged particles (balanced or not) are permanently receiving unpredictable impulses. This has two main consequences: First, the accelerated charged particles radiate all the absorbed energy. Second, the unpredictable impulses prevent quantal particles to follow predictable paths. Even so, the overall motion obeys the Hamilton's principle which is founded on trajectories. How can all this happen?

2 The quantum potential and the ensemble of virtual trajectories

The answer to the above question lay in the fact that the natural behavior of any moving particle, at any time, is obeying the classical dynamical principle. This must be interpreted as follows: In the absence of random forces, they move along extreme action trajectories. However, in the case of particles which are significantly affected by the ZPF the situation is drastically modified. Indeed, homogeneous, isotropic and random forces (including beck reaction forces) are not part of the traditional classical description of the motion.

Here, it will be proved that the quantal motion occurs as follows: Immediately before any particle-field random inter-

action the particle is over a given trajectory (obedience to the dynamical principle), but upon receiving an unpredictable impulse it is withdrawing from this trajectory to an unpredictable place. Again, in the new position it continues obeying the dynamical principle; that is, the particle is over another trajectory. As this is a permanent process, then the particle occupies these possible trajectories only instantly (virtual trajectories). In a sense, we can say that the unpredictable impulse has created initial conditions (arbitrary) for a new trajectory.

In the light of the foregoing, at each position actually occupied by the particle pass an infinite number of such virtual trajectories. This assumption is in agreement with the following facts: First, Eq. (2) represents an ensemble of unpredictable trajectories; $P(\mathbf{x}, t)$ — preserving its uniqueness — can take any value at $\mathbf{x}$. Moreover, ∇P is not deterministic. Second, energy and momentum in quantum mechanics are independent of coordinates. This means that everywhere there are equivalent ensembles of partial derivatives $\partial S/\partial t$ and ∇S — requiring continuous virtual functions S — which on average give the corresponding observed quantities. This statement implies the same uncertainty everywhere (non locality). Thirty, Probability density, classically, is defined over trajectories; it is canonically conjugate to the action function S (this remains valid in the equations above). Over extreme action trajectories $\partial P/\partial t = 0$ (we know where the particle is at the time t). Therefore, if $\partial P/\partial t \neq 0$, then it means that the particle was "banned" from its trajectory.

To formally prove that the trajectories represented by the virtual ensemble (2) are instantly visited by the particle, it is necessary finding a valid expression which leads to the idea that such trajectories (or momenta ∇S) are randomly chosen (or induced) where the particle is. This is better made after knowing the meaning of the quantum potential.

If a moving particle is not actuated by random forces, then, given the potential V and the initial conditions, we can predict its extreme action trajectory. However, the presence of random forces — exactly like that found in the ZPF — modify this classical way to see the motion. This rupture relates to the fact that now there is only a probability of finding the particle at a given position at the time t.

Whenever a particle is removed from a given position by random forces, the probability of find it there is diminished. Consequently, as probability is a conserved quantity, this decrease of probability leads to the emergence of an outgoing compensatory probability current. Formally, following standard techniques and considering the ZPF properties, at each position there is a diffusion of probability density currents ($P\mathbf{v}$), in such a way that

$$\frac{\partial P}{\partial t} + \nabla \cdot (P\mathbf{v}) = 0\,. \tag{6}$$

In true, $P\mathbf{v}$ represents all possible local outflows of matter whose velocities $\mathbf{v}$ have the directions of the vectors ∇P. Therefore, all currents obey

$$P\mathbf{v} = \alpha \nabla P, \tag{7}$$

where α is a proportionality factor, to be determined.

Being the matter-field interaction conservative, then there is no net momentum transfer to the particle. This implies that the average probability density current is zero, i.e.

$$\int P\,(P\mathbf{v})\; d^3r = \int P\,(\alpha \nabla P)\; d^3r = 0\,. \tag{8}$$

Integrating the second form by parts and considering that $P \to 0$ at infinity, we find that its null value is plenty satisfied if α is a constant. In true, it is an imaginary diffusion constant because there is no effective dislocation of matter in all directions (this is a single-particle description). In fact, in accordance with the imaginary part of the effective action (1), the unpredictable impulses received by the particle are given by

$$m\mathbf{v} = \nabla \left(i\,\frac{\hbar}{2}\,\ln P \right) = i\,\frac{\hbar}{2}\,\frac{\nabla P}{P}\,, \tag{9}$$

which, compared with (7), implies that $\alpha = i\hbar/2m$.

The consequent average kinetic energy induced by the ZPF on the particle is

$$\langle T_{ZPF} \rangle = \int P \left(\frac{1}{2}\, m|\mathbf{v}|^2 \right) d^3r\,, \tag{10}$$

which considering (9), reads

$$\langle T_{ZPF} \rangle = \frac{\hbar^2}{8m} \int \frac{(\nabla P)^2}{P}\; d^3r. \tag{11}$$

However, the implicated acceleration makes the electrical charge radiates. So, we must appeal to the general rule concerning accelerated charged particles, namely: The change in the kinetic energy in the absorption-emission process is equal to the work done by the field minus the radiated energy. This is the energy conservation implicit in the determination of the Abraham-Lorentz back reaction force.

Therefore, varying the average kinetic energy, that is, taking the functional derivative of (11) with respect to P, we find that the remaining energy due to particle-field interactions is

$$\delta\langle T_{ZPF} \rangle = \frac{\hbar^2}{8m} \left(\frac{\nabla P \cdot \nabla P}{P^2} - 2\,\frac{\nabla \cdot \nabla P}{P} \right), \tag{12}$$

where, therefore, the first term relates to absorption of radiation, and the second to emission.

Coincidentally, this remaining energy is the quantum potential (4) which, therefore, is the expression of the required energy conservation implied in the so-called quantum equilibrium.

At this point we have sufficient valid information to prove that extreme action trajectories are randomly chosen at each position actually occupied by the particle.

Indeed, the probability density conservation (6), considering (9), reads

$$\frac{\partial P}{\partial t} + i\,\frac{\hbar}{2m}\nabla^2 P = 0\,, \tag{13}$$

which has the shape of a diffusion equation; local diffusion of probability density currents or virtual outflows of matter at the actual particle position.

The validity of this equation is unquestionable. In fact, it is absolutely equivalent to Eq. (3), or

$$\frac{\partial(\psi^*\psi)}{\partial t} + i\,\frac{\hbar}{2m}\,\nabla\cdot(\psi^*\,\nabla\psi - \psi\,\nabla\,\psi^*) = 0\,, \tag{14}$$

as can be proven from $|\nabla\psi|^2 = -\psi^*\nabla\psi$ and the parameterized forms of S and P in terms of ψ.

Very important, the equations (13) and (3) represent the same diffusion at each position $\mathbf{x}$ actually occupied. Equivalently, these two ways of expressing probability conservation contain implicitly all possibilities for the particle flow at $\mathbf{x}$. As Eq. (3) expresses this in terms of ∇S, then ∇S must represent all possible momenta at $\mathbf{x}$. However, as these partial derivatives require continuous action functions, then there pass multiple virtual trajectories. One of them infallibly will be occupied, but only for a moment because in the next position the same phenomenon is repeated.

In this sence, the obedience to the dynamical principle, implicit in the effective action (1), is traduced as follows: At a given time the particle is over a trajectory represented by the action S (real part), but at this very moment there is a choice for the next motion, which is dictated by the probability dependent local action (imaginary part). In other words, the imaginary part chose the next action function (S) representing another trajectory to be occupied during an infinitesimal time; and so on.

Now, it is possible to correct the interpretation given to (5) in the article [1]. Just rewrite Eq. (13) in the energy form

$$i\,\frac{\hbar}{2}\frac{1}{P}\frac{\partial P}{\partial t} = \frac{\hbar^2}{4m}\frac{\nabla\cdot\nabla P}{P}\,, \tag{15}$$

which implies that

$$\int_{all} P\left(i\,\frac{\hbar}{2}\frac{1}{P}\frac{\partial P}{\partial t}\right)d^3r = \int_{all} P\left(\frac{\hbar^2}{4m}\frac{\nabla\cdot\nabla P}{P}\right)d^3r = 0\,. \tag{16}$$

Being the second member of (15) the emitted energy of the balance (12), then the result (5) means that the involved energy doesn't remain in the particle.

3 Conslusion

The subsequent particle's positions, randomly chosen in the interactions, are on different trajectories. Therefore, there are continuous trajectories, but never followed by quantal particles. They simply represent the obedience to the mechanical principle, regardless of where the particle is. Nevertheless, as these virtual trajectories are inherent to the Schrödinger picture, then it is expected that they — properly determined and used as statistical tools - can give the same predictions. However, the convenience of such procedure needs to be better discussed.

On the other hand, were highlighted permanent emissions and absorptions of radiation, meaning that particles are actuated by forces and back reaction forces, which, on average, are zero. This explains why the interactions become transparent in the quantum description. Nevertheless, speculating, these permanent absorptions and emissions of electromagnetic waves (a delicate asymmetry accompanying particles everywhere) may be important to interpret certain properties of matter.

Submitted on March 3, 2014 / Accepted on March 11, 2014

References

1. Ogiba F. Phenomenological derivation of the Schrödinger equation. *Prog. Phys.*, 2011, no.4, 25–28.

Views about the "Oxford Questions". Wave Function Collapse and Schrödinger's Cat: Are They Real Scientific Topics or Plain Fictions?

Spiridon Dumitru

Department of Physics (retired), "Transilvania" University, B-dul Eroilor 29, 500036 Braşov, Romania
E-mail: s.dumitru42@yahoo.com

Motivated by the recently published "Oxford Questions" we review the foundational character of the wave function collapse theme. We show that the respective theme, as well as its twin analogue represented by the Schrödinger's cat problem, are not real scientific topics but plain and rather trivial fictions. Consequently, we suggest that the related items of the "Oxford Questions" have to be perceived with some epistemic caution.

1 Introduction

The newly diffused *The Oxford Questions on the Foundations of Quantum Physics* [1], known also as "*Oxford Questions*, aims to formulate "*a list of main open questions about the foundations of quantum physics*". Within the respective list, the issue "*whether or not the 'collapse of the wave packet' is a physical process*" is approached in "*several Oxford Questions: in particular, 1b, 2a, 2c, 3a, 3c and 5a*". The issue is mainly brought into attention in 3c: "*How can the progressive collapse of the wave function be experimentally monitored?*".

It is expected that, in the future, the Oxford Questions will stimulate more or less extensive studies in both advanced and pedagogic research. Previous to these studies, it is important to examine the correctness of the items gathered in the Oxford Questions, particularly the ones pertaining to the above-mentioned quantum collapse. Such an examination is intended in this short paper, by using some ideas noted in some of our recent works. Section 2 is focused on the theme of Wave Function Collapse. Additionally, in Section 3, we examine the case of Schrödinger's Cat Thought Experiment which in fact is a twin analogue of the Wave Function Collapse. We find that both the Wave Function Collapse and the Schrödinger's Cat Thought Experiment are not real scientific topics but only pure fictions.

The present paper ends in Section 4 with some closing thoughts, particularly with the suggestion that, for real science, the invalidated Oxford Questions items have to be regarded as needless.

2 On the wave function collapse

Historically speaking, the Wave Function Collapse concept was brought into scientific debate by the conflict between the following two suppositions:

$\mathbf{s}_1$ The old opinion that a Quantum Measurement of a (sub)atomic observable should be regarded as a single sampling (trial) which gives a unique deterministic value. ■

$\mathbf{s}_2$ The agreement, enforced by theoretical considerations, is such that to describe such an observable one should resort to probabilistic (non-deterministic) entities represented by an operator together with a wave function. ■

To avoid conflict between suppositions $\mathbf{s}_1$ and $\mathbf{s}_2$ it was in diffused the thesis that, during a Quantum Measurement, the corresponding wave function collapses into a particular eigenfunction associated with a unique (deterministic) eigenvalue of the implied operator. Such a thesis has led to the Wave Function Collapse concept regarded as a true dogma. The respective concept was assumed, in different ways and degrees, within a large number of mainstream publications (see [2–8] and references therein). But, as a rule, the previously mentioned assumptions were (and still are) not accompanied with adequate elucidations concerning the initial correctness of the alluded concept in relation to the natural themes of Quantum Mechanics.

Now, explicitly or implicitly, the Oxford Questions [1] put forward the problems:

$\mathbf{p}_1$ Whether or not the "collapse of the wave packet" is a physical process. ■

$\mathbf{p}_2$ How can the progressive collapse of the wave function be experimentally monitored? ■

$\mathbf{p}_3$ According to which theoretical scheme, justified by physical reality alone, can a Wave Function Collapse be described properly? (This is in the situation [6] where a whole "*zoo of collapse models*" have already been invented. ■

In order to generate significant remarks on the above-mentioned Oxford Questions problems $\mathbf{p}_1$–$\mathbf{p}_3$, now we wish to bring into attention some ideas prefigured and to a certain extent argued in our recent paper [9, 10]. We mainly pointed out the ephemeral character (i.e. caducity) of the Wave Function Collapse concept. Basically our argumentations are grounded on the following indubitable facts. Mathematically, a quantum observable (described by a corresponding opera-

tor) is a true random variable. Then, in a theoretical framework, such a variable must be regarded as endowed with a spectra of eigenvalues. For a given quantum state/system the mentioned eigenvalues are associated with particular probabilities incorporated within the wave function of the mentioned state/system. Consequently, from an experimental perspective, a measurement of a quantum observable requires an adequate number of samplings finished through a significant statistical group of data/outcomes. That is why one can conclude that the supposition $\mathbf{s}_1$ of the Wave Function Collapse concept appears as a false premise while the whole respective concept proves oneself to be a useless fiction.

The previously noted conclusion can be consolidated indirectly by mentioning the quantum-classical probabilistic similarity (see [11–14]) among quantum mechanical observables and macroscopic random variables, studied within the thermodynamic theory of fluctuations. On the whole, a macroscopic random variable is characterized by a continuous spectra of values associated with an intrinsic probability density. Then, for measuring a macroscopic random variable, a single experimental sampling delivering a unique value (result) is worthless. Such a sampling is not described as a collapse of the mentioned probability density. Similarly, a quantum measurement must not be represented as a wave function collapse. Moreover, a true experimental evaluation of a macroscopic random variable requires an adequate lot of samplings finished through a statistical set of individual results. A plausible model for a theoretical description of the alluded evaluation can be done [14–16] through an information transmission process. In the respective model, the measured system appears as an information source while the measuring device plays the role of an information transmission channel to the recorder of measurement data. As part of the mentioned measuring process, the quantum mechanical operators (describing quantum observables) preserve their mathematical expressions. Additionally, the transmission to the the recorder of quantum probabilistic attributes is described by means of linear transformations for probability density and current(associated with the corresponding wave function).

Taking into account the above mentioned indubitable arguments, we think that in natural perception the "collapse of the wave function" cannot be considered as a physical process. Consequently, the Wave Function Collapse concept does not have the qualities of a real scientific topic, it being only a purely trivial and worthless fiction. Moreover, the above noted problems $\mathbf{p}_2$ and $\mathbf{p}_3$ make no sense. That is why the further studies expected to be raised by the Oxford Questions would be more appropriate if ignoring all the elements regarding the Wave Function Collapse concept.

3 As regards the Schrödinger's cat

Subsidiarily to the above considerations about the Wave Function Collapse concept, some remarks can be brought into question [9] concerning the famous Schrödinger's Cat Thought Experiment. The essential element in the respective experiment is represented by a single decay of a radioactive atom (which, through some macroscopic machinery, kills the cat). But the individual lifetime of a single decaying atom is a random variable. That is why the mentioned killing decay is in fact a twin analogue of the above mentioned single sampling taken into account in supposition $\mathbf{s}_1$ of the Wave Functions Collapse concept. So, the previous considerations reveal the notifiable fact that is useless (even forbidden) to design experiments or actions that rely solely on a single deterministic sampling of a random variable (such is the decay lifetime). Accordingly, the Schrödinger's Cat Thought Experiment appears as a twin analogue of the Wave Functions Collapse i.e. as a fiction (figment) and a deontology without any real scientific value.

The previously mentioned fictional character of the Schrödinger's Cat Thought Experiment can be argued once more by observation [9] that it is possible to imagine a macroscopic thought-experiment completely analogous with Shrödinger's quantum one. Within the respective analogue, a cousin of Schrödinger's cat can be killed through launching a single macroscopic ballistic projectile. More specifically, the killing macroscopic machinery is activated by the reaching of the projectile in a probable hitting point. But the respective point has characteristics of a true macroscopic (non-quantum) random variable. Consequently, the launching of a single projectile is a false premise, similar to the supposition $\mathbf{s}_1$ of the Wave Function Collapse concept. Add here the known fact that within the practice of traditional artillery (operating only with macroscopic ballistic projectiles but not with propelled missiles) designed for an expected destruction of a military objective, one uses a considerable (statistical) number of projectiles but not a single one. So the whole situation with a macroscopic killing projectile is completely analogous with the Schrödinger's Cat Thought Experiment which uses a single quantum radioactive decay. Therefore, the acknowledged classical experiment makes clear once more the fictional character of the Schrödinger's Cat Thought Experiment.

According to the above-noted remarks, certain things must be regarded as being worthless, i.e. allegations such as: *"the Schrödinger's cat thought experiment remains a topical touchstone for all interpretations of quantum mechanics"*. Note that such or similar allegations can be found in many science popularization texts, e.g. in the ones disseminated via the Internet.

4 Closing thoughts

Through the contents of the previous sections, we have brought into attention a few significant remarks regarding the themes of the Wave Function Collapse and the Schrödinger's Cat Thought Experiment. Through the respective remarks, we argue that the mentioned themes are not real scientific

topics but pure and trivial fictions. So we find that the Oxford Questions have an important, prolonged drawback and, consequently, their invalidated items have to be regarded as needless things for science.

Submitted on February 27, 2014 / Accepted on March 12, 2014

References

1. Briggs G.A.D., Butterfield J.N., Zeilinger A. The Oxford Questions on the foundations of quantum physics. *Proc. Royal Soc. A*, 2013, v.469, 20130299; arXiv:1307.1310.
2. Stamatescu I.-O. Wave function collapse. In: *Compendium of Quantum Physics*, Springer, 2009, 813–822.
3. Ghirardi C. Collapse theories. The Stanford Encyclopedia of Philosophy. Winter 2011 Edition, http://plato.stanford.edu/archives/win2011
4. Omnes R. Decoherence and wave function collapse. *Foundations of Physics*, 2011, v.41, 1857–1880; arXiv: 1105.0831.
5. Weinberg S. Collapse of the state vector. *Phys. Rev. A*, 2012, v.85, 062116; arXiv: 1109.6462.
6. Bassi A., Lochan K., Satin S., Singh T.P., and Ulbricht H. Models of wave-function collapse, underlying theories, and experimental tests. arXiv: 1204.4325.
7. Cowan C.W., Tumulka R. Epistemology of wave function collapse in quantum physics. arXiv: 1307.0827.
8. Bassi A., Ulbricht H. Collapse models: from theoretical foundations to experimental verifications. arXiv:1401.6314.
9. Dumitru S. Caducity of idea about wave function collapse as well new views on Schrödinger's cat and quantum measurements. *Progress in Physics*, 2013, v.9, no.2, 63–68.
10. Dumitru S. Annotations regarding the Oxford Questions. arXiv: 1311.2581.
11. Dumitru S. Fluctuations and thermodynamic inequalities. *Physica Scripta*, 1974, v.10, 101–103.
12. Dumitru S. The Planck and Boltzmann constants as similar generic indicators of stochasticity: some conceptual implications of quantum-nonquantum analogies. *Physics Essays*, 1993, v.6, 5–20.
13. Dumitru S., Boer A. Fluctuations in the presence of fields — phenomenological Gaussian approximation and a class of thermodynamic inequalities. *Phys. Rev. E*, 2001, v.64, 021108; arXiv: cond-mat/0011444.
14. Dumitru S. Reconsideration of the uncertainty relations and quantum measurements, *Progress in Physics*, 2008, v.4, no.2, 50–68; arXiv:1205.3892.
15. Dumitru S. Phenomenological theory of recorded fluctuations. *Physics Letters A*, 1974, v.48, 109–110.
16. Dumitru S., Boer A. On the measurements regarding random observables. *Romanian Journal of Physics*, 2008, v.53, 1111–1116; http://www.nipne.ro/rjp/2008_53_9-10.html

The Electron and Proton Planck-Vacuum Coupling Forces and the Dirac Equation

William C. Daywitt

National Institute for Standards and Technology (retired), Boulder, Colorado, U.S.A.
E-mail: wcdaywitt@me.com

This short paper derives the electron and proton Planck-vacuum coupling forces so that both the electron and proton, and their antiparticles, possess a Compton radius and obey the Dirac equation.

1 Introduction

The Dirac equation can be expressed as [1] [2]

$$e_*^2\left(i\frac{\partial}{\partial ct}+\boldsymbol{\alpha}\cdot i\nabla\right)\psi = mc^2\beta\psi \tag{1}$$

where in the Planck vacuum (PV) theory the coefficients e_*^2 and mc^2 are particle-PV coupling constants associated with the polarization and curvature forces

$$\frac{(\pm e_*)(-e_*)}{r^2} = \mp\frac{e_*^2}{r^2} \qquad \text{and} \qquad \frac{mm_*G}{r_*r} = \frac{mc^2}{r} \tag{2}$$

where $(\pm e_*)$ and mc^2 are the charge and rest mass energy of the free-space Dirac particles and $(-e_*)$ refers to the separate Planck particles making up the PV continuum. G is Newton's gravitational constant, m_* and r_* are the mass and Compton radius of the Planck particles, and e_* is the massless bare charge. The 'Dirac particles' refer in the present paper to the electron and proton and their respective antiparticles.

The coupling constants in (1) and (2) are presently associated with the rest-frame coupling forces [3]

$$F(r) = \mp\frac{e_*^2}{r^2} - \frac{mc^2}{r} \tag{3}$$

but there is a problem. The negative polarization force in (3) is due to the positive charge in $(\pm e_*)$ of (2) and yields the equation

$$-e_*^2\left(i\frac{\partial}{\partial ct}+\boldsymbol{\alpha}\cdot i\nabla\right)\psi = mc^2\beta\psi \tag{4}$$

which, because of the negative sign, is not a Dirac equation. Thus these coupling forces do not lead to a Dirac particle in the positron and proton cases — nor can they produce their corresponding Compton radii $r_c = e_*^2/mc^2$ from (3), where $F(r_c)$ must vanish. So there is something wrong with these coupling forces and, to resolve the problem, it is necessary to look more closely at the foundation of the PV theory.

2 Single superforce

The two observations: "investigations point towards a compelling idea, that all nature is ultimately controlled by the activities of a single *superforce*", and "[a living vacuum] holds the key to a full understanding of the forces of nature" ; come from Paul Davies' popular 1984 book [4, p.104] entitled "*Superforce: The Search for a Grand Unified Theory of Nature*". This living vacuum consists of a "seething ferment of virtual particles", and is "alive with throbbing energy and vitality". These statements form the foundation of the PV theory [5] [6] that, among other things, derives the primary constants associated with Newton's constant $G\,(=\,e_*^2/m_*^2)$, Planck's reduced constant $\hbar\,(=\,e_*^2/c)$, and the fine structure constant $\alpha\,(=e^2/e_*^2)$.

The single-superforce idea is taken here to mean that the superforces associated with General relativity [5] and the Newton and Coulomb forces have the same magnitude. In particular it is assumed that

$$\frac{m_*^2G}{r_*^2} = \frac{c^4}{G} = (\pm)\frac{e_*^2}{r_*^2} \tag{5}$$

where the first, second, and third ratios are the superforces for Newton's gravitational force and General relativity, and the free-space forces and superforces associated with the Coulomb force.

Equating the first and second ratios in (5) leads to

$$\frac{c^4}{G} = (\pm)\frac{m_*c^2}{r_*} \tag{6}$$

where, since c^4 and G are positive-definite constants, the negative sign in (6) must refer to some other aspect of the ratio — this other aspect is the c^4/G association with the two-term particle-PV coupling forces. Equating the second and third ratios in (5) and using (6) yields

$$(\pm)\frac{m_*c^2}{r_*} = (\pm)\frac{e_*^2}{r_*^2} \tag{7}$$

both sides of which are coupling forces.

Equating the first and third ratios in (5) gives

$$G = \frac{e_*^2}{m_*^2} \tag{8}$$

as the definition of the secondary constant G in terms of the primary constants e_*^2 and m_*^2.

Using the curvature and polarization forces in (7), the two-term coupling forces take the form

$$F(r_*) = (\pm)\frac{e_*^2}{r_*^2}(\pm)\frac{m_*c^2}{r_*} \tag{9}$$

where the proper choice of the plus and minus signs leads to coupling forces consistent with the existence of a Compton radius. Thus the proper choice is

$$F(r_*) = \pm\left(\frac{e_*^2}{r_*^2} - \frac{m_*c^2}{r_*}\right) \tag{10}$$

defining coupling forces that vanish at the Compton radius ($r_* = e_*^2/m_*c^2$) of the Planck particle. The vanishing of (10) reveals a basic property of the PV state that establishes how the stable free-space particle interacts with the vacuum — i.e., via a two-term coupling force that generates a characteristic Compton radius ($r_c = e_*^2/mc^2$) for the particle.

For the free-space electron and proton and their antiparticles, the results of the previous paragraph suggest that their coupling forces should be

$$F(r) = \pm\left(\frac{e_*^2}{r^2} - \frac{m_ec^2}{r}\right) = \begin{cases}\text{electron}\\ \text{positron}\end{cases} \tag{11}$$

and

$$F(r) = \mp\left(\frac{e_*^2}{r^2} - \frac{m_pc^2}{r}\right) = \begin{cases}\text{proton}\\ \text{antiproton}\end{cases} \tag{12}$$

where the plus and minus signs correspond to the particles indicated on the right of the braces, and the subscripts 'e' and 'p' refer to the electron and proton respectively. These coupling forces replace the problematic forces in (3). The radius r in these equations is the radius from the free-space Dirac particle to the separate particles of the PV.

The vanishing of equations (10)–(12) leads to the important string of Compton relations

$$r_em_ec^2 = r_pm_pc^2 = r_*m_*c^2 = e_*^2 \quad (= c\hbar) \tag{13}$$

relating the Dirac particles to the Planck particles.

3 Conclusions and comments

The forces (11) and (12) vanish at the electron and proton, and their respective antiparticle, Compton radii

$$r_e = \frac{e_*^2}{m_ec^2} \qquad \text{and} \qquad r_p = \frac{e_*^2}{m_pc^2} \tag{14}$$

and lead to the Dirac equations

$$\pm e_*^2\left(i\frac{\partial}{\partial ct} + \boldsymbol{\alpha}\cdot i\nabla\right)\psi = \pm mc^2\beta\psi\,. \tag{15}$$

Dividing through by $\pm mc^2$ gives

$$r_c\left(i\frac{\partial}{\partial ct} + \boldsymbol{\alpha}\cdot i\nabla\right)\psi = \beta\psi \tag{16}$$

where the Compton radius r_c ($= e_*^2/mc^2$) and m now represent any of the Dirac particles ($r_c = r_e, r_p$).

The particle-PV potential energy associated with the coupling forces in (11) and (12) is defined as

$$V(r) = -\int_{r_c}^{r} |F(r)|\,dr \tag{17}$$

for $r \leqslant r_c$, resulting in (using (13))

$$\frac{V(r)}{mc^2} = \frac{r_c}{r} - 1 - \ln\frac{r_c}{r} \tag{18}$$

where $V(r_c) = 0$. The potential increases as the Dirac-particle cores ($\pm e_*, m$) are approached (as r decreases), making the negative energy vacuum susceptible to free-space (where the cores reside) perturbations. This susceptibility leads to an internal vacuum structure for the Dirac particles; where, in the "The Dirac Proton and its Structure" calculations [6] [7], quantitative confirmation for the preceding Dirac-particle calculations is provided.

Submitted on March 6, 2014 / Accepted on March 17, 2014

References

1. Daywitt W.C. Understanding the Dirac Equation and the Electron-Vacuum System. *Progress in Physics*, 2013, no. 4, 78.
2. Daywitt W.C. The Electron-Vacuum Coupling Force in the Dirac Electron Theory and its Relation to the Zitterbewegung. *Progress in Physics*, 2013, no. 3, 25.
3. Daywitt W.C. Particles and Antiparticles in the Planck Vacuum Theory. *Progress in Physics*, 2011, no. 1, 55.
4. Davies P. *Superforce: the Search for a Grand Unified Theory of Nature*. Simon and Schuster, Inc., New York, 1984.
5. Daywitt W.C. The Planck Vacuum. *Progress in Physics*, 2009, no. 1, 20. See also www.planckvacuum.com.
6. Daywitt W.C. The Proton and its Structure. This paper has been submitted the the Canadian "*Applied Physics Research*" Journal for publication. See also www.planckvacuum.com.
7. Barut A.O. and Bracken A.J. Zitterbewegung and the Internal Geometry of the Electron. *Phys. Rev. D*, 1981, v. 23, no. 10.

Further Insight Relative to Cavity Radiation II: Gedanken Experiments and Kirchhoff's Law

Pierre-Marie Robitaille

Department of Radiology, The Ohio State University, 395 W. 12th Ave, Columbus, Ohio 43210, USA.
E-mail: robitaille.1@osu.edu

Kirchhoff's law of thermal emission states that cavity radiation must always be black, or normal, irrespective of the nature of the walls. Arbitrary cavity radiation must be solely dependent upon the equilibrium temperature and the frequency of observation. Despite such theoretical claims, it is well established that laboratory blackbodies are not constructed from arbitrary materials, but rather from nearly perfect absorbers of radiation over the frequency of interest. In the laboratory, arbitrary cavities do not contain black radiation. This experimental fact stands in direct conflict with Kirchhoff's formulation. Nonetheless, Kirchhoff's law of thermal emission endures, in part, due to Gedanken experiments whose errors in logic are difficult to ascertain. In this work, thought experiments are discussed in order to expose some logical shortcomings. It will be demonstrated that Kirchhoff's law cannot be supported in this context.

If a space be entirely surrounded by bodies of the same temperature, so that no rays can penetrate through them, every pencil in the interior of the space must be so constituted, in regard to its quality and intensity, as if it had proceeded from a perfectly black body of the same temperature, and must therefore be independent of the form and nature of the bodies, being determined by temperature alone... In the interior therefore of an opake red-hot body of any temperature, the illumination is always the same, whatever be the constitution of the body in other respects.

Gustav Robert Kirchhoff, 1860 [1]

1 Introduction

Recently, the validity of Kirchhoff's law [1, 2] and the universality of the laws of thermal emission [3–6] have been brought into question [7–13]. This reformulation of an established thermodynamic principle has repercussions throughout the fields of physics and astronomy. The issues at hand not only concern our understanding of the nature of the stars [14] and the microwave background [15], but also the universality endowed upon Boltzmann's and Planck's constants [12]. Thus, although 150 years have passed since Kirchhoff's law was formulated [1, 2], it is appropriate to carefully reconsider its authenticity. In this respect, the author has argued against the validity of this law of thermal emission [7–13].

Stewart's law [16], not Kirchhoff's [1, 2], properly accounts for the equivalence between emissivity and absorptivity in thermal equilibrium. Unlike his contemporaries [1,2,6], Stewart [16] does not require that all radiation within cavities be black, or normal. In this work, the variable nature of cavity radiation is affirmed by addressing a Gedanken experiment which is often invoked to justify Kirchhoff's law, either in the classroom or within textbooks.

2 Experiment I: Two ideal cavities

In this experiment, two cavities of the same dimensions are imagined to exist in an empty universe at the same temperature (see Fig. 1A). In order to ensure that the heat contained within each cavity cannot escape, let us surround the exterior of these enclosures with an adiabatic wall. The interior of each cavity is then placed under vacuum to prevent convective processes. The inner surface of the first enclosure (cavity 1) is comprised of an ideal, or perfect, emitter (Emissivity (ϵ) = 1, Reflectivity (ρ) = 0; at the frequency of interest). The interior of cavity 2 is constructed from an ideal, or perfect, reflector ($\epsilon = 0$, $\rho = 1$; at the frequency of interest). For pedagogical purposes, a perfectly adiabatic structure is selected for the inner wall of cavity 2. The cavities are in temperature equilibrium with a third object in the same universe, which is also surrounded by an adiabatic wall.

The physics community currently maintains that, under these conditions, both cavities must contain black radiation, in accordance with Kirchhoff's law [1,2], despite the fact that the second cavity, being fully adiabatic, acts as a perfect reflector and, hence, is unable to emit a single photon. How can it be argued that cavity 2 is filled with black radiation?

Let the two cavities come into contact with one another and place a small hole between them, as displayed in Fig. 1B. When this occurs, photons must cross from cavity 1 (perfectly emitting) into cavity 2 (perfectly reflective). Yet, if cavity 2 is devoid of black radiation, it will not be able to transfer a photon back into the first cavity. As a result, since the first cavity would be losing net photons into the second cavity, its energy content or temperature would drop. Conversely, the energy content of the second cavity would rise. This cannot be permitted according to the zeroth law of thermodynamics, since all three objects are already at the same temperature. Consequently, it is argued that the perfectly reflecting cavity

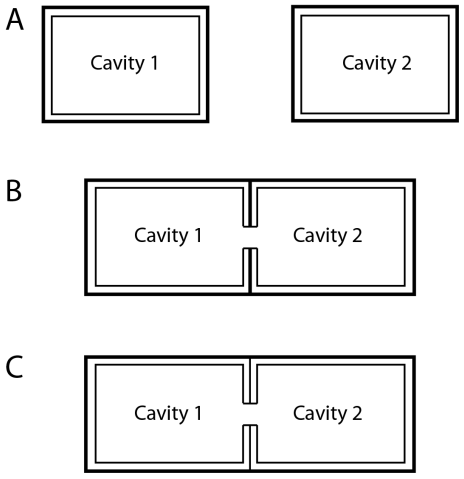

Fig. 1: Schematic representation of our thought experiments. A) Two cavities are presented. Cavity 1 is constructed from a perfect emitter ($\epsilon = 1$, $\rho = 0$) surrounded by an adiabatic wall. Cavity 2 represents a perfect reflector ($\epsilon = 0$, $\rho = 1$). In this case, we assume that both the inner lining and the outer wall are fully adiabatic. B) The cavities displayed in A are brought together and a small hole is made between them in order to permit radiation to flow from one enclosure into the other. C) Two cavities are presented which again have been brought in contact with one another. The inner surface of cavity 1 is constructed from graphite, or soot, and is assumed to act as a perfect emitter ($\epsilon = 1$, $\rho = 0$). The inner surface of cavity 2 is constructed from silver which is assumed to act as a perfectly reflector ($\epsilon = 0$, $\rho = 1$). Both cavities are surrounded by adiabatic walls. However, when the two cavities are brought together, the adiabatic walls between them are removed. This allows for direct thermal contact of the two inner surfaces. A small hole is included to permit radiation to move from one enclosure into the other.

must have contained black radiation all along, such that radiative equilibrium could always be maintained and that the temperature of the cavities can remain intact.

The error in such arguments must be found in permitting net energy to be transferred from cavity 1 into cavity 2. This cannot be allowed, simply based on the zeroth law of thermodynamics, if both cavities are said to be at the same temperature. A logical misstep must have been made in this thought experiment. The two cavities must not have been properly conceived.

The problem can be attributed to the inner surface of the second cavity and in the fact that both cavities must be surrounded by an adiabatic wall to prevent the emission of photons into the surrounding empty universe. This was central to maintaining the energy/temperature stability of each subsystem.

In designing the second cavity from a perfectly adiabatic wall, a physical regimen has been adopted which has no relationship to the best reflectors. Adiabatic walls are immune to all thermal processes. As a consequence, scientists who invoke their use in this setting, fail to recognize that such walls cannot be characterized with a temperature. Thus, if Kirchhoff's law is invalid and there are actually no photons within cavity 2, one cannot even set a temperature for the second system. By default, adiabatic walls cannot store energy within themselves. Namely, in addition to being perfectly reflective, they cannot support thermal conduction or electron flow. This stands in direct opposition to the known properties of the best reflectors and real heat shields.*

In reality, all good reflectors are also good conductors. As a case in point, silver constitutes a very efficient reflector in the infrared, but it is also one of the best electrical and thermal conductors.†

Since the formulation of a law of physics must depend upon the proper characterization of the physical world, one must be careful not to invoke a mathematical or physical regimen which has lost all relation to reality. The use of a fully adiabatic perfectly reflecting cavity has not allowed for sufficient degrees of freedom in which to store energy, as it cannot sustain any phonons within its walls. The only degree of freedom which might be available to such a cavity would rest in its ability to contain a radiation field. However, can cavity 2 actually have the ability to spontaneously generate such a field, despite its complete lack of phonons and perfect reflection, simply driven by a law of physics which is currently under question?

As cavity 2 is perfectly reflecting, the proper conclusion remains that it cannot self-generate a single photon. Thus, it should initially be devoid of a radiation field. Because it also cannot hold any energy in its adiabatic walls, cavity 2 cannot be characterized by *any* temperature.

Consequently, at the beginning of the experiment, cavity 2 cannot be in thermal equilibrium with cavity 1. Therefore, cavity 1 is allowed to transfer photons into cavity 2, simply because there is no thermal equilibrium initially. The temperature of cavity 1 must drop, as it pumps photons into cavity 2. Thus, cavity 1 falls out of thermal equilibrium with the third object, and Kirchhoff's law has not been proven.

Obviously, there are shortcomings in cavity 2. As such, the cavities should be redesigned, such that the validity of Kirchhoff's law can be assessed from a slightly different perspective.

*Superconducting magnets for MRI utilize heat shields in their interior that may well represent the closest example of an adiabatic shield in nature. Such shields are typically made from a highly reflective and conductive metal. They are suspended in the interior of the cryostat using very thin and insulating fiberglass rods which act to help eliminate all conductive thermal contact between the shield and other portions of the magnet system (i.e. the liquid helium Dewar containing the magnet windings, other heat shields, the liquid nitrogen Dewar, the outer casing of the magnet, etc.). These heat shields are typically suspended in a vacuum environment. This is done in order to minimize any convective contact between the shield and the rest of the magnet.

†Silver is amongst the best conductors with a resistivity of only $\sim 1.6 \times 10^{-8}$ Ω m at 300 K and of $\sim 0.001 \times 10^{-8}$ Ω m at 4 K [17]. It is also an excellent reflector in the infrared, our frequency range of interest.

3 Experiment II: Two cavities in thermal contact

Once again, each cavity is surrounded, under vacuum, with an adiabatic wall such that heat radiation cannot be lost into the universe and the temperature of each cavity can be maintained. As before, these two cavities are in temperature equilibrium with a third object in the same universe, which is also surrounded by an adiabatic wall.

The inner surface of cavity 1, the perfectly emitting cavity, will be constructed from graphite, or soot. These materials are known to be very good physical examples of blackbodies in the laboratory [18–21]. Departure from physical reality will consist solely in assuming that the emissivity of the inner surface is perfect ($\epsilon = 1, \rho = 0$).

Silver will be used to line the inner surface of cavity 2. This metal is perhaps the best known reflector in the laboratory. In parallel fashion, a single departure is made from physical reality, namely in assuming that the reflectivity of the silver interior will be perfect ($\epsilon = 0, \rho = 1$), much like the second cavity in section 2.

Each cavity has a total energy which is now equal to the sum of the energy it contains in the photons it encloses and in the phonons which exists in its walls.* In this sense, each cavity is given access to only two possible degrees of freedom: 1) the vibrational/phonon system in its walls and 2) the radiation field.

Since the systems must be in thermal equilibrium, net conduction is forbidden in accordance with the requirements set forth by Max Planck [6, p. 23].

Let us now bring the two cavities together. But this time, before making the small hole, let us remove the adiabatic outer wall from that section of the cavities which come into direct contact. In this manner, thermal conduction can occur between the two cavities, if necessary. Finally, let us make the small hole and permit cavity 1 to transfer a photon into cavity 2 (see Fig. 1C).

Under these conditions, if a photon from cavity 1 enters cavity 2, an identical quantum of energy instantly propagates from the second perfectly reflecting cavity, through conduction and phonon action, into the walls of the first cavity. In a sense, cavity 1 has instantly converted this phonon into the photon it just expelled. As a result, cavity 1 has simply acted as a transformer of energy. It has taken phonon energy from cavity 2, created a photon, and sent energy back into cavity 2. Cavity 1 has not lost any net photons. The total energy of each system does not change and the zeroth law is not violated.

Thus, when a small hole is made between the two enclosures, each cavity eventually becomes filled with blackbody radiation when thermal equilibrium is reestablished. This conclusion has previously been demonstrated mathematically [9] and was recognized long ago in the laboratory. The net result is that no net energy has been exchanged. The temperature does not change, and no laws of thermodynamics have been violated. Yet, for the period of time when photon and phonon transfer was occurring, the entire system fell out of thermal equilibrium, even if temperature equilibrium was being maintained. Eventually however, thermal equilibrium is re-established and both cavities are filled with black radiation.

Over the course of this experiment, something very important has occurred in cavity 2. The energy which this cavity contained has been redistributed amongst its two degrees of freedom. Although the net temperature of cavity 2 has not changed, phonon energy has been lost to the radiation field. This simple observation has consequences in physics, as it signifies that the law of equipartition which characterizes so much of statistical thermodynamics cannot hold. The energy of a system is not necessarily distributed equally between all of its available degrees of freedom.

It could be argued, of course, that a behavior has been demanded from real materials which can never exist. This is a question of how closely physical reality can be modeled. Is it a more grievous error to assume 1) that a perfectly adiabatic cavity can exist, a material which cannot emit photons, cannot sustain conduction in any form, or be associated with any temperature, or 2) that graphite and silver come to represent two 'perfect' examples of emissivity and reflectivity, respectively?

Relative to this question, it is clear that the construction of a perfectly reflecting cavity from an ideally adiabatic wall (Experiment I) constitutes the greater departure from physical reality. Adiabatic surfaces, with their inability to emit any photons and their incapability of sustaining thermal or electrical conduction simply are not approached by anything in nature. It is impossible to state that a truly adiabatic wall is at any given temperature, as temperature in the physical world must be associated with energy content and adiabatic walls contain none. They represent a convenient intellectual concept and offer very little relative to properly modeling physical reality. For this reason, their use results in the finding that all cavities must be filled with blackbody radiation, even if their walls lack the physical ability to emit a single photon. Obviously, a logical conflict has been produced which highlights that our model has deviated too far from physical reality. As a result, it is unlikely that such a model (Experiment I) provides a proper proving ground relative to the validity of Kirchhoff's formulation.

Conversely, it is known that laboratory blackbodies constructed from graphite, or soot (carbon black, lampblack), can reach rather high emissivities over certain frequencies [18–21]. The requirement that these materials can come to have an emissivity of 1 is very close to reality. At the same time, silver can manifest an excellent reflectivity over certain frequencies. Silver surfaces are the best reflectors known. As a result, the assumption that silver can exhibit a reflectivity of 1, is not very far from experimental fact. In this regard,

*For the purpose of this discussion, the energy associated with the electrons in conduction bands, or any other degree of freedom, can be neglected, as these do not provide additional insight into this problem.

it must be concluded that Experiment II constitutes a much better representation of nature. It is known that laboratory blackbodies are always made from near perfect emitters of radiation, like graphite or soot [10, 11]. They are never made of excellent reflectors, such as silver [10, 11].

The silver cavity was initially devoid of any radiation, precisely because it can emit none. It is only when it is placed in contact with a perfectly absorbing cavity, that the energy contained in its vibrational degrees of freedom can be transformed into a radiation field. This directly highlights that Kirchhoff's formulation cannot be correct. We do not find an equal ability to construct blackbody cavities in the laboratory irrespective of the nature of the walls. Silver cavities cannot hold black radiation unless they have been subjected to the action of a perfect absorber [9].

4 Conclusions

When properly analyzed, Gedanken experiments reveal that Kirchhoff's law of the thermal emission cannot be valid. The proper analysis of cavity radiation must be open to realistic treatments of energy balance within real materials. When this is correctly accomplished, cavity radiation becomes absolutely dependent on the nature of the enclosure. Phonon transfer can balance photon transfer. As such, Kirchhoff's law holds no validity, either mathematically, in the experimental setting, or in the context of thought experiments [7–13]. Cavity radiation is not always black, but is absolutely dependent on the nature of the enclosure. As demonstrated in Experiment II, two cavities can be at the same temperature, but not contain identical radiation. The introduction of black radiation into opaque enclosures absolutely depends on the presence, or action, of a perfect emitter. Based on this presentation, the constants of Planck and Boltzmann are not universal [12].

Beyond Kirchhoff's law, the analysis of cavity radiation leads to the conclusion that the equipartition theorem cannot be valid across all systems. The amount of energy associated with a given degree of freedom at temperature equilibrium is not necessarily equal to that contained in all other degrees of freedom. The zeroth law of thermodynamics, by which temperature is defined, is not concerned with radiation fields, but simply temperature equilibrium. If two objects are at the same temperature, they are by definition in thermal equilibrium, provided that their is no net emission, conduction, and convection taking place in the systems of interest.

In Experiment II, a system is initially placed under temperature and thermal equilibrium. It then is allowed to remain under temperature equilibrium, while it temporarily falls out of thermal equilibrium, as the small hole is created to enable the exchange of phonons and photons. At any time, if the two cavities are physically separated and the hole filled, they would immediately regain both temperature and thermal equilibrium. At that point, the second cavity would contain an arbitrary number of photons and not black radiation. It is only if cavity 1 is given sufficient time to act that cavity II will contain black radiation. However, the action of the first cavity was absolutely critical to this transformation. A perfect emitter had to be present. It is not simply a question of time, but of physical action by a perfect emitter.

Experiment II is indicating that it is not necessarily possible to equilibrate the energy contained within the degrees of freedom within real materials. Under these conditions, equipartition cannot hold. Equipartition requires that all degrees of freedom have the same ability to contain energy. This cannot be correct. The most compelling example is illustrated by the hydrogen and hydroxyl bonding systems within water [14]. The force constants in these two systems are drastically different. As a result, the hydrogen bonding system is likely to be filled with energy at temperatures just above absolute zero (~3K). This is the reason, in fact, why the microwave background which surrounds the Earth does not vary in intensity in response to seasonal changes [14]. Equipartition is also invalid in the photosphere, where dramatic differences in the energy content of the translational and vibrational degrees of freedom are likely to exist [22].

Throughout his treatise on heat radiation [6], Max Planck invoked a carbon particle, which he surmised to act as a simple catalyst (see [10] for a detailed review). However, he inserted a perfect emitter into his cavity. This particle could then fill the cavity with black radiation, provided that it was placed in physical contact with the energy source to be converted. It did not matter how much carbon was inserted, as this only governs the time involved. For this reason, when Planck introduced the carbon particle into his cavity [6], it was as if he had lined it completely with carbon [10]. He had not demonstrated that all cavities contained black radiation, only that all perfectly emitting cavities are black.

Acknowledgment

Sylvain Bréchet is recognized for valuable insight relative to phonon transfer during conduction. Luc Robitaille is acknowledged for the preparation of Fig. 1.

The first draft of this work was completed at the home of Professor Lawrence J. Berliner immediately following a discussion which took place at my poster (H1.00227 — The Sun on Trial) during the APS March Meeting. Larry and his wife Barbara are recognized for their unceasing encouragement and for welcoming me into their Denver home.

Dedication

This work is dedicated to my father, Noel Antoine Robitaille (born on December 22, 1929). He devoted his life to the practice of family and emergency medicine, delivering over 800 babies and tending the medical needs of the communities in which he resided, both in Canada and Iowa. He retired on August 30, 2013, at the age of nearly 84, after having, for

many years, served at his small clinic in LaPorte City and making visits to the local nursing home. A few years ago, as he walked with nostalgia in the cemetery of his village, he recalled how so many buried there were once his patients and friends. His daughter-in-law, to help lighten the atmosphere, had inquired: "So Noel, do you think you were a good doctor?"

In February 2014, he passed the 50 year anniversary of receiving the rare privilege, as a white man, to be named an honorary Indian Chief — "Kitchitouagegki". He was the first named by any of the Three First Nations: The Council of Three Fires (Ojibway, Odawa, and Potawatomi). In describing the honor conferred upon him, Allen Toulouse recalled, *"His presence contributed to reducing the infant mortality rate of the Sagamok First Nation (Reducing the number of deaths during pregnancy for both the mothers and their babies). He also made many actions to improve the conditions of the people of Sagamok — including having running water and wells installed in the reserve in the early 1960s"* [23]. It appears that his elevation to Chief represents *"the first official case of a First Nation bestowing this honor upon a Caucasian medical doctor in North-American history"* [23].

Fig. 2: Noel Antoine Robitaille, honorary chief "Kitchitouagegki". Photo courtesy of Allen Toulouse and Christine Robitaille.

Submitted on: March 17, 2014 / Accepted on: March 19, 2014
First published online on: March 19, 2014

References

1. Kirchhoff G. Über das Verhältnis zwischen dem Emissionsvermögen und dem Absorptionsvermögen der Körper fur Wärme und Licht. *Poggendorfs Annalen der Physik und Chemie*, 1860, v. 109, 275–301. (English translation by F. Guthrie: Kirchhoff G. On the relation between the radiating and the absorbing powers of different bodies for light and heat. *Phil. Mag.*, 1860, ser. 4, v. 20, 1–21).
2. Kirchhoff G. Über den Zusammenhang zwischen Emission und Absorption von Licht und Wärme. *Monatsberichte der Akademie der Wissenschaften zu Berlin*, sessions of Dec. 1859, 1860, 783–787.
3. Wien W. Über die Energieverteilung in Emissionspektrum eines schwarzen Körpers. *Ann. Phys.*, 1896, v. 58, 662–669.
4. Stefan J. Über die Beziehung zwischen der Wärmestrahlung und der Temperatur. *Sitzungsberichte der mathematisch naturwissenschaftlichen Classe der kaiserlichen Akademie der Wissenschaften*, Wien 1879, v. 79, 391–428.
5. Planck M. Über das Gesetz der Energieverteilung im Normalspektrum. *Annalen der Physik*, 1901, v. 4, 553–563.
6. Planck M. The theory of heat radiation. P. Blakiston's Son & Co., Philadelphia, PA, 1914.
7. Robitaille P.-M. On the validity of Kirchhoff's law of thermal emission. *IEEE Trans. Plasma Sci.*, 2003, v. 31, no. 6, 1263–1267.
8. Robitaille P.M. Robitaille P. M. L. An analysis of universality in blackbody radiation. *Progr. Phys.*, 2006, v. 2, 22–23; arXiv:physics 0507007.
9. Robitaille P.-M. A critical analysis of universality and Kirchhoff's law: A return to Stewart's law of thermal emission. *Progr. Phys.*, 2008, v. 3, 30–35.
10. Robitaille P.-M. Blackbody radiation and the carbon particle. *Progr. Phys.*, 2008, v. 3, 36–55.
11. Robitaille P.-M. Kirchhoff's law of thermal emission: 150 Years. *Progr. Phys.*, 2009, v. 4, 3–13.
12. Robitaille P.-M. Blackbody radiation and the loss of universality: Implications for Planck's formulation and Boltzmann's constant. *Progr. Phys.*, 2009, v. 4, 14–16.
13. Robitaille P.-M. Further Insight Relative to Cavity Radiation: A Thought Experiment Refuting Kirchhoff's Law. *Progr. Phys.*, 2014, v. 10(1), 38–40.
14. Robitaille P.-M. Water, hydrogen bonding, and the microwave background. *Progr. Phys.*, 2009, v. 2, L5–L8.
15. Robitaille P.-M. Fourty lines of evidence for condensed matter — The Sun on trial: Liquid metallic hydrogen as a solar building block. *Progr. Phys.*, 2013, v. 4, 90–142.
16. Stewart B. An account of some experiments on radiant heat, involving an extension of Prévost's theory of exchanges. *Trans. Royal Soc. Edinburgh*, 1858, v. 22, no. 1, 1–20.
17. Electrical Resistivity of Pure Metals. In, *CRC Handbook of Chemistry and Physics*, 2013–2014, CRC Press, Baca Raton, FL, p. 12–42.
18. Touloukian Y.S., DeWitt D.P. Thermal radiative properties of nonmetallic solids. Vol. 8 in: Thermophysical Properties of Matter, IFI/Plenum, New York, 1972.
19. Burchell T.D. Thermal properties and nuclear energy applications. In: Graphite and Precursors, Gordon and Breach Science Publishers, Amsterdam, The Netherlands, 2001, 87–109.
20. Harris L. The optical properties of metal blacks and carbon blacks. MIT and The Eppley Foundation for Research, Monograph Ser., 1, New Port, R.I., Dec. 1967.
21. Pierson H.O. Handbook of Carbon, Graphite, Diamond and Fullerenes. Noyes Publications, Park Ridge, NJ, 1993, p. 109.
22. Robitaille P.-M. On the Temperature of the Photosphere: Energy Partition in the Sun. *Progr. Phys.*, 2011, v. 3, 89–92.
23. Toulouse A. Sagamok Anishinabek News, Dec. 2013, p. 13. http://issuu.com/sagamok/docs/sagamok_news_december_digital_versi (Accessed online 3/8/2013).

Electrical Conductivity of Metals: A New Look at this Subject

Paulo Roberto Silva

Departmento de Física (Retired Associate Professor), ICEx, Universidade Federal de Minas Gerais, Belo Horizonte, MG, Brazil. E-mail: prsilvafis@gmail.com

Various parameters tied to the electrical conductivity of typical metals are estimated and are expressed in terms of universal constants. It happens that they are close to those found in metallic copper at room temperature. The fact that the realization of the model occurs at room temperature is explained by using the Landauer's erasure principle. The averaged collision time of the electron of conduction is also thought as a particle lifetime. Finally an analogy is established between the motion of the electron of conduction and the cosmological constant problem, where a spherical surface of radius equal to the electron mean free path has been thought as a surface horizon for the charge carriers.

1 Introduction

Highly purified water is a bad electrical conductor. However, the addition of small amounts of sodium chloride (NaCl) to this liquid, can increase its electrical conductivity in a substantial way. At the ambient temperature (295K), the water's dielectric constant of 80, permits the Na+ and Cl- ions to move freely through the liquid and this feature can account for the change in its conductive behavior. It seems that the concentration of free charge carriers has the most relevant role in determining the electrical conductivity of the substances. But what to say about electrical conductivity in metals? Isolated metallic atoms have their inner electrons belonging to closed shells and hence tightly bound to their corresponding atomic nucleus. However the electrons of the outer most shell are weakly bonded to its respective nucleus. When arranged in a crystal lattice structure, the bond weakness of these outer electrons is enhanced due to the interactions among neighbor atoms of the lattice, so that the electrons of conduction are free to travel through the whole crystal. Resistance to their motion is due to the thermal vibrations (phonons) and defects provoked by the presence of impurities and lattice dislocations. In a perfect crystal at zero absolute temperature, these free electrons can be described by using the quantum mechanical formalism of the Bloch waves [1, 2]. The concentration of free electrons plays an important role in the description of the electrical conductivity in metals.

2 Evaluation of typical parameters tied to the electrical conductivity of metals

A possible way to estimate the concentration of conduction electrons in a typical good metal will be next presented. An alternative form to estimate the Casimir force between two parallel uncharged metallic plates separated by a close distance d was developed in reference [3]. There, we considered the cutting of a cubic cavity of edge d in a metallic block. We imagined that the free electrons in metal as a gas of non-relativistic particles confined by the vacuum pressure in the interior of a cubic box of edge equal to d. On the other hand as was pointed out by Jaffe [12], the Casimir force can be calculated without reference to the vacuum fluctuations, and like other observable effects in QED, it vanishes as the fine structure constant α goes to zero.

In reference [3], we treated a non-relativistic Fermi gas confined by the vacuum pressure B and found the relation

$$Bd^3 = \frac{2}{5} E_{av}\,, \tag{1}$$

where E_{av} stands for the average energy of the gas. Meanwhile it is convenient to consider that an equivalent way to treat the problem is by taking in account the electromagnetic interaction through the dependence of the energy levels of the system on the fine structure constant α. We reproduce here some steps of the reasons outlined in reference [3]. One of the simplest models which exhibits energy levels dependence on the fine structure α is the Bohr atom, namely

$$E_n = -\frac{\alpha^2 mc^2}{2n^2} = -\frac{E_1}{n^2}\,. \tag{2}$$

By taking the maximum occupied energy level equal to $\frac{N}{2}$, we get the maximum energy E_M of the system

$$E_M = -\frac{4E_1}{N^2}\,. \tag{3}$$

The average energy could be estimated as

$$E_F = \frac{2}{N}\int_1^{\frac{N}{2}} (-)\, E_1\, n^{-2} dn = \frac{2}{N}\, E_1\, \frac{2-N}{N}\,. \tag{4}$$

In the limit, as $N \gg 1$, we have

$$E_{av} = -\,2\,\frac{E_1}{N}\,. \tag{5}$$

Now let us estimate the vacuum pressure. We have

$$Bd^3 = -\frac{2}{5}\frac{\alpha^2 mc^2}{N} = \frac{2}{5}\, E_{av}\,. \tag{6}$$

By taking $p_0 = \frac{\alpha mc}{2}$ and $\lambda_0 = \frac{h}{p_0} = \frac{2h}{\alpha mc}$, it is possible to make the choice

$$N = \frac{d}{\lambda_0} = \frac{\alpha mcd}{2h}. \quad (7)$$

Inserting equation (7) into equation (6), we obtain

$$B = -\frac{8}{5\pi}\frac{\alpha\pi^2\hbar c}{d^4}. \quad (8)$$

Therefore we notice that by making the choice indicated by equation (7), the explicit dependence of B on the electron mass m and on the maximum quantum number N has disappeared. The alternative way we have used in order to treat the Casimir force problem, permit us to calculate a typical density of charge carriers in good metals. Let us write

$$nd^3 = \frac{4\pi}{3} N^3 3! = 8\pi N^3. \quad (9)$$

In equation (9), we have considered the volume of a sphere in the N-space, and the possible number of permutations among the N_x, N_y and N_z quantum numbers. Putting equation (7) into equation (9) we obtain

$$n = \pi\left(\frac{\alpha mc}{h}\right)^3. \quad (10)$$

Numerical evaluation of equation (10) gives $n = 8.56 \times 10^{28}\,\mathrm{m}^{-3}$, which could be compared with $8.45 \times 10^{28}\,\mathrm{m}^{-3}$, the density of charge carriers in metallic copper [1, 2]. Meanwhile the Fermi energy of metals could be expressed as [1, 4]

$$E_F = \frac{h^2}{8m}\left(\frac{3n}{\pi}\right)^{\frac{2}{3}}. \quad (11)$$

Inserting equation (10) into equation (11), we get

$$E_F = \frac{3^{\frac{2}{3}}}{8}\alpha^2 mc^2. \quad (12)$$

Numerical estimate of equation (12) gives $E_F = 7.07\,\mathrm{eV}$, which naturally is very close to the value found in metallic copper.

In order to proceed further, let us compute the electrical conductivity of a typical good metal. To do this we first suppose that we have n scatters per unit of volume and by considering a prism shaped tube having longitudinal size equal to the electron mean free path ℓ, width ℓ_F equal to half of the Fermi wavelength of the electron, and thickness ℓ_C equal to half of its Compton wavelength. If we consider that the electrical conductivity always happens in a regime of charge neutrality, the number of scatters per unit of volume will be equal to the number density of charge carriers, and we can write

$$n\ell_F\ell_C\ell = n\frac{h}{2mv_F}\frac{h}{2mc}v_F\tau = 1. \quad (13)$$

In equation (13), ℓ_C stands for the wavelength of a photon with a momentum related to the creation of a electron-positron pair and this corresponds to a minimum thickness of the prism, which also implies in a maximum τ, the average time between collisions. From equation (13) we obtain the relation

$$n\tau = \frac{m^2c}{\pi^2\hbar^2}. \quad (14)$$

Now, Drude formula for the electrical conductivity σ is given by (Kittel [1])

$$\sigma = \frac{e^2 n\tau}{m}. \quad (15)$$

Inserting $n\tau$ of equation (14) into equation (15), we obtain

$$\sigma = \frac{e^2 mc}{\pi^2\hbar^2}. \quad (16)$$

Numerical estimate of the electrical resistivity ρ, gives $\rho = \frac{1}{\sigma} = 1.57 \times 10^{-8}\Omega\mathrm{m}$ which can be compared with the resistivity of the metallic copper measured at the temperature of 295 K, namely $\rho_{copper} = 1.70 \times 10^{-8}\Omega\mathrm{m}$. From equation (10) and equation (14) we also obtain the averaged time between collisions

$$\tau = \frac{1}{\alpha^3}\frac{4h}{\pi mc^2}. \quad (17)$$

Numerical estimate of equation (17) gives $\tau = 2.65 \times 10^{-14}\mathrm{s}$. This umber must be compared with the value estimated of $\tau_{copper} = 2.5 \times 10^{-14}\mathrm{s}$, for copper at the room temperature as quoted by Allen [2]. It is also interesting to write formulas for the Fermi velocity v_F and the electron mean free path ℓ. We have

$$v_F = \left(\frac{2E_F}{m}\right)^{\frac{1}{2}} = \frac{3^{\frac{1}{3}}}{2}\alpha c, \quad (18)$$

and

$$\ell = v_F\tau = \frac{3^{\frac{1}{3}}2h}{\alpha^2\pi mc}. \quad (19)$$

These relations for the quantities associated to the electrical conduction in typical metals are exhibited in table 1, as well their respective numerical estimates and are also compared with the corresponding ones quoted for copper at the room temperature.

3 Realization at the room temperature: a possible explanation

It is an intriguing question why a model describing the electrical conductivity of a typical good metal just realizes itself in copper crystals at room temperature. The answer to this question could be elaborated through these reasons.

- As was pointed out by Jacobs [9], Landauer's erasure principle [8] states that: whenever a single bit of information is erased, the entropy in the environment to which the information storing system is connected must increase at least $k_B \ln 2$, where k_B is the Boltzmann's constant;

- A free electron in a metal travels in average a distance equal to its mean free path, with a constant velocity v_F, until to collide with the ionic vibrations (phonons). In the collision process, the free electron looses its memory.

We think that we may associate to the Fermi energy E_F, a string of length equal to its Fermi wavelength, composed by unit cells having a length equal to the Compton wavelength of the electron. Let us to introduce a quasi-particle with a mass-energy μc^2 defined as

$$\mu c^2 = E_F \frac{v_F}{c} . \tag{20}$$

As we can see from equation (20), this quasi-particle has a mass-energy equal to the Fermi energy divided by the number of cells in the string. Defining

$$\Delta F = \Delta U - T\Delta S = \frac{1}{2}\mu c^2 - k_B \ln 2 . \tag{21}$$

And after making the requirement that

$$\Delta F|_{T=T^\star} = 0 , \tag{22}$$

we obtain the relation

$$E_F^3 = \left(k_B T^\star\right)^2 2\,(\ln 2)^2\, mc^2 . \tag{23}$$

Putting $E_F = 7.1\text{eV}$ (table 1) and $mc^2 = 0.511\text{MeV}$ in equation (23) and solving for $k_B T^\star$, we find

$$k_B T^\star = 26\ meV \tag{24}$$

The above number for the characteristic temperature $T^\star$ must be compared with $k_B T_{Room} = 25\,\text{meV}$. Therefore the obtained result for the characteristic temperature given by equation (24) seems to make sense to the fact that the realization of the model for the electrical conductivity of good metals to happen for copper crystals at the room temperature.

4 Three characteristic lenghts and the grow of a polymer chain

In a paper dealing with the cosmological constant problem [6], the time evolution of the universe world line was compared with the growing of a polymer chain by making use of a Flory-like free energy. It is possible to think the electron mean free path as the length of a polymer chain, composed by monomers of size equal to the Compton wavelength of electron. Within this analogy, the radius of gyration of the chain is identified with the Fermi wavelength of electron. We consider as in the de Gennes derivation [7] two contributions for the Flory's free energy. The first term which goes proportional to $\frac{N^2}{R^d}$, corresponds to a repulsive-like monomer-monomer interaction. A second term which comes from an entropic contribution, namely a logarithm of a Gaussian distribution (a signature of a random walk process) goes as $\frac{R^2}{(N\lambda_C)^2}$. We write

$$F = \frac{N^2\lambda_C^d}{R^d} + \frac{R^2}{N\lambda_C^2} , \tag{25}$$

where F is a Flory-like free energy, λ_C is the Compton length, N is the number of monomers in the chain, and d is the space-time dimension. Setting $\ell = N\lambda_C$ and minimizing equation (25) relative to R, we obtain for the radius of gyration R_g the relation

$$R_g = \ell^{\frac{3}{2+d}} \lambda_C^{\frac{d-1}{2+d}} . \tag{26}$$

We identify $R_g(d = 4)$ with the Fermi length of the electron, λ_F. We have

$$\lambda_F = (\ell\lambda_C)^{\frac{1}{2}} . \tag{27}$$

We observe that equation (27) , relating the three characteristics lengths of the problem, agrees with the upper bound to the electron mean free path found in reference [13]. Please see equation (21) of the cited reference. It is worth to notice that the agreement between both calculations occurs just when the radius of gyration is evaluated in the space-time dimension $d = 4$.

5 High temperature behaviour of the collision time

It would be interesting to evaluate a relation expressing the high temperature behavior of the collision time appearing in the Drude formula for the electrical conductivity. By considering a viscous force which depends linearly on the velocity, the power dissipated by this force can be written as

$$\frac{dE}{dt} = -F_{viscous} v = -\frac{1}{\tau} pv . \tag{28}$$

The power dissipated by this viscous force acting on the charge carrier will appear as an increasing in the internal energy of the lattice and we write

$$\frac{dU}{dt} = -\frac{dE}{dt} = \frac{1}{\tau} pv . \tag{29}$$

By taking

$$p = \frac{\hbar}{2R} \text{ and } vdt = dR , \tag{30}$$

where the first relation in equation (30) comes from the uncertainty principle, we get

$$dU = \frac{\hbar}{2\tau}\frac{dR}{R} . \tag{31}$$

Performing the integration of equation (31) between the limits $R_0 = \frac{\hbar}{mc}$ and $R_1 = \frac{\hbar}{mv_F}$, we obtain

$$\Delta U = \frac{\hbar}{2\tau} \ln \frac{c}{v_F} . \tag{32}$$

Now, let us consider an entropy variation given by

$$\Delta S = k_B \ln 2^D = D k_B \ln 2 . \tag{33}$$

In equation (33), we have written an entropy variation similar to that considered in applying the Landauer's erasure principle [8], but here putting $D = 4$, by taking in account the four dimensions of the space-time. Taking the extremum of the free energy, namely writing

$$\Delta F = \Delta U - T\Delta S = 0\,, \tag{34}$$

and solving for τ, we have

$$\tau = \frac{\hbar}{8k_BT}\ln\frac{c}{v_F}\,. \tag{35}$$

In the case of copper $\left(v_F = 1.57\times10^6\mathrm{m\ s^{-1}}\right)$ at the room temperature ($T = 300\,\mathrm{K}$), we find

$$\tau_{copper}\,(300\,\mathrm{K}) = 2.4\times10^{-14}\mathrm{s}. \tag{36}$$

As we can see in table 1, the result of equation (36) is very close to the room temperature mean collision time of the electrons of conduction in copper, as quoted in the literature.

6 Average collision time as a particle lifetime

There are two characteristics linear momenta that we can associate to the free electrons responsible for the electrical conductivity in good metals. They are: the Fermi momentum mv_F and the Compton momentum mc. By taking into account that the free electron has a fermionic character, we will write a non-linear Dirac-like equation describing the "motion" of this particle. We have

$$\frac{\partial\Psi}{\partial x} - \frac{1}{c}\frac{\partial\Psi}{\partial t} = \frac{mv_F}{\hbar}\Psi - \frac{mc}{\hbar}\left|\Psi^\star\Psi\right|\Psi\,. \tag{37}$$

We see that equation (37) contains only first order derivatives of the field Ψ. Besides this, the field Ψ has not a spinorial character. Making the two sides of equation (37) equal to zero and solving for $|\Psi^\star\Psi|$, we get

$$\left|\Psi^\star\Psi\right| = \frac{v_F}{c} = \frac{3^{\frac{1}{3}}}{2}\,\alpha\,. \tag{38}$$

In obtaining equation (38), we also used the result for v_F shown in table 1. On the other hand in the collision process, the free electron loss its memory. We may think that this feature looks similar to the annihilation of a particle- antiparticle pair, each of mass-energy equal to E_F. Putting this thing in a form of the uncertainty principle yields

$$2E_F\Delta t = \frac{h}{2} \quad\text{or}\quad \frac{h\nu}{2} = 2E_F\,. \tag{39}$$

Solving equation (39) for ν, we get

$$\nu = \frac{1}{\Delta t} = 4\frac{E_F}{h} = \frac{3^{\frac{2}{3}}}{2h}\alpha^2mc^2. \tag{40}$$

By combining the results of equation (38) and equation(40) we obtain the line width Γ tied to the "particle" decay

$$\Gamma = \nu\left|\Psi^\star\Psi\right| = \frac{3}{4h}\,\alpha^3mc^2\,. \tag{41}$$

Finally the "particle" lifetime τ is given by

$$\tau = \frac{1}{\Gamma} = \frac{4h}{3\alpha^3mc^2}\,. \tag{42}$$

Comparing τ giving by equation (42) with the time between collisions shown in table 1, we verify that the present result displays the number 3 in the denominator, instead of the number π which appears in table 1.

Table 1: Formulas related to the electrical conductivity of typical metals, in terms of universal constants (this work). Numerical estimates of them are compared with those quoted for Copper at room temperature.

Formula	Numerical estimates	Copper at room temperatures
$n = \pi\left(\frac{\alpha mc}{h}\right)^3$	$8.56\times10^{28}\,\mathrm{m^{-3}}$	$8.45\times10^{28}\,\mathrm{m^{-3}}$ [1,2]
$E_F = \frac{3^{\frac{2}{3}}}{8}\,\alpha^2mc^2$	7.07 eV	7.0 eV [1]
$\rho = \frac{1}{\sigma} = \frac{\pi^2\hbar^2}{e^2mc}$	$1.57\times10^{-8}\,\Omega\mathrm{m}$	$1.70\times10^{-8}\,\Omega\mathrm{m}$ [1,2]
$\tau = \frac{1}{\alpha^3}\frac{4h}{\pi mc^2}$	$2.65\times10^{-14}\,\mathrm{s}$	$2.5\times10^{-14}\,\mathrm{s}$ [2,5]
$v_F = \frac{3^{\frac{1}{3}}}{2}\,\alpha c$	$1.6\times10^6\,\mathrm{m\ s^{-1}}$	$1.6\times10^6\,\mathrm{m\ s^{-1}}$ [1]
$\ell = \frac{3^{\frac{1}{3}}2h}{\alpha^2\pi mc}$	419Å	400Å [5]

7 Analogy with the cosmological constant problem

In this section we assume, for simplicity, that $\hbar = c = k_B = 1$. One worth point we can consider now is the analogy that can be made with the cosmological constant problem. Hsu and Zee [10] have proposed an effective action A_{eff} as a means to deal with the cosmological constant problem. They wrote

$$A_{eff} = -\left(\Lambda L^4 + \frac{M_P^4}{\Lambda}\right) + \text{independent of }\Lambda\text{-terms}, \tag{43}$$

where M_P is the Planck mass, L is the radius of the event horizon of the universe and Λ is the cosmological constant. Taking the extremum of this action they got

$$\Lambda = \left(\frac{M_P}{L}\right)^2. \tag{44}$$

We could think A_{eff} above as a four-dimensional representation of a kind of free energy, where the first term plays the role of the internal energy and the second one is related to the entropy S. The absolute temperature is taken to be equal to one. We propose that

$$\Omega \sim \exp\left(\frac{M_P^4}{\Lambda}\right) \tag{45}$$

with

$$S = \ln \Omega. \tag{46}$$

On the other hand, there is a proposal [11] that the universe can be considered as a black hole with its entropy being evaluated by counting the number of cells contained in the area of its event horizon (the holographic principle), namely

$$S_{universe} \sim \left(\frac{L}{L_P}\right)^2 = L^2 M_P^2 . \tag{47}$$

By considering the two equivalent ways of the entropy evaluation, from equation (46) and equation (47) relations, we can write

$$L^2 M_P^2 = \frac{M_P^4}{\Lambda}, \tag{48}$$

which reproduces the results of Hsu and Zee [10], please see equation (44). Turning to the problem of the electrical conductivity in good metals, let us consider for instance in a copper crystal an electron of the conduction band which just suffered a collision. In the absence of an external electric field, all the directions in the space have equal probability to be chosen in a starting new free flight. Therefore if we take a sphere centered at the point where the electron has been scattered, with a radius equal to the electron mean free path, the surface of this sphere may be considered as an event horizon for the phenomena. Any electron starting from this center will be on average scattered when striking the event horizon, loosing the memory of its previous free flight. Besides this, all the lattice sites of the metallic crystal are treated on equal footing, due to the translational symmetry of the system. Based on the previous discussion and inspired on the black hole physics, let us to define the entropy related on the event horizon for the electron of conduction in metals. We write

$$S_{Metal} = \pi \left(\frac{\ell}{w}\right)^2, \tag{49}$$

where ℓ is the electron mean free path and w is the equivalent to the Planck length of the problem. It is possible to write an action analogous to that of Hsu and Zee [10], in order to describe the electrical conductivity in metals. We have

$$A_{Metal} \sim \left(\Lambda_M \ell^4 + \frac{1}{\Lambda w^4}\right). \tag{50}$$

Making the equality between the two ways of writing the entropy, namely equaling the entropy of a surface horizon of radius ℓ and ultra-violet cutoff w with the last term of equation(50), we get

$$\pi \left(\frac{\ell}{w}\right)^2 = \frac{1}{\Lambda_M w^4}, \tag{51}$$

which leads to

$$\Lambda_M^{\left(-\frac{1}{4}\right)} = \pi^{\frac{1}{4}} (\ell w)^{\frac{1}{2}}. \tag{52}$$

Upon to identify $\Lambda_M^{\left(-\frac{1}{4}\right)}$ with the Fermi wavelength of the electron λ_F and w with its Compton wavelength λ_C, we obtain

$$\lambda_F = \pi^{\frac{1}{4}} (\ell \lambda_C)^{\frac{1}{2}}. \tag{53}$$

Relation (53) must be compared with equation (27).

Submitted on March 14, 2014 / Accepted on March 17, 2014

References

1. Kittel C. Introduction to Solid State Physics. 5th Ed, Wiley, 1976, Chapter 6.
2. Allen P.B. Electrical Conductivity. *The Physics Teacher*, v. 17(6), September 1979, 362–366.
3. Silva P.R. Casimir force: an alternative treatment. arXiv: 0901.0908.
4. Tipler P.A. Modern Physics. Worth Pub. Inc., New York, 1978, Chapter 9.
5. Halliday D. et al. Fundamentals of Physics, 3th Edition, Extended Version, Wiley, 1988, Chapter 28.
6. Silva P.R. Cosmological constant and polymer physics. *Braz. J. Phys.*, 2008, v. 38, 587–590; arXiv: 0812.4007.
7. de Gennes P-G. Scaling Concepts in Polymer Physics. Cornell University Press, 1979, Chapter 1.
8. Landauer R. *IBM J. Res. Develop.*, 1961, v. 5, 183.
9. Jacobs K. arXiv: quant-ph/0512105.
10. Hsu S. and Zee A. arXiv: hep-ph/0406142.
11. Susskind L. The world as a hologram. arXiv: hep-th/9409089.
12. Jaffe R.L. *Phys. Rev. D*, 2005, v. 72, 021301.
13. Silva P.R. et al. Quantum conductance and electric resistivity. *Phys. Lett. A*, 2006, v. 358, 358–362.

LETTERS TO PROGRESS IN PHYSICS

On the Equation which Governs Cavity Radiation

Pierre-Marie Robitaille

Department of Radiology, The Ohio State University, 395 W. 12th Ave, Columbus, Ohio 43210, USA
E-mail: robitaille.1@osu.edu

In this work, the equation which properly governs cavity radiation is presented. Given thermal equilibrium, the radiation contained within an arbitrary cavity depends upon the nature of its walls, in addition to its temperature and its frequency of observation. With this realization, the universality of cavity radiation collapses. The constants of Planck and Boltzmann can no longer be viewed as universal.

Science enhances the moral value of life, because it furthers a love of truth and reverence...

Max Planck, Where is Science Going? 1932 [1]

When Max Planck formulated his law [2, 3], he insisted that cavity radiation must always be black or normal, as first proposed by Gustav Robert Kirchhoff [4, 5]. The laws of thermal emission [2–7] were considered universal in nature. Based on Kirchhoff's law [4, 5], cavity radiation was said to be independent of the nature of the walls and determined solely by temperature and frequency. Provided that the cavity walls were opaque, the radiation which it contained was always of the same nature [2–5]. All cavities, even those made from arbitrary materials, were endowed with this property.

Cavity radiation gained an almost mystical quality and Planck subsequently insisted that his equation had overarching consequences throughout physics. The constants contained within his formulation, those of Planck and Boltzmann (h and k), became fundamental to all of physics, leading to the development of Planck length, Planck mass, Planck time, and Planck temperature [3, p. 175].

However, it can be demonstrated that cavity radiation is not universal, but depends on the nature of the cavity itself [8–15]. As such, the proper equation governing cavity radiation is hereby presented.

It is appropriate to begin this derivation by simply considering Kirchhoff's law [4, 5]

$$\frac{\epsilon_\nu}{\kappa_\nu} = f(T, \nu)\,, \tag{1}$$

where $f(T, \nu)$ is the function provided by Max Planck [2]. As Eq. 1 was hypothesized to be applicable to all cavities, we can adopt the limits of two extremes, namely the perfect absorber and the perfect reflector.

First, the condition under which Kirchhoff's law is often presented, the perfectly absorbing cavity, can be considered (emissivity (ϵ) = 1, absorptivity (κ) = 1, reflectivity (ρ) = 0; at the frequency of interest, ν). In setting κ to 1, it is apparent that the mathematical form of the Eq. 1 remains valid.

Second, if a perfectly reflecting cavity is utilized ($\epsilon = 0$, $\kappa = 0$, $\rho = 1$), it is immediately observed that, in setting κ to 0, Kirchhoff's law becomes undefined. This simple mathematical test indicates that arbitrary cavities cannot be black, as Kirchhoff's law cannot be valid over all conditions. The problem arises because reflection has not been properly included in Kirchhoff's formulation. In this respect, it is possible to invoke Stewart's law of thermal emission [16] which states that, under conditions of thermal equilibrium, the emissivity and absorptivity are equal

$$\epsilon_\nu = \kappa_\nu\,. \tag{2}$$

It is recognized that, for any material, the sum of the emissivity and reflectivity is always equal to 1. This constitutes another formulation of Stewart's law [10, 16] which can also be expressed in terms of absorptivity

$$\epsilon_\nu + \rho_\nu = \kappa_\nu + \rho_\nu = 1\,. \tag{3}$$

As such, let us substitute these relations into Kirchhoff's law (Eq. 1). This mathematical operation is permitted in this exceptional case, since Stewart's law (Eqs. 2, 3) is valid under conditions of thermal equilibrium. The effects of reflection are inserted into Kirchhoff's law. In so doing, the possibility that Eq. 1 can become undefined, when absorptivity is equal to 0, is removed, as reflectivity will be equal to 1. Hence, the following is obtained:

$$\frac{\epsilon_\nu + \rho_\nu}{\kappa_\nu + \rho_\nu} = f(T, \nu)\,. \tag{4}$$

Since, $\kappa_\nu + \rho_\nu$ can be set to 1, with rearrangement, the law for arbitrary cavity radiation under conditions of thermal equilibrium, can be obtained. This law is now properly dependent on the nature of the cavity walls, because it includes the reflectivity observed in real materials

$$\epsilon_\nu = f(T, \nu) - \rho_\nu\,. \tag{5}$$

Dedication

This work is dedicated to our mothers on whose knees we learn the most important lesson: love.

Submitted on: March 25, 2014 / Accepted on: March 26, 2014
First published online on: March 26, 2014

References

1. Planck M. The new science — 3 complete works: Where is science going? The universe in the light of modern physics; The philosophy of physics. [Translated from the German by James Murphy and W.H. Johnston], Meridian Books, New York, 1959.
2. Planck M. Über das Gesetz der Energieverteilung im Normalspektrum. *Annalen der Physik*, 1901, v. 4, 553–563.
3. Planck M. The theory of heat radiation. P. Blakiston's Son & Co., Philadelphia, PA, 1914.
4. Kirchhoff G. Über das Verhältnis zwischen dem Emissionsvermögen und dem Absorptionsvermogen. der Körper fur Wärme und Licht. *Poggendorfs Annalen der Physik und Chemie*, 1860, v. 109, 275–301. (English translation by F. Guthrie: Kirchhoff G. On the relation between the radiating and the absorbing powers of different bodies for light and heat. *Phil. Mag.*, 1860, ser. 4, v. 20, 1–21).
5. Kirchhoff G. Über den Zusammenhang zwischen Emission und Absorption von Licht und. Wärme. *Monatsberichte der Akademie der Wissenschaften zu Berlin*, sessions of Dec. 1859, 1860, 783–787.
6. Wien W. Über die Energieverteilung in Emissionspektrum eines schwarzen Körpers. *Ann. Phys.*, 1896, v. 58, 662–669.
7. Stefan J. Über die Beziehung zwischen der Warmestrahlung und der Temperature. *Sitzungsberichte der mathematischnatur wissenschaftlichen Classe der kaiserlichen Akademie der Wissenschaften*, Wien 1879, v. 79, 391–428.
8. Robitaille P.-M. On the validity of Kirchhoff's law of thermal emission. *IEEE Trans. Plasma Sci.*, 2003, v. 31, no. 6, 1263–1267.
9. Robitaille P.M. Robitaille P. M. L. An analysis of universality in blackbody radiation. *Progr. Phys.*, 2006, v. 2, 22–23; arXiv: physics 0507007.
10. Robitaille P.-M. A critical analysis of universality and Kirchhoff's law: A return to Stewart's law of thermal emission. *Progr. Phys.*, 2008, v. 3, 30–35.
11. Robitaille P.-M. Blackbody radiation and the carbon particle. *Progr. Phys.*, 2008, v. 3, 36–55.
12. Robitaille P.-M. Kirchhoff's law of thermal emission: 150 Years. *Progr. Phys.*, 2009, v. 4, 3–13.
13. Robitaille P.-M. Blackbody radiation and the loss of universality: Implications for Planck's formulation and Boltzmann's constant. *Progr. Phys.*, 2009, v. 4, 14–16.
14. Robitaille P.-M. Further Insight Relative to Cavity Radiation: A Thought Experiment Refuting Kirchhoff's Law. *Progr. Phys.*, 2014, v. 10(1), 38–40.
15. Robitaille P.-M. Further Insight Relative to Cavity Radiation II: Gedanken Experiments and Kirchhoff's Law. *Progr. Phys.*, 2014, v. 10(2), 116–120.
16. Stewart B. An account of some experiments on radiant heat, involving an extension of Prévost's theory of exchanges. *Trans. Royal Soc. Edinburgh*, 1858, v. 22, no. 1, 1–20.

Progress in Physics is an American scientific journal on advanced studies in physics, registered with the Library of Congress (DC, USA): ISSN 1555-5534 (print version) and ISSN 1555-5615 (online version). The journal is peer reviewed and listed in the abstracting and indexing coverage of: Mathematical Reviews of the AMS (USA), DOAJ of Lund University (Sweden), Zentralblatt MATH (Germany), Scientific Commons of the University of St.Gallen (Switzerland), Open-J-Gate (India), Referential Journal of VINITI (Russia), etc. Progress in Physics is an open-access journal published and distributed in accordance with the Budapest Open Initiative: this means that the electronic copies of both full-size version of the journal and the individual papers published therein will always be acessed for reading, download, and copying for any user free of charge. The journal is issued quarterly (four volumes per year).

Electronic version of this journal: http://www.ptep-online.com

Postal address:
Department of Mathematics and Science, University of New Mexico,
705 Gurley Avenue, Gallup, NM 87301, USA

Printed in the United States of America